Faculty 4: Production Engineering
Mechanical Engineering & Process Engineering
Space Engineering I (SpE I)

Master Thesis

submitted in partial fulfilment
of the requirements for the degree of

Master of Science in *Space Engineering*

Design of an Alignment and Levelling Kinematic for Exploration Landing Platforms

Auslegung einer Ausricht- und Nivellier-Kinematik für Explorationslandeplattformen

---

by

Jan Alexander Bertram

Matriculation Number: 6091313

1. Reviewer Prof. Dr. Andreas Rittweger
Head of the Institute of Space Systems
German Aerospace Center (DLR)
Research Group 29 - Aerospace Engineering
University of Bremen

2. Reviewer & Supervisor Dr. Lars Witte
Head of Landing and Exploration Technologies
German Aerospace Center (DLR) - Institute of Space Systems

23rd August 2023

Jan Alexander Bertram
Design of an Alignment and Levelling Kinematic for Exploration Landing Platforms
Master Thesis, 23rd August 2023
Reviewers: Prof. Dr. Andreas Rittweger and Dr. Lars Witte
Supervisor: Dr. Lars Witte

University of Bremen
Space Engineering I (SpE I)
Mechanical Engineering & Process Engineering
Faculty 4: Production Engineering
ZARM, Am Fallturm 2
28359 Bremen

German Aerospace Center (DLR)
Institute of Space Systems
Landing and Exploration Technologies
Robert-Hooke-Straße 7
28359 Bremen

Abstract

The interest for the exploration of the Lunar surface has re-blossomed recently with the start of programs like NASA's *Artemis program* and the *European Exploration Envelope Program (E3P)* of the ESA. For these missions new Lunar landers are required, which enable delivery of cargo, production equipment, and power generation equipment to support crewed missions. Testing of new exploration technologies or science rovers is conceivable as well. Until now, large ground slopes and obstacles like boulders prevented many parts of the Lunar surface from being possible touchdown locations. By implementing a new technology, able to move the interface of the landing legs primary strut vertically up and down the side of the lander body, it is possible to change the geometry of the lander as a whole. This allows the alignment and levelling of the landing platform after touchdown. Thus expanding the number of potential landing sites and increasing the versatility and accessibility of landers.

This thesis compiles the needed mathematical foundations for the geometry, motion, and force calculation and implements them into a tool for computation. The results of this calculation are then used to design a first iteration of an alignment and levelling kinematic to get an understanding of the added mass, power requirement, and viability of such a system.

Zusammenfassung

Das Interesse an der Erforschung der Mondoberfläche ist in jüngster Zeit mit dem Start von Programmen wie dem *Artemis-Programm* der NASA oder dem *European Exploration Envelope Program (E3P)* der ESA wieder aufgeblüht. Für diese Missionen werden neue Mondlandegeräte benötigt, die den Transport von Fracht, Produktions- und Energieerzeugungsanlagen zur Unterstützung von Missionen mit Besatzung ermöglichen. Auch die Erprobung neuer Erkundungstechnologien oder wissenschaftlicher Rover ist denkbar. Bislang verhindern starke Bodenneigungen und Felsbrocken, dass große Teile der Mondoberfläche als mögliche Landeorte in Frage kommen. Durch den Einsatz neuer Technologie, welche es ermöglicht den Anbindungspunkt der Primärstrebe der Landebeine vertikal an der Seite des Landerkörpers auf und ab zu bewegen, kann die Geometrie des Landers im Ganzen verändert werden. Dies erlaubt das Ausrichten und Nivellieren der Landeplattform nach dem Aufsetzen auf der Monoberfläche und die Erschließung neuer Landeplätze. Außerdem wird die Flexibilität und Zugänglichkeit des Landers erhöht.

In dieser Arbeit werden die notwendigen mathematischen Grundlagen für die Geometrie-, Bewegungs- und Kraftberechnung zusammengetragen und in ein Berechnungswerkzeug implementiert. Die Ergebnisse der Berechnung werden daraufhin verwendet, um einen ersten Entwurf einer Ausricht- und Nivellierkinematik zu erstellen und ein Verständnis für die zusätzliche Masse, den Energiebedarf und die Realisierbarkeit eines solchen Systems zu erlangen.

Preface and Acknowledgement

After seven years of studying, first for four and a half years at the Hochschule Bremen and for the last two and a half years at the University of Bremen, this thesis marks conclusion of my studies (for now?). In addition to my master studies, I got the opportunity to work as a graduate research assistant at the DLR (Deutsches Zentrum für Luft- und Raumfahrt) Institute of Space Systems in Bremen, where I was able to apply the knowledge I acquired in the university in my day-to-day business. Additionally, I was fortunate enough to get the trust of my co-workers to work on some really interesting projects like the vertical take-off and vertical landing rocket stage demonstrator CALLISTO, the Mars Boundary Layer Explorer MABLE, or the reusable first stage rocket demonstrator project SALTO.

First, I have to thank my supervisor and head of the department for Landing and Exploration Technologies Dr. Lars Witte. He came up with the topic proposal of my thesis and enabled me to work on it besides my daily work in his department. He encouraged me to develop my skills and nudged me in the correct direction during the process of working on my thesis. Another thanks goes out to Prof. Dr. Andreas Rittweger, head of the institute and of the Aerospace Engineering research group at the University of Bremen who kindly agreed to act as first reviewer of my thesis.

My second thanks goes to all my direct co-workers in the department for Landing and Exploration Technologies. I always enjoyed working with each and everyone in the team and experienced a very supporting and friendly work environment. Special thanks goes out to Caroline Krämer, who helped me a lot during the direct stiffness method calculation. Also to Anton Schneider and Dr. Christian Grimm, both of which always had an open ear for any problems I encountered and helped me think of new ideas to solve them. Last, but definitely not least, special thanks to my fellow student in this department Arne Schlichting, with whom I share an office. He started his work in this department shortly before I started working on my thesis and we quickly became friends. During my work, I had many discussions with him, he always listened to the problems I encountered whenever I got stuck and came up with suggestions to keep going. He also helped with some decisions, especially

regarding the depictions used in this thesis. Without him, this thesis would most likely have looked a lot different.

Besides my work contacts, I have to thank all of my great friends who always stood by my side and helped me get my mind off my work. Special thanks at this point to my two best friends Isabell Wittekind, whom I shared many walks along the Werdersee with discussing my thesis or just everything and anything, and Christoph Diederichs, whom I have known for approximately 18 years now and with whom I can basically talk about everything and always get great advise. Also my awesome Pub-Quiz group "Die Fantastischen Bierwesen", whom I usually saw at least once a week for our Quiz-night in the Neustadt. Over the last one and a half to two years, they became some of my favourite people in the world and I would not want to miss them. Thank you Jan Pollex, Nora Volling, and Mareen Czech!

Finally, I have to thank my parents and their partners. My father Klaus Bertram and his spouse Barbara Pfeifer, and my mother Sabine Bertram and her life partner Fred Born. Without their parenting, education, care, support, and love I would not have become the person I am today! I can not thank you enough for everything you've done! I love you!

Jan Bertram

> *All we have to decide is what to do with the time that is given to us.*[a]

— J. R. R. Tolkien
English writer and philologist

---

[a]Gandalf in The Fellowship of the Ring, 1954

Contents

List of Figures

List of Tables

Abbreviations

A.D.	Anno Domini
abs	absolute
CAD	Computer Aided Design
CFRP	Carbon Fibre Reinforced Plastic
CNES	Centre National d'Études Spatiales
CoG	Centre of Gravity
COTS	Commercially available Off-The-Shelf
DC	Direct Current
DIN	Deutsches Institut für Normung
DLR	Deutsches Zentrum für Luft- und Raumfahrt
DoF	Degree(s) of Freedom
DSM	Direct Stiffness Method
dyn	dynamic
E3P	European Exploration Envelope Program
EBAD	Ensign-Bickford Aerospace & Defense
ECSS	European Cooperation for Space Standardization
EL3	European Large Logistics Lander
ESA	European Space Agency
FEA	Finite Element Analysis
FEM	Finite Element Method
FOS	Factor of Safety
GPS	Global Positioning System
IF#	Interface and Leg Number
ISO	International Organization for Standardization
JAXA	Japan Aerospace Exploration Agency
MATLAB	Matrix Laboratory
MSC	MacNeal-Schwendler Corporation
N/A	Not Applicable
NASA	National Aeronautics and Space Administration
Nastran	NASA Structural Analysis
PS	Primary Strut
rel	relative

S1	Strut 1 (Primary Strut)
S2	Strut 2 (Secondary Strut – left)
S3	Strut 3 (Secondary Strut – right)
seg	Segment
SLS	Space Launch System
SS	Secondary Strut
VTVL	Vertical Take-Off and Vertical Landing
w/o	without

Symbols

Roman Letters

Symbol	Definition	Symbol	Definition
A	Area	d	Diameter
A_{root}	Root area	d	Distance
C	Rotation matrix (12x12)	d_m	Mean diameter
C^T	Transposed C matrix (12x12)	d_{root}	Root diameter
E	Young's modulus	e	Unit vector
F	Force	f_c	Column buckling factor
FOS	Factor of safety	f_{cost}	Cost function
G	Shear modulus	g	Gravitational acceleration
I	Second moment of area	h	Height
I	Principal moment of inertia	k	Element stiffness matrix
I_3	Identity matrix (3x3)	k^b	Stiffness matrix of a beam
IF	Interface	l	Screw lead
K	Stiffness matrix	m	Mass
L	Length	$\overrightarrow{n}$	Normal vector
M	Moment	$\overrightarrow{n_0}$	Unit normal vector
P	Point	s	Element stiffness relation
R	Rotation matrix (3x3)	s^b	Stiffness relation of a beam
R, r	Radius	t	Thickness
S	Stiffness relation	u	Element displacement vector
T	Torque	u^b	Displacement vector of a beam
U	Displacement vector	x, y, z	Coordinate directions
X, Y, Z	Coordinate directions	xyz	Coordinate vector

Greek Letters

Symbol	Definition
α	Half of thread angle
α, β, γ	Tait-Bryan angles
α_{gnd}	Ground slope angle
θ	Pitch
θ_e	Rotation angle (Axis-angle representation)
μ	Coefficient of friction
ν	Poisson's ratio
π	Pi
σ_u	Ultimate strength
σ_y	Yield strength
φ	Roll
ϕ	Angle/Angular position
ω	Angular velocity

Indices

Symbol	Definition
CoG	Centre of Gravity
FP	Footprint
L, $lander$	Lander
P/L	Payload
PS	Primary Strut
$S1$	Strut 1 (Primary Strut)
$S1, seg1$	Strut 1, upper segment
$S1, seg2$	Strut 1, lower segment
$S2$	Strut 2 (Secondary Strut – left)
$S3$	Strut 3 (Secondary Strut – right)
SS	Secondary Strut

Symbol	Definition
$axis$	Axis direction
$body$	Body-coordinate-system
$foot$	Footpad
$glob$	Global-coordinate-system
lcl	Local
max	Maximum
min	Minimum
$struct$	Structure
tot	Total
$tube$	Tube
x, y, z	Coordinate directions

Others

Symbol	Definition
’	Arc minute
°	Degree
®	Registered trademark
™	Trademark

1 Introduction

> *Here men from the planet Earth first set foot upon the moon. July 1969 A.D. We came in peace for all mankind.*[a]
>
> **— NASA**

[a] Inscription on the Apollo 11 Lunar plaque, the Moon, 1969

After the *Apollo program* ended more than 50 years ago, with "Apollo 17" being the last crewed mission to the surface of the moon in 1972, exploration of the Lunar surface was deferred in an effort of pursuing other scientific programs. In recent years, interest in the scientific exploration of the Lunar surface has re-blossomed with programs like NASA's *Artemis program* and the *European Exploration Envelope Program (E3P)* of the European Space Agency (ESA) [1][2]. Especially following the first flight of the *Space Launch System (SLS)* with "Artemis I", which launched successfully on the 16th of November 2022, the second era of Lunar exploration comes within reach again.

The planned missions within these programs include the delivery of cargo, production equipment, and power generation equipment, thereby supporting future crewed missions. Exploration of the Lunar surface using science rovers and testing of new exploration technologies will increase our understanding of the Moon. Lastly, the return of samples to Earth will most likely be conducted, among many other conceivable mission goals. [3]

Unfortunately, these landing systems, be it on Earth or other celestial bodies like Moon or Mars, can not just land at any point on the surface of the celestial body but require rather narrowly defined conditions, which the landing site has to fulfil. These include the slope of the ground at the landing site, ground conditions like the composition and rigidity of the soil, as well as the presence of large or small boulders or other possible hazards in the targeted area. Because of that, chosen landing sites, especially in the beginning of Lunar and Martian exploration, have almost always been more or less level with the local gravitational vector and featured few boulders or other factors that could be hazardous to the lander. Unfortunately,

it is very difficult to get a high enough resolution of the landing area beforehand. Ruling out the presence of small boulders in the range of less than 0.5 m in diameter becomes almost impossible because of that. However, even these relatively small boulders can still damage the lander severely should it happen to impact on one of them. Feedback loops were implemented in the systems to map the landing area during approach and take measures to try and avoid possible detected hazards at the same time. However, all landers have to intersect the targeted landing site from an orbital path, meaning horizontal velocities will almost always be present and the exact landing location on the ground plane in many cases just happens to be the one where the landers trajectory intersects this plane and reaches a height of 0 m above ground. This can lead to unacceptable risks when choosing scientifically interesting but very small landing sites, such as craters with steep slopes and rough terrain, or ones that are littered with hazards broken only rarely by safe landing positions in-between. [4][5]

As reconnaissance quality of the landing areas, technological capability of landing systems, and accuracy and quality of simulations have increased in recent years, smaller and more challenging landing sites became feasible [6][7]. Landing sites in Lunar pole craters or on comets, as well as scientifically interesting areas with rough terrain on Mars or one of its moons Phobos and Deimos have been suggested as points of interest for these future missions [8].

Together with the desire to send humans back to the Moon to explore, very flexible landing systems that are easy to access by an astronaut are needed in order to meet the requirements of the different possible payloads.

These European lander projects for Lunar exploration currently operate under names like "Argonaut", or "European Large Logistics Lander" (EL3), and offer payload capacities of approximately 1.5 t [3]. In order to simplify the access to the payload compartment for rovers and astronauts, a mechanism that aligns and lowers the entire landing platform would be very helpful. Experiments using observatories or ascent stages atop the landing platform would also benefit hugely from the alignment and levelling capabilities such a mechanism would offer. Additionally, more control over the alignment of the lander could increase the number of possible touch down regions to those with rougher terrain and steeper slopes which were considered unsuitable for current systems. There are even proposals for actively controlled dampening systems. These systems, however, are still in early development and it is questionable whether they are fast enough to be utilized on landers in the near future. Furthermore, most of them only aim for ensuring safe landing without the risk of tipping over by implementing active dampening (e.g. [5][9][10]), or changing the geometry of the legs before touchdown (e.g. [11][12]). Some also try to offset the decrease of leg length induced by crushing of honeycomb elements by

implementing the possibility to slightly change the legs length using a lead screw inside of the primary strut after touchdown (e.g. [13]). None of them, however, tries to completely level and align the lander after touchdown.
A new, simple approach for these challenges has to be found, which does not only have to be lightweight, but also be based on readily available technologies. The mechanism needed for this would have to change the geometry of the lander, making it able to compensate for the rough, sloped terrain underneath. While multiple different concepts are conceivable to address this problem, from i) the already mentioned active control of the dampening system before and during touchdown, over ii) changing the length of the landing legs after touchdown, to iii) moving the interface of each legs primary strut by either attaching it to a swing arm or simply implementing some form of linear actuator to move the interface up and down, not all of them are similarly promising. This thesis addresses the variant of linear displacement of the primary interface. Analogous to a parallel manipulator used widely in the field of robotics, alignment, levelling, and lowering of the landing platform can be achieved this way. The alignment and levelling of the lander will be broken down into multiple steps, for each of which the exact primary interface position and acting forces are computed. Afterwards, the linear motion concept will be examined in more detail and a possible technical solution is presented, allowing for an estimation of required mass, volume, and power.

1.1 Legged lander basics

Before getting to in depth mathematical, geometrical, and mechanical explanations on how the legs of the lander have to be moved and what kind of mechanisms are needed to do so, this section will give a short introductory explanation on how a typical lander looks and works, and how the different parts and subsystems of such landers are called. The standard naming conventions of the field will be used in most cases, however, if any naming convention is not used, this section will clear up any possible misunderstandings regarding the denomination used in this thesis.

1.1.1 General design of legged landing platforms

Legged landing platforms are used in most if not all large stationary lander designs. These landers consist of a main body (or landing platform) which sits atop multiple landing legs. In most cases, there are either three or four of these legs, which themselves consist of three struts each [4]. The main or primary strut experiences

the larger share of the loads while the two secondary struts provide stability to and relieve some of the strain on the primary strut. Additionally, these legs always contain some form of dampening or initial landing shock absorption capabilities in the form of dampers or honeycomb crush structures. This decreases the shock loads transferred to the structure upon first impact with the ground of the celestial body. The leg kinematics design of a legged landing platform can generally be categorized into one of two categories: "*Cantilever*" or "*Inverted Tripod*". While the secondary struts of the leg attach to the immovable part of the primary strut in the Cantilever design, they attach to the movable part closer to the footpad in the Inverted Tripod design. The main characteristics of such a system including dynamic stability, energy absorption, and ground clearance depend on properties of the lander including but not limited to type of leg kinematic, length and number of legs, mass of the system, position of the CoG (h_{CoG}), as well as landing gear footprint radius (r_{FP}). Figure 1.1 shows some of these properties. [14], [15]

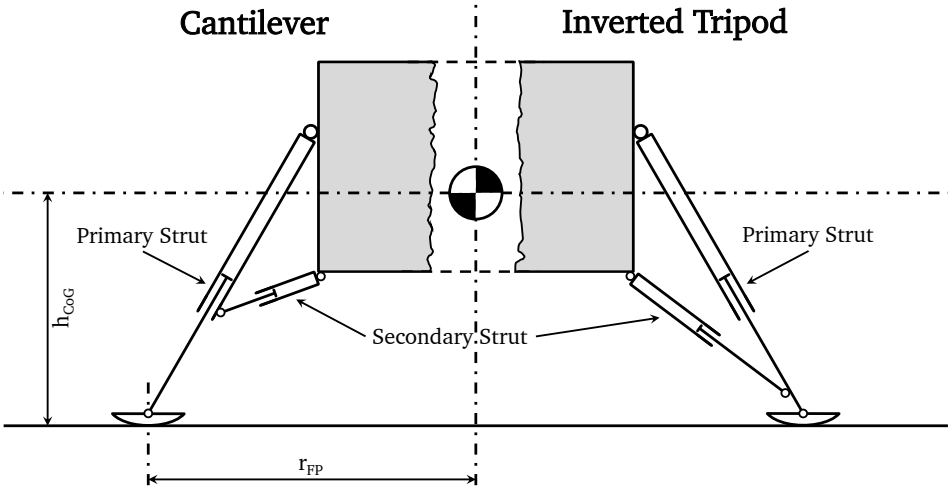

Fig. 1.1.: Leg kinematics and geometric properties: *The Cantilever principle (left) attaches the secondary strut to the upper tube of the primary strut, the Inverted Tripod principle (right) attaches the secondary strut to the moving lower tube of the primary strut* (adapted from [14]).

An example for the Cantilever design is the *Apollo Lunar Module* described by Rogers in [15], while the Inverted Tripod design can be found e.g. on the *Viking Lander* described by Holmberg et al. in [16]. According to Rogers, the Cantilever design usually shows a decreased overall weight due to shorter secondary struts even though the primary strut has to be reinforced as it experiences higher bending loads compared to the Inverted Tripod design. Additionally, Rogers states that the Cantilever design minimizes interference of the struts and increases stability of the lander due to a usually lower centre of gravity. Even if this sounds like a compelling argument to use a Cantilever design over an Inverted Tripod design, this

is not always the case as other factors than those mentioned here also play a role in the design process and may lead to the Inverted Tripod being the better choice. Examples of this could be reduced bending loads in the primary strut for very large and heavy landers or a lowered risk of buckling of the struts as the load is shared more equally on the three struts. Additionally, as the honeycomb dampeners in the struts are compressed, the geometry of the legs changes differently depending on which of the two kinematics designs was used. While the footprint radius decreases in the Cantilever design, it increases in the Inverted Tripod design, making the Inverted Tripod more stable as it settles.

1.1.2 Denomination

In order to avoid any possible confusion later in this thesis, the most important designations of parts which make up the landing system, will be explained here.

Legged lander The term "*legged lander*" (from now on just *lander* for short) is used to denote a spacecraft which uses a system of legs to land softly on an astronomical body. Depending on the landing site they can be fitted with different systems including systems for aerodynamic stabilisation, retro-thrusters, and a landing gear or landing legs with footpads. [4]

Landing platform The term "*landing platform*" (sometimes also "*lander body*" or just "*body*") in this thesis only refers to the part of the lander, which sits atop the landing legs. It is comparable to a satellite bus as it encompasses the landers main structural body as well as any subsystems. It also contains the payload which, however, is not a part of the landing platform itself.

Landing leg The "*landing legs*" are attached to the landing platform and, with their footpads, form the main interface towards the ground on which the lander stands. Typically, most landers feature three or four legs [4]. While designs with more legs are also possible, they are not utilized often as they quickly become very heavy. This diminishes the increased stability they offer, especially at the small size most landers have. The legs are made up of a primary and two secondary struts.

Strut (primary/secondary) The "*primary strut*" (sometimes also called "*main strut*") carries most of the load the lander exerts on the legs while the main purpose of the "*secondary struts*" is providing stability to the leg. Depending on the leg design (Cantilever or Inverted Tripod), the secondary struts might also support a large amount of the landers weight. For example, the closer the interface between primary and secondary strut is towards the footpad and therefore the ground, the higher the share of the load carried by the secondary strut. Additionally, the primary strut is usually split into multiple segments as it functions as a telescopic rod. In this thesis, however, when mentioning the "*upper segment*" of the primary strut it refers to the upper part from the interface to the lander body (IF1) down to the attachment point of the secondary struts. The "*lower segment*" refers to the lower part of the primary strut from this attachment point all the way down to the footpad.

Footpad The "*footpad*" (sometimes also just called "*foot*") is the contact point between the landing leg and the ground. It provides the necessary friction on hard surfaces as well as limiting the sinking in soft soils, thereby stabilizing the lander during touchdown.

1.2 Structure of thesis and methods used

The development of a first model for the motion of a landing platform requires multiple steps that have to be made in succession to one another. These steps form the chapters and sections of this thesis. Figure 1.2 shall provide an overview of these main chapters and their successive structure. The following chapter description provides a more detailed explanation of the applied methods and used tools.

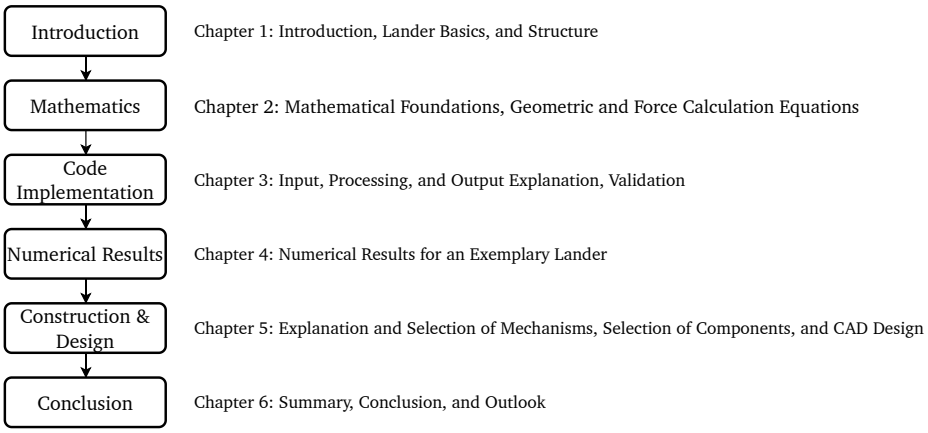

Fig. 1.2.: Flowchart and structure of this thesis

Chapter 1 (this chapter) gives an overall introduction into the topic of movable landing leg kinematics and the distinction between the Cantilever and Inverted Tripod designs of landers. Additionally, the basic parts of a lander were explained and differentiated.

Chapter 2 explains the mathematics required to calculate the geometric motion of a lander and the forces and loads acting during this motion. The geometric dimensions of a lander are explained (section 2.2.1) followed by the explanation of the used coordinate-systems (section 2.2.2). After setting some basic definitions and assumptions for the motion of the lander (section 2.2.3), the approaches for the different parts of the geometric calculation are described (section 2.3). This includes transformation matrices, positioning of points in three-dimensional space, the definition of the ground plane, and the calculation of intermediate positions between the initial state of the lander after touchdown and the final state of the lander in which it is fully levelled. Afterwards, the approach for the calculation of forces and loads acting on the lander and its parts is explained (section 2.4).

Chapter 3 illustrates the implementation of the mathematics from chapter 2 into a MATLAB script. The basic input via MS Excel (section 3.2), the processing flow of the code itself (section 3.3), and the output of the results (section 3.4) are explained to give the reader an overview of the inner workings of the code. Additionally, a validation of the force calculation using MSC Patran and MSC Nastran can be found here as well (section 3.5).

Chapter 4 specifies the characteristics and parameters for an exemplary realistic lander (section 4.1) for which the forces on the primary interface are calculated for different orientations of the lander on an inclined plane (sections 4.2 and 4.3). Based on these results, the key design drivers for a construction of a mechanism are identified (section 4.4).

Chapter 5 includes requirements for a movement mechanism (section 5.1) and the explanation of different linear movement mechanisms (section 5.2), leading to the selection of one design approach. Based on the requirements, off-the-shelf components are selected (section 5.3) and custom components are designed using CAD software (section 5.4). The chapter ends with a mass and power estimation for the designed mechanism (sections 5.5 and 5.6).

Chapter 6 summarises the results of this thesis. It includes a final discussion and closing remarks. It ends in an outlook on open points for possible future works.

Mathematical Foundations

2

> *Everything is physics and math.*
>
> **— Katherine Johnson**
> American mathematician at NASA

To get a profound understanding of what happens or has to happen in order to level and align a landing platform, the mathematical correlations of the system have to be understood. By comparing the lander to already existing systems from the field of robotics, i.e. parallel manipulators, and getting an understanding of possible similarities and differences as well as problems that may emerge in the description of these systems, the characterisation of the lander system can be simplified. Additionally, the geometry of the lander as well as the coordinate system that will be used must be defined. Once this is done, the transformation of coordinates between these different coordinate systems has to be defined after which the actual movement of the lander may be computed. In a further step, the forces acting inside the struts of the landing legs can be calculated from the geometry of the lander, its mass, and the local gravitational vector.

2.1 Parallel manipulators and inverse kinematics

Classical serial manipulators, with the most prominent example being articulated robot arms, use actuators that are connected in series from an anchor point to the end-effector. To achieve full freedom of motion in all spatial dimensions, a system with six DoF (Degrees of Freedom) is needed, three for the translational movement along each axis of space and three for rotating about these axes. An example of such a manipulator can be seen in figure 2.1a. In the classic mathematical consideration, a system with just five DoF also only moves in five dimensions (usually the yaw around the vertical axis is not considered in this case), while a system with more than six DoF offers the possibility of so called *zero-space movement* as every additional DoF introduces a redundant axis into the system. This can be used to move parts of the manipulator without moving the attached end-effector. [17]
A parallel manipulator is a system in which two platforms are connected to each

other via multiple movable struts connected in parallel. One of the two platforms stays still, while the other one is moved by manipulating the connecting struts or legs. The means of moving these struts can be very different from one another, e.g. using multiple jointed struts similar to an articulated robot arm, or telescopic struts that can extend and retract. The most commonly recognised variant of this is probably the so called *hexapod* or *Stewart platform*, an example of which can be seen in figure 2.1b. [17], [18]

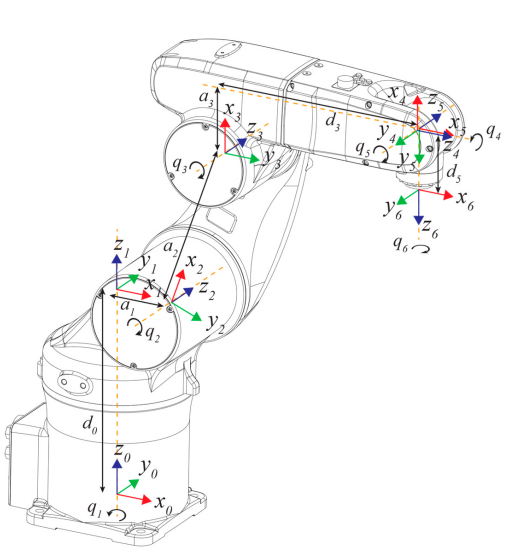

(a) Example for a serial manipulator: *The image shows a robotic arm with its respective reference frames; from [19], used under Creative Commons CC BY 4.0 licence.*

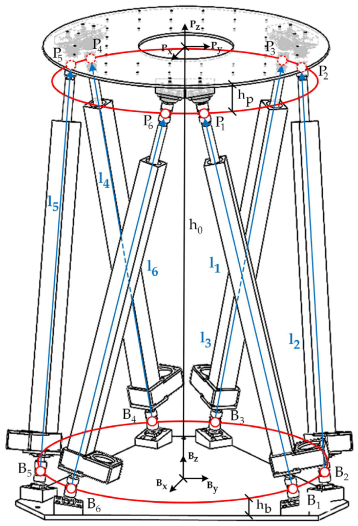

(b) Example for a parallel manipulator: *The image shows the geometric structure of a general Gough-Stewart platform; cropped from [20], used under Creative Commons CC BY 4.0 licence.*

Fig. 2.1.: Serial and parallel manipulator

There are, however, also manipulators of this type with fewer than six connections and less DoF. This can lead to so called *parasitic motion* where movement in axes, that are assumed to be locked, happens because of geometric constraints in the system. If, for example, only three DoF are considered in the calculation (as will also be the case for the calculations in this thesis), e.g. two rotational and one translational, the combination of movement in these axes can lead to movement along or around the other axes, which is not supposed to happen. To get the most accurate results, this has to be dealt with in the kinematic analysis of the system in order to explain the real world behaviour of the system. [21][22]
This, however, would drastically exceed the scope of this thesis and will therefore be neglected for now.
Controlling parallel manipulators requires solving for the actuator states based on the desired final position of the end-effector using so called *inverse kinematics*. Contrary

to direct kinematics in which the joint/actuator states are known and the position and alignment of the end-effector is calculated, in inverse kinematics the state of the end-effector at the end of the kinematic chain is known and the joint/actuator parameters have to be calculated from that. This approach is more complicated to the extent that inverse kinematics lead to strongly non-linear systems of equations. While numerical approaches work for all kinds of manipulators, they do require more computational power. Finding analytical solutions, however, is non-trivial for serial manipulators while for hexapods, for example, no analytical solution exists at all. [17] Because of this, a numerical approach will be used for the calculation in this thesis.

2.2 Geometric definition of the lander

Before the mathematical approach can be explained, first the geometry of the basic lander has to be defined. The mathematical scripts shall be parametrised in order to be used for different landers with different interface positions as well as different landing leg kinematics. Therefore, an easily adaptable, generic geometrical definition, which still includes every parameter, is needed for the calculation.

2.2.1 Lander dimensions

The most important dimensions of a generic Lunar lander, which are used in this thesis, are shown in figure 2.2 and explained in table 2.1. They consist of the dimensions of the lander body, the position of the centre of gravity, and the strut lengths. Additionally, the definition of the interface numbering is shown in the figure as well. The primary strut (strut 1/S1) is connected to IF1, and the secondary struts (strut 2/S2 and strut 3/S3) are connected to IF2 and IF3. When looking straight onto a leg, the left secondary strut is denoted as strut 2 and the right secondary strut as strut 3. The intersection between the primary and secondary struts is denoted as $IF_{PS,SS}$.

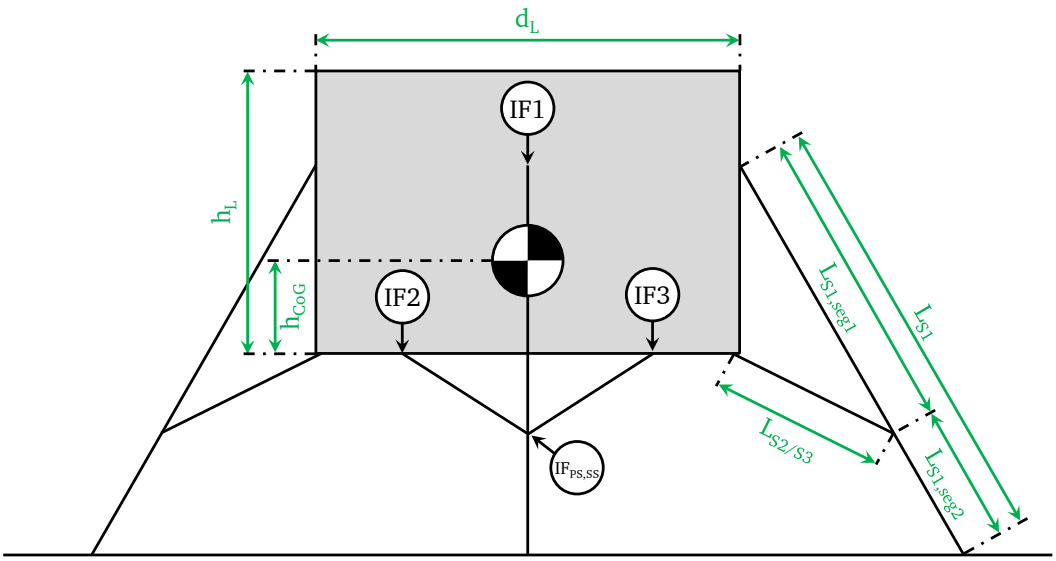

Fig. 2.2.: Dimensions of a generic Lunar lander

Tab. 2.1.: Dimensions of a generic Lunar lander

Symbol	Parameter
d_L	Lander diameter
h_L	Lander height
L_{S1}	Length of primary strut
L_{S2}	Length of secondary struts
L_{S3}	
$L_{S1,seg1}$	Distance IF1 to secondary strut attachment
$L_{S1,seg2}$	Distance secondary strut attachment to foot
h_{CoG}	Height of CoG

2.2.2 Coordinate-systems

For the description of the lander legs, two different coordinate-systems are being used. It is necessary to be able to transform coordinates from one of these systems to another in order to be able to do all the necessary calculations and describe the movement and forces in an understandable manner. How this transformation of coordinates between the coordinate systems works is explained in section 2.3.1.

2.2.2.1. Body-coordinate-system

First, there is the lander- or body-coordinate-system. It is used to describe the interface positions of the legs primary and secondary strut to the landing platform and forces or movement relative to the landing platform. A qualitative example of this can be seen in figure 2.3. The origin of this coordinate-system is set at the central point of the lower side of the landing platform. The x-axis points in a radial direction towards the primary strut interface (IF1) of leg 1. The y-axis is rotated 90° counter-clockwise pointing towards leg 2 (in the case of a four legged lander). The z-axis is perpendicular to the xy-plane, pointing upwards towards the upper side of the lander body in accordance with the right hand rule.
A simplification can be used to make the definition of the interface positions between struts and landing platform easier. As these interfaces show rotational symmetry right after landing, this can be used to reduce the number of legs for which the interface coordinates have to be defined as these coordinates are the same for all legs. This, however, changes later on when the primary strut interfaces are moved in the direction of the vertical axis in order to level and align the landing platform. After defining the interface coordinates for leg 1, transformation matrices are used to rotate these coordinates to the correct position for each of the other landing legs. By using this technique, it is also easier to parametrise the number of legs the lander shall have.

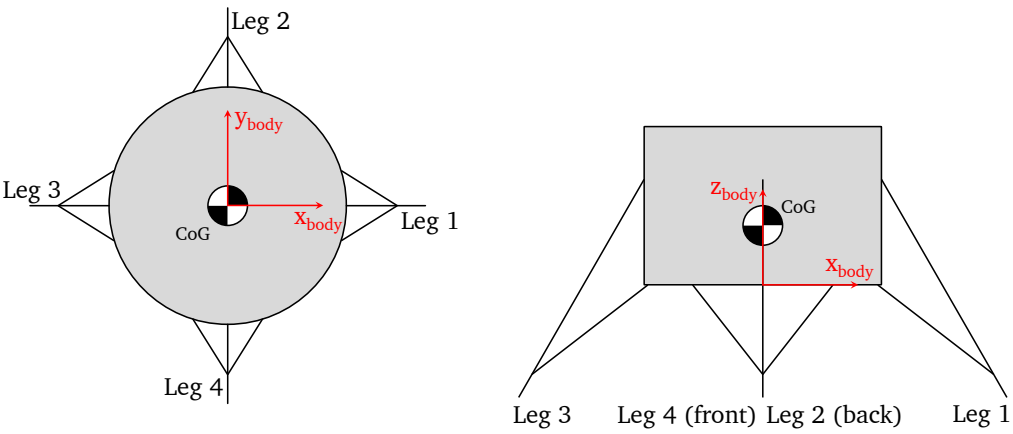

(a) Top view

(b) Side view

Fig. 2.3.: Body-coordinate-system

2.2.2.2. Global-coordinate-system

The second coordinate-system used is the global-coordinate-system which is shown for an exemplary lander with four legs in figure 2.4. The origin of the coordinate-system is kept at the initial central point of the lower side of the landing platform right after touchdown of the lander. It stays at this global point even when the landing platform is lowered at a later point in time. The directions of the axes, however, are different from the body-coordinate-system. The positive z-axis z_{glob} now points upwards against the direction of the local gravitational vector. The global x-axis x_{glob} is again perpendicular to z_{glob} lying in the same rotational plane as x_{body} and z_{body}, provided the lander is only pitched (roll $\varphi = 0$). Under these circumstances, the y-axes of global- and body-coordinate-system coincide ($y_{glob} = y_{body}$ for $\varphi = 0$). Should the lander only be rolled and not pitched (pitch $\theta = 0$), the x-axes of the two coordinate-systems coincide ($x_{glob} = x_{body}$ for $\theta = 0$), while the angle between the two y-axes is equal to φ.

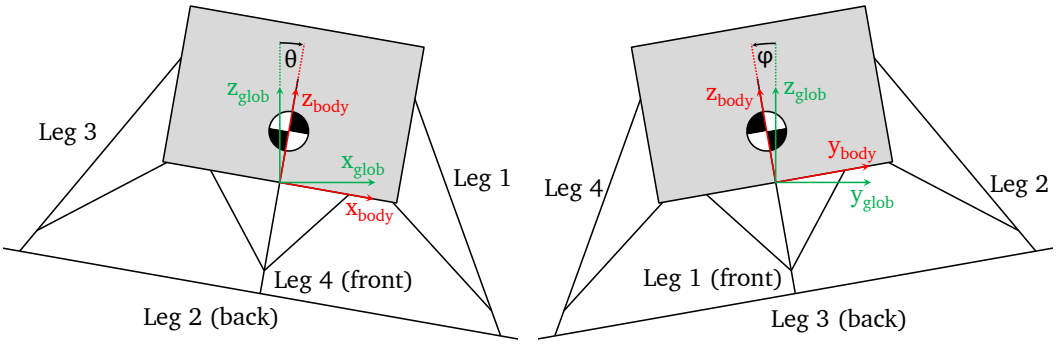

(a) Definition of x_{glob}: *Lander on a 10° slope (tilted around the y-axis)* $\longrightarrow y_{glob} = y_{body}$

(b) Definition of y_{glob}: *Lander on a 10° slope (tilted around the x-axis)* $\longrightarrow x_{glob} = x_{body}$

Fig. 2.4.: Global-coordinate-system

In this global coordinate system, all coordinates are defined/calculated for the whole movement of the landing platform from its landing position to its aligned and levelled position. A more detailed explanation on how the transformation and the calculation of the other interface coordinates works follows in section 2.3.

2.2.3 Lander geometry and motion - definitions and assumptions

While some properties of the lander like its geometry and orientation are known by definition or measurement, some assumptions have to be made for other properties. This is necessary to make the script easily adaptable while still keeping it in a feasible operational framework without too many redundant code pieces.

Definitions and known parameters

D1. The orientation of the lander after it has landed is known in the form of roll around the global x-axis and pitch around the global y-axis

D2. The lengths of all landing leg struts (primary and secondary) after landing and crushing of the dampening elements are known and they do not change

D3. The position of all primary and secondary strut interfaces relative to the lander-centred-coordinate-system is known based on the lander design

Assumptions

A1. The platform is assumed to be sufficiently described with three DoF: translational movement along the vertical z-axis, rotational movement around the x-axis [roll] and the y-axis [pitch]; other translational movement is neglected because of A4 and rotation around the z-axis (yaw) can be neglected as the lander is assumed to feature rotational symmetry, i.e. it can be sufficiently described by only using pitch and roll; parasitic motion is neglected

A2. The position of the primary strut interfaces only change in the direction of the vertical axis (z-axis) relative to the lander-centred-coordinate-system

A3. The position of the secondary strut interfaces does not change relative to the lander-centred-coordinate-system as they are assumed not to be actuated

A4. As a first approximation, the ground is assumed to be locally described by a plane without any bumps or changes in inclination

A5. The movement of the platform is assumed to happen slowly so inertial effects can be neglected and all forces are assumed to be quasi-static

This calculation, based on alignment and height above ground, is only meant as a first estimate of i) the length needed for the linear drive of the primary strut interface to the lander and ii) the loads on the legs and the forces needed to drive the lander from its landing position into the final desired position. In no means does it give exact results. For a possible system design at a later point in time, more advanced dynamic simulations might be needed.

2.3 Mathematical approach for the calculation of lander geometry

The numerical approach chosen for the calculation combines vectorial calculus and trigonometry, as well as non-linear numerical optimisation, in order to calculate the interface positions of each leg for the desired height and alignment of the landing platform.
In a first step, the positions of all interfaces right after landing have to be determined in order to calculate the ground plane. This sets a lower boundary for the positions of the footpads. In a following step, the interface positions needed for any pitch θ, roll φ, and height above ground can be calculated (explained in section 2.3.5).
To be able to compute the position of the interface between the primary and secondary struts $IF_{PS,SS}$, a form of positioning algorithm, similar to those that GPS satellites use, has to be implemented (explained in section 2.3.2). After that, the positions of the footpads and therefore the parameters needed to describe the ground plane can be computed using vectorial calculus (explained in sections 2.3.3 and 2.3.4).

2.3.1 Transformation matrix

As already mentioned in section 2.2.2, the coordinates of the interfaces have to be transformed between coordinate-systems in order to calculate and describe all effects happening while the landing platform is aligning itself.
For this, the standard transformation matrix using Euler angles, or more specifically *Tait-Bryan angles*, is utilized. Here, the angles about x, y, and z are γ, β, and α, respectively. It is very important to keep one sequence in which the rotations around the axes is computed, as changing the order of the rotations leads to different results for the same angles. The most common order of rotations used in the spaceflight regime is x-y-z (extrinsic rotations) or z-y'-x" (intrinsic rotations), which is also utilized in this thesis. Figure 2.5 shows an exemplary rotation from a global xyz-system into a body-fixed XYZ-system.
To get the angles α, β, and γ, the global pitch (θ) and roll (φ) angle are first transformed into the axis-angle representation. In this representation, a rotation of a vector is simply defined by an axis, in the form of a unit vector $\vec{e}$, around which the vector is rotated by a specific amount θ_e. In this case, the axis around which the coordinates have to be rotated is a line orthogonal to the vertical axes of the two coordinate-systems between which the coordinate transformation shall take place.

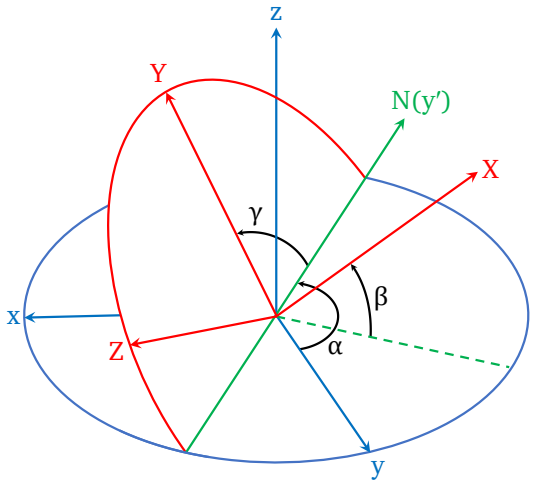

Fig. 2.5.: Tait-Bryan angles: *z-y'-x" sequence (intrinsic rotations; N coincides with y', X coincides with x"), corresponds to an α, β, γ angle sequence; based on similar image by "Juansempere", used under Creative Commons CC BY 3.0 licence, via Wikimedia Commons.*

It can be computed by forming the dot product of unit vectors in the two vertical axes. For example the axis around which a rotation between the global- and the body-coordinate-system happens.

$$\vec{e} = \vec{z}_{glob} \cdot \vec{z}_{body} \tag{2.1}$$

The angle θ_e is simply the angle between the two vectors $\vec{z}_{glob}$ and $\vec{z}_{body}$.

$$\cos\theta_e = \frac{\vec{z}_{glob} \cdot \vec{z}_{body}}{|\vec{z}_{glob}|\,|\vec{z}_{body}|} \tag{2.2}$$

The euler angles α (yaw), β (pitch), and γ (roll) are computed in the next step.

$$\alpha = \arctan\left(\frac{e_x \cdot e_y \cdot (1-\cos\theta_e) + e_z \cdot \sin\theta_e}{1-\left(e_y^2+e_z^2\right)\cdot(1-\cos\theta_e)}\right) \tag{2.3a}$$

$$\beta = \arcsin\left(-(e_x \cdot e_z \cdot (1-\cos\theta_e) - e_y \cdot \sin\theta_e)\right) \tag{2.3b}$$

$$\gamma = \arctan\left(\frac{e_y \cdot e_z \cdot (1-\cos\theta_e) + e_x \cdot \sin\theta_e}{1-(e_x^2+e_y^2)\cdot(1-\cos\theta_e)}\right) \tag{2.3c}$$

Now that the Euler angles are known, the rotation matrix may be computed by using equation 2.4 below. The rotation matrix has to be premultiplied with whichever vector shall be rotated.

$$
\begin{aligned}
R &= R_z(\alpha)R_y(\beta)R_x(\gamma) \\
&= \overset{yaw}{\begin{bmatrix} \cos\alpha & -\sin\alpha & 0 \\ \sin\alpha & \cos\alpha & 0 \\ 0 & 0 & 1 \end{bmatrix}} \overset{pitch}{\begin{bmatrix} \cos\beta & 0 & \sin\beta \\ 0 & 1 & 0 \\ -\sin\beta & 0 & \cos\beta \end{bmatrix}} \overset{roll}{\begin{bmatrix} 1 & 0 & 0 \\ 0 & \cos\gamma & -\sin\gamma \\ 0 & \sin\gamma & \cos\gamma \end{bmatrix}} \\
&= \begin{bmatrix} \cos\alpha\cos\beta & \cos\alpha\sin\beta\sin\gamma - \sin\alpha\cos\gamma & \cos\alpha\sin\beta\cos\gamma + \sin\alpha\sin\gamma \\ \sin\alpha\cos\beta & \sin\alpha\sin\beta\sin\gamma + \cos\alpha\cos\gamma & \sin\alpha\sin\beta\cos\gamma - \cos\alpha\sin\gamma \\ -\sin\beta & \cos\beta\sin\gamma & \cos\beta\cos\gamma \end{bmatrix}
\end{aligned}
\tag{2.4}
$$

It should be noted that the direction of the angles is defined by the right hand rule and reversing the transformation, i.e. rotating back to the original coordinate-system from the new coordinate-system, requires transposing the rotation matrix before premultiplying with the vector. Additionally, this approach does not work if both roll φ and pitch θ are 0° or if one of them is equal to 90°. The 90° exception can be neglected for this thesis as the maximum tilt of the lander from the global plane shall be in the order of 15°. If both angles are equal to 0° the rotation matrix is simply the identity matrix I_3.
After the interface positions of the struts to the landing platform have been rotated according to the current orientation of the lander, the remaining positions of the interfaces between primary and secondary strut can be calculated using the steps explained in section 2.3.2.

2.3.2 Positioning of primary to secondary strut interface

Because of the different amount of strut stroke of each leg during touchdown and because any measurement is innately inaccurate, the exact position of the interface between primary and secondary strut ($IF_{PS,SS}$) can not be derived directly. By using an approach similar to the one geopositioning satellites use to determine the position of a point from their own known position and their distance to that point, it is possible to calculate the coordinates of $IF_{PS,SS}$. Considering the coordinates of the interfaces as the centre of a sphere with their radii r being the distance to the wanted interface point, the point where all spheres meet is the position of the interface. Figure 2.6 shows a visual representation of the spheres which overlap exactly on the interface between the struts. The implementation into a calculation

script and the constraint function, which restricts the solution geometrically, are explained in section 3.3.2.

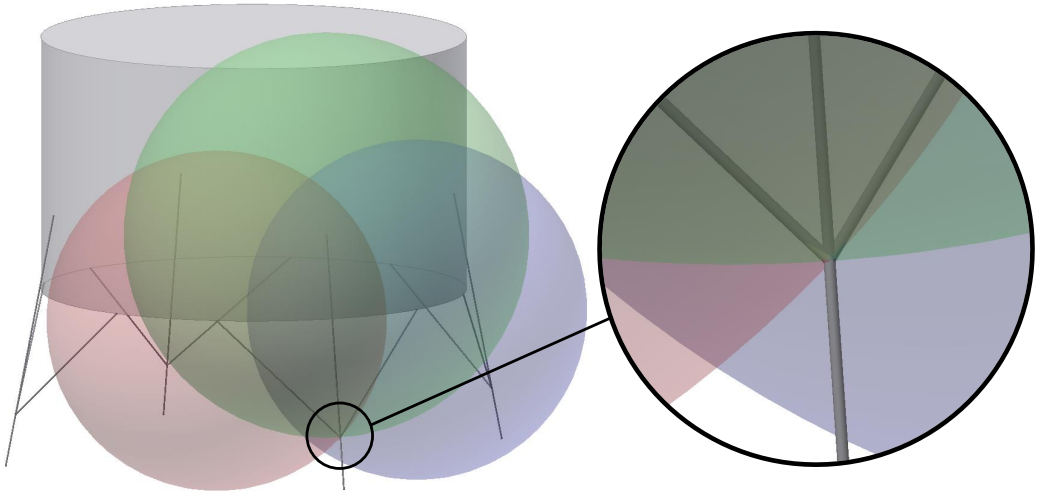

Fig. 2.6.: Positioning of interface position using spheres: *The right circle shows a zoomed in section of a lander on the left.*

2.3.3 Computation of foot positions using vectorial calculus

Based on the now known position of $IF_{PS,SS}$ for each leg, the position of the footpads follows by using simple vectorial calculus. A unit vector from IF1 to $IF_{PS,SS}$ can be calculated by subtracting the coordinates of the former from the coordinates of the latter interface and dividing the result by the distance between the two. By then multiplying the resulting unit vector that points in the direction of the primary strut by its length and adding that to the coordinates of IF1, the resulting coordinates x, y, and z determine the position of the footpad xyz_{foot}.

$$xyz_{foot}(x,y,z) = IF1 + L_{PS} \cdot \left(\frac{IF_{PS,SS} - IF1}{d} \right) \tag{2.5}$$

where:

$$d = \sqrt{(IF1_x - IF_{PS,SS;x})^2 + (IF1_y - IF_{PS,SS;y})^2 + (IF1_z - IF_{PS,SS;z})^2}$$

2.3.4 Equation of the ground plane

The ground plane is described using the *Hesse normal form*, where a plane has an unit normal vector $\overrightarrow{n_0}$ and a distance from the origin d. By providing the x-, y-, and

z-coordinates of any three points on the plane (e.g. $P1$, $P2$, and $P3$) these values can easily be calculated. Here, these values correspond to the coordinates of footpad 1 to footpad 3 (footpad 4 is assumed to be on the plane described by the first three footpads).
First, the normal of the plane is calculated using

$$\overrightarrow{n} = (\overrightarrow{P1} - \overrightarrow{P2}) \times (\overrightarrow{P1} - \overrightarrow{P3}) \tag{2.6}$$

Depending on the exact location of the plane, the unit normal vector of the plane is then calculated using

$$\overrightarrow{n_0} = \begin{cases} \frac{\overrightarrow{n}}{|\overrightarrow{n}|} \text{ for } \overrightarrow{P1} \cdot \overrightarrow{n} \geq 0 \\ - \frac{\overrightarrow{n}}{|\overrightarrow{n}|} \text{ for } \overrightarrow{P1} \cdot \overrightarrow{n} < 0 \end{cases} \tag{2.7}$$

The distance to the origin follows from

$$d = \overrightarrow{P1} \cdot \overrightarrow{n_0} \tag{2.8}$$

thereby fully describing the ground plane in the *Hesse normal form*. The normal vector can later also be used to calculate the angle between the ground and the landing leg struts in order to compute the acting forces. The z-value of the plane can be calculated for every point on the xy-plane of the coordinate-system using equation 2.9. For example, if at state 0 (landed state at rest) the origin of the coordinate-system is set as input for the equation, the result is the height of the lander above ground as the origin of the coordinate-system is set at the centre of the lower face of the lander.

$$z(x, y) = \frac{d - \overrightarrow{n_0}(1) \cdot x - \overrightarrow{n_0}(2) \cdot y}{\overrightarrow{n_0}(3)} \tag{2.9}$$

2.3.5 Motion of the lander and intermediate positions

Once the positions of the interfaces in the initial state 0 are known and the ground plane was calculated, the intermediate positions between state 0 and the end state, in which the landing platform is aligned and levelled, can be calculated. In this context, the word *state* refers to a configuration of the lander. For example, in the initial state 0, none of the primary interfaces have been moved from their initial fixed position, while they have moved slightly in state 1, and have reached their final position in the final state n (depending on how many are calculated). By incrementally adjusting roll, pitch, and height of the lander, the new positions of

all interfaces can be calculated for each intermediate state until the desired zero degrees of roll and pitch and the specified height above ground are reached.

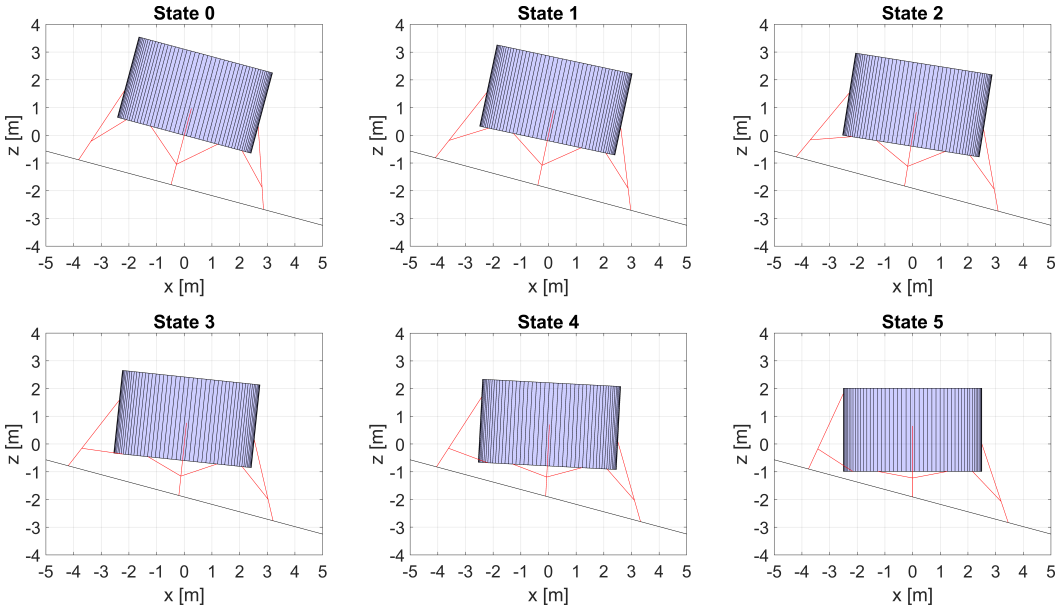

Fig. 2.7.: Transition of lander from landing position to aligned and levelled position: *Example of movement of the lander on a ground slope of 15° from 'state 0' (right after landing) to the final state (here 'state 5') in which the lander is aligned and levelled.*

Doing this requires recalculating the interface positions of IF1, IF2, and IF3 for the new height and orientation of the lander. This can be achieved by offsetting the z-coordinates of the interfaces and rotating them according to the pitch and roll of each intermediate state following the procedure explained in section 2.3.1. The footpads will not coincide with the ground plane anymore after doing this. At this point, the mechanism that will actually move the lander in reality comes into play. The interfaces of the primary struts (IF1) are moved in z-direction (in the body-coordinate-system) thereby changing the angle of the struts and allowing the lander to stand in this new state. The position IF1 is calculated iteratively for each leg by i) initially guessing the interface coordinates, ii) calculating the new foot position of the leg based on this guess, and iii) adjusting the interface position again until the foot coordinates coincide with the ground plane within a reasonable error frame. At this point, the lander stands in its new state 1. This procedure is then repeated for each state until the specified end state is reached. Figure 2.7 shows this for an exemplary ground slope of 15° in five steps from the state right after landing to the aligned and levelled lander in the last state.

2.4 Calculation of forces on the landing legs

After the positions of each of the struts of the landing legs from the landing to the aligned state along multiple intermediate positions are known, the forces on each of the struts have to be calculated to estimate the power needed for moving the lander. It is important to note that only the maximum expected boundary value of the force on the leg is needed for this as this extreme dictates the maximum power needed for moving the lander and therefore drives the design and component selection.
In a first step, the reaction forces on the footpads must be calculated.

2.4.1 Reaction forces on footpads for a three legged lander

For a lander with three legs ($n = 3$), the computation of the reaction forces is a trivial task as it is possible to find three equilibrium conditions for the entire system. By simplifying the system so that only forces in the direction of the global z-axis, or in other words in the direction of the local gravitational vector, are considered, the number of equations is reduced to the force equilibrium in direction of the z-axis, as well as the torque equilibria around the x- and y-axis. These equilibrium conditions can be seen in equations 2.10.
It should be noted that the x- and y-axis are moved into the CoG for this purpose, which is why the distance of the force to the axes in equations 2.10b and 2.10c is set in relation to the CoG. Towards where they are moved does not make any difference as the moment of the system has to be in equilibrium no matter where the axes are placed, otherwise the system would tilt around that axis. For the equations here, however, the assumption that they go through the CoG has to be made as they would be incorrect otherwise because of the missing weight of the lander in these equations, which cancels out when the axes go through the CoG. Furthermore, this approach reduces the reaction forces to a single force in the direction of the z-axis, which does not reflect reality, where this force is split into a force normal to the ground, as well as friction tangential to the ground. Directly calculating all of these forces in this step would, however, increase the complexity of the equations drastically. Each of the distances has to be calculated using vector calculus and the approach of splitting the result into their respective components afterwards simplifies the matter at hand

by a lot as they can be directly calculated using trigonometry and the orientation of the ground plane.

$$\sum F_z = 0 = \sum_{i=1}^{n} F_{z,i} - m_{lander} \cdot g_{lcl} \tag{2.10a}$$

$$\sum M_x = 0 = \sum_{i=1}^{n} M_{x,i} = \sum_{i=1}^{n} F_{z,i} \cdot (y_i - y_{CoG}) \tag{2.10b}$$

$$\sum M_y = 0 = \sum_{i=1}^{n} M_{y,i} = \sum_{i=1}^{n} F_{z,i} \cdot (x_i - x_{CoG}) \tag{2.10c}$$

2.4.2 Reaction forces on footpads for a four legged lander

Given the case of a four legged lander, the three equilibrium conditions of equations 2.10 do not sufficiently limit the system as there are now four legs ($n = 4$), which means four variables but only three equations to calculate them. Because of that, it is not possible to find one definitive solution without an additional equation or boundary condition. This problem has range of possible solutions, some of which will be shortly outlined here.

2.4.2.1. Maximum boundary values and forces for three legs

The simplest solution would be only considering the most extreme boundary condition of the lander. In that case, it is possible to assume that only three of the four legs have to support the entire weight of the lander, while the fourth leg sees no load at all. Doing this effectively removes one of the legs from consideration, thereby lowering the number of legs to three ($n = 3$), allowing for a calculation based on the approach and equations from section 2.4.1. This introduces an error compared to the reality where most certainly all of the legs will support at least some of the weight. It would, however, be reasonable to use this case with its maximum force as the driving value for dimensioning as a very conservative estimate allowing the mechanism to support and move the lander even in the most extreme cases. Even so, it is more desirable to actually know the load on each of the legs and to introduce a safety factor based on these values instead of using an unknown safety factor purely based on a faulty calculation that does not show the whole picture.

2.4.2.2. Analytical solutions using simplified lander configurations

By simplifying the problem to one where the footpads either stand in an exact rectangle (or square), it is possible to determine the forces on the footpads using geometric relations. Analogous to a simply supported beam with asymmetric load, the entire force in the CoG can be split into forces on two opposing sides (e.g. $\overline{\mathrm{AD}}$ and $\overline{\mathrm{BC}}$). After that, the results can be divided again to get the reaction forces of each of the four individual supports. In its entirety, this simplifies to the following statement:
The force in each vertical support corresponds to the ratio between the rectangular area opposing the vertex (that stretches from the opposing vertex to the CoG) and the entire area of the rectangle multiplied by the force in the CoG. This can also be seen in figure 2.8, where an exemplary area and corresponding support are shaded equally.

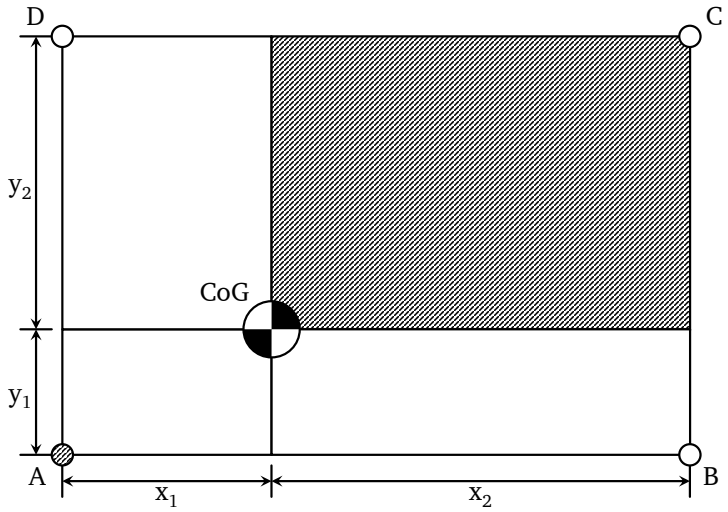

Fig. 2.8.: Force ratio of vertices in a rectangle: *The reaction force in each support is equal to the force in the CoG multiplied with ratio between the opposing area and the entire area (e.g.* $F_A = F_{CoG} \cdot \frac{A_{shaded}}{A_{\mathrm{ABCD}}} = F_{CoG} \cdot \frac{x_2 \cdot y_2}{(x_1+x_2)\cdot(y_1+y_2)}$*).*

Unfortunately, this does not work if the quadrilateral that stretches between the footpad positions is not a square or rectangle when looking at the lander from above. However, this will not be the case most of the time. If this approach is still used, it introduces an error that increases with an increasing deviation from a rectangle.
Alternatively, if two of the legs stand in a line that is orthogonal to the plane between the gravity vector and the normal vector of the ground plane, the forces on these two legs can be assumed to be equal in magnitude. This is the case for two legs in the so called 1-2-1 configuration and for two sets of two legs in the 2-2 configuration. This way, the system reduces to three (1-2-1 configuration) or

even just two unknowns (2-2 configuration). If this is the case, the equilibrium equations 2.10 from section 2.4.1 may be used to compute the forces on the footpads. For a visual representation of this see figure 2.9.

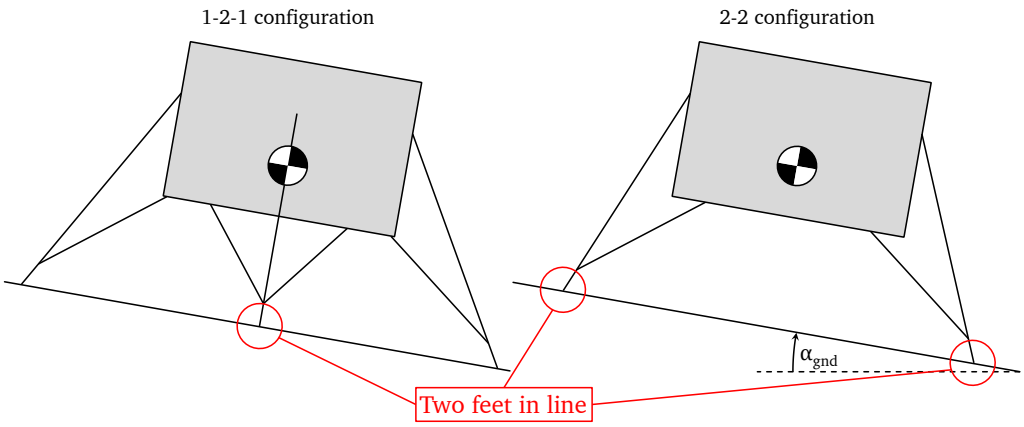

Fig. 2.9.: Alignment of a four legged lander with the line between two legs orthogonal to ground slope: *The red circle signifies two footpads behind each other on one line. In the left image (1-2-1 configuration), there are three unknowns and in the right (2-2 configuration) only two.*

As these simplifications can not be made for most of the possible positions the lander could stand in, this approach would be faulty in most cases, which is why it won't be used in the final version of the calculation.

2.4.3 General solutions

Some possible approaches are not limited to a specific number of legs in order to work, two of which will be shortly discussed here.

2.4.3.1. Principle of virtual work

Usually, in basic mechanic studies when dealing with statically indeterminate systems, the principle of virtual work is used to calculate the reaction forces of the supports. In a nutshell, this works by removing the additional reaction forces that make the system statically overdetermined, therefore allowing the supporting node to move slightly due to deformation under the external load. The work along this so called *virtual displacement* may then be calculated. By reintroducing a reaction force at the support which undoes the virtual displacement and pushes the node back to its original position, it is possible to calculate the reaction force.
Unfortunately, it is necessary to know in which way the system will be deformed in

order to calculate the displacement and work of the external force along this displacement. For simple beam systems, this is rather easy, however, the more complex a system becomes the more complicated the solution gets. As we are dealing with too many uncertainties regarding the exact geometry and stiffness of the system, calculating the forces this way would be rather complicated and not lead to desirable results.

2.4.3.2. Direct Stiffness Method

The direct stiffness method is the basis for most modern Finite Element Analysis (FEA) applications. It uses a matrix based approach which is fast and uses less memory than other methods to calculate the forces acting inside a truss like structure. By coupling nodes and their translation due to external forces using a stiffness matrix, the acting forces in the system can be calculated. [23]–[25]
Of course it would also be possible to use any FEM-program to do a FEA and calculate the reaction forces this way. However, transferring the coordinates to a FEM-program, creating the mesh, applying the correct material properties and so forth, requires a translation program which transfers the MATLAB values into ones that are logical to the FEM-program. This is no simple task if it shall be automated and would go beyond the scope of this thesis. The cost-benefit ratio of creating this translation makes it not worth the time it would take to create it and work out all of the possible bugs. Therefore, this is not a justified solution for this particular case. Even still, by breaking the FEA down into its most basic components, it is possible to create a simple calculation using the direct stiffness method.
In a first step, the system has to be simplified into a truss structure consisting of nodes and connecting beams. An example of a simplified lander system with all of the struts can be seen in a trimetric representation in figure 2.10. Figures 2.11 and 2.12 show additional view directions. Here, the struts that actually exist, i.e. the legs of the system, are depicted in different shades of red while the additional struts that connect the legs, and act as the mechanical support the lander body would usually give to the system, are depicted in shades of grey. In the front, one of the legs is shown in fully saturated colours. It is clearly visible that each leg of the lander has a total of four red leg-struts and six struts connecting the interfaces with each other and the CoG. Additionally, one strut is used to connect each 'corner' of the lander with the one next to it.

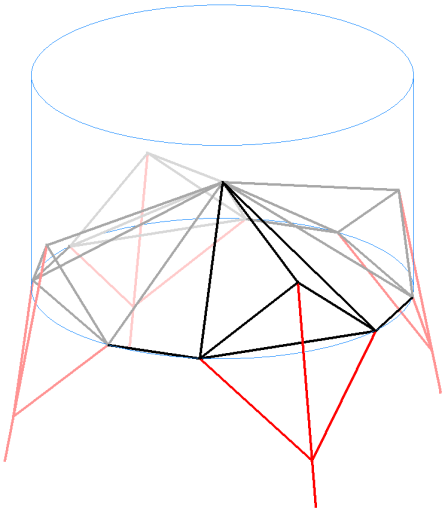

Fig. 2.10.: Trimetric view of the truss structure of a four legged lander

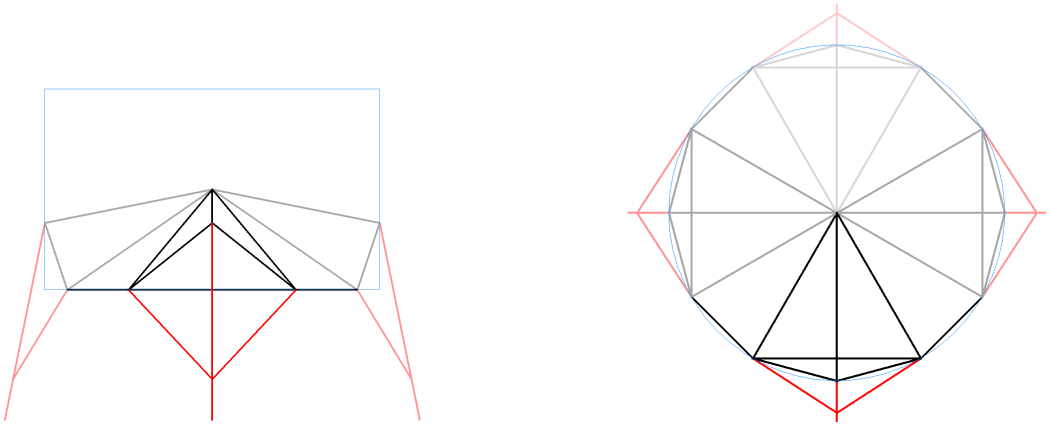

(a) Side view **(b)** Top view

Fig. 2.11.: Truss structure of a four legged lander in 1-2-1 configuration

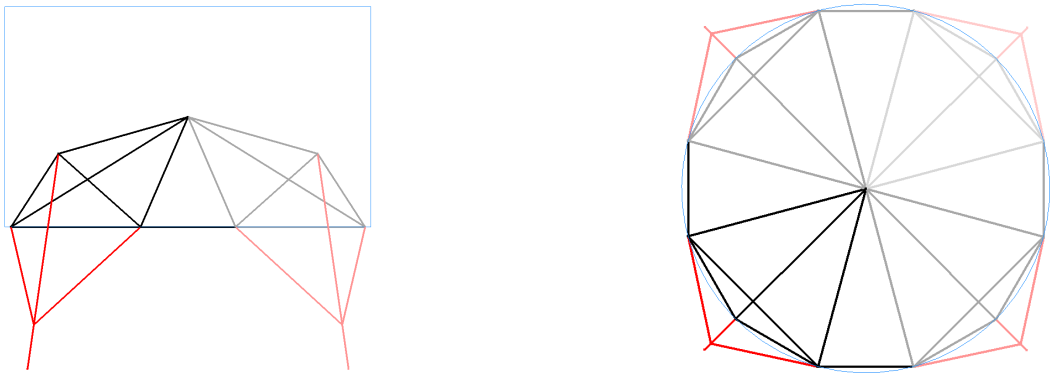

(a) Side view **(b)** Top view

Fig. 2.12.: Truss structure of a four legged lander in 2-2 configuration

Each of these beams has a total of twelve degrees of freedom in three-dimensional space. Two ends with three translational and three rotational DOF each. The local coordinate-system for each of the struts has its x_1-axis in the direction of the beam. As we assume rotationally symmetric beams, the exact direction of the x_2- and x_3-axis is not important as long as they are orthogonal to the beam direction and each other. The free body forces are assumed to be positive in the axis directions. [23][24]
Once all of the nodes and beams are defined, the displacements and stress resultants at the end nodes of each beam can be connected with one another [23][24]. This has to be done for each of the beams and is here explained exemplary for one beam element b connecting the nodes j and k.

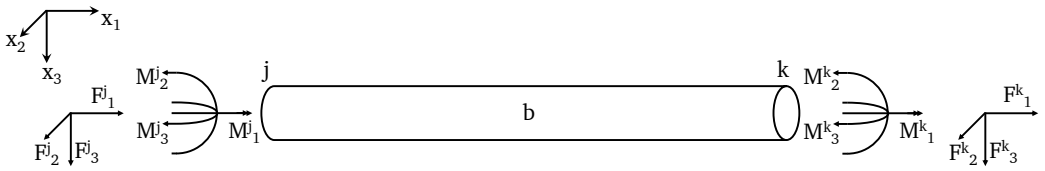

Fig. 2.13.: Beam element with complete stress resultants in three-dimensional space (adapted from [24])

The resulting forces at the ends j and k of the beam b, which can be seen in figure 2.13, are combined into a stiffness relation s^b. This vector is the result of multiplying the stiffness matrix k^b of the beam with its displacement u^b, which can be seen in equation 2.11:

$$s^b = \begin{pmatrix} F_1^j \\ F_2^j \\ F_3^j \\ M_1^j \\ M_2^j \\ M_3^j \\ F_1^k \\ F_2^k \\ F_3^k \\ M_1^k \\ M_2^k \\ M_3^k \end{pmatrix} = k^b \begin{pmatrix} u_1^j \\ u_2^j \\ u_3^j \\ \varphi_1^j \\ \varphi_2^j \\ \varphi_3^j \\ u_1^k \\ u_2^k \\ u_3^k \\ \varphi_1^k \\ \varphi_2^k \\ \varphi_3^k \end{pmatrix} = k^b u^b \tag{2.11}$$

where:

$$k^b = \begin{bmatrix} \frac{EA}{L} & 0 & 0 & 0 & 0 & 0 & \frac{-EA}{L} & 0 & 0 & 0 & 0 & 0 \\ & \frac{12EI_{33}}{L^3} & 0 & 0 & 0 & \frac{6EI_{33}}{L^2} & 0 & \frac{-12EI_{33}}{L^3} & 0 & 0 & 0 & \frac{6EI_{33}}{L^2} \\ & & \frac{12EI_{22}}{L^3} & 0 & \frac{-6EI_{22}}{L^2} & 0 & 0 & 0 & \frac{-12EI_{22}}{L^3} & 0 & \frac{-6EI_{22}}{L^2} & 0 \\ & & & \frac{GI_{11}}{L} & 0 & 0 & 0 & 0 & 0 & \frac{-GI_{11}}{L} & 0 & 0 \\ & & & & \frac{4EI_{22}}{L} & 0 & 0 & 0 & \frac{6EI_{22}}{L^2} & 0 & \frac{2EI_{22}}{L} & 0 \\ & & & & & \frac{4EI_{33}}{L} & 0 & \frac{-6EI_{33}}{L^2} & 0 & 0 & 0 & \frac{2EI_{33}}{L} \\ & & & & & & \frac{EA}{L} & 0 & 0 & 0 & 0 & 0 \\ & & & & & & & \frac{12EI_{33}}{L^3} & 0 & 0 & 0 & \frac{-6EI_{33}}{L^2} \\ & & & & sym. & & & & \frac{12EI_{22}}{L^3} & 0 & \frac{6EI_{22}}{L^2} & 0 \\ & & & & & & & & & \frac{GI_{11}}{L} & 0 & 0 \\ & & & & & & & & & & \frac{4EI_{22}}{L} & 0 \\ & & & & & & & & & & & \frac{4EI_{33}}{L} \end{bmatrix} \tag{2.12}$$

These local vectors and matrices have to be transformed into a global-coordinate-system in order to calculate the stiffness matrix for the whole system. By using rotation matrices as those in equation 2.4, the local stiffness matrices are rotated into the global-coordinate-system. Because the system contains a total of four three-dimensional vectors (two force vectors and two torque vectors, one for each end of the beam), a large 12x12 rotation matrix C has to be constructed from the small 3x3 rotation matrix R following the pattern shown in equation 2.13. Transformation from global to local coordinates can be done by premultiplying the C-matrix with the global coordinates. Reversing this operation requires using the transposed rotation matrix C^T. [23][24]

$$C = \begin{bmatrix} R & 0 & 0 & 0 \\ 0 & R & 0 & 0 \\ 0 & 0 & R & 0 \\ 0 & 0 & 0 & R \end{bmatrix} \tag{2.13}$$

Transformation of the local stiffness matrix to the global one follows the scheme shown in equation 2.14, which is based on equation 2.11 as well as the transformation logic described in the last paragraph.

$$k^b_{glob} = \frac{s^b_{glob}}{u^b_{glob}} = \frac{C^T s^b_{lcl}}{u^b_{glob}} = \frac{C^T k^b_{lcl} u^b_{lcl}}{u^b_{glob}} = \frac{C^T k^b_{lcl} C u^b_{glob}}{u^b_{glob}} = C^T k^b_{lcl} C \tag{2.14}$$

Once all global stiffness relations have been computed, they are combined into an overall stiffness relation $S = KU$ for the entire lander truss system as shown in figure 2.10. This is done by splitting the matrix and vectors of each strut as depicted in equation 2.15 and sorting their parts into the system stiffness relation. For each node, the degrees of freedom are defined in the U vector while the forces and torques are defined in the S vector. External forces can now be inserted into the correct positions of the S vector. By setting the movement of the bearing nodes in the U vector to 0, according to the boundary conditions of the system, rigid-body

movement is blocked and the system is defined. If this part is neglected, the system becomes singular and therefore unsolvable. [23][24]

$$\begin{pmatrix} s_j^b \\ s_k^b \end{pmatrix} = \left[\begin{array}{c|c} k_{jj}^b & k_{jk}^b \\ \hline k_{kj}^b & k_{kk}^b \end{array}\right] \begin{pmatrix} u_j^b \\ u_k^b \end{pmatrix} \tag{2.15}$$

Sorting the four sub-matrices of the global element stiffness matrix k_{glob} of each strut into K it follows that:

$$K = \begin{bmatrix} \sum_{i=1}^{n} k_{11}^i & \cdots & \sum_{i=1}^{n} k_{1m}^i \\ \vdots & \ddots & \vdots \\ \sum_{i=1}^{n} k_{m1}^i & \cdots & \sum_{i=1}^{n} k_{mm}^i \end{bmatrix} \tag{2.16}$$

where:

n = number of struts
m = number of nodes

After the external forces, boundary conditions, and stiffness matrices are sorted into their corresponding space, the equation system can be solved. It should be noted that solving the equation system is done in two steps:

1. First all rows as well as their corresponding columns in the K matrix in which the U vector has a 0 are erased and this reduced system is solved.
2. In a second step, the solution of the reduced system is reintroduced into the entire system, which can then be solved as a whole and yields the reaction forces of the bearing nodes as a result.

In order to get the forces in the beam elements, the displacements of the nodes bordering the element have to be rotated back into the local coordinate-system. By using equation 2.11, the forces in the element may be calculated. [23][24]
The entire concept is also shown for an easy example in figure 2.14.

2.4.4 Chosen approach

As the results of calculations using an analytical approach lack accuracy, the principle of virtual work requires better knowledge of displacement that happens under load and the full FEA would go beyond the scope of this thesis, the direct stiffness method will be used for calculating the forces acting on the nodes of the lander. It works for

landers with as many or as few legs as needed, can be automated, and allows for easy adaptation of the properties of the system, e.g. regarding boundary conditions. It is very accurate for small displacements, offers the ability to individually change the mechanical properties of each of the struts easily, and also includes effects of bending of the struts. Doing this also allows to include effects like the mechanical compliance of the dampening elements in the struts as well as of the interaction between the footpads and the Lunar regolith. All of this, combined with a great cost-benefit-ration of implementation of this method, makes it the perfect candidate for this thesis.
The method was verified using an FEA with MSC Patran as pre/post-processor and MSC Nastran as solver. Additional information on the validation can be found in section 3.5.

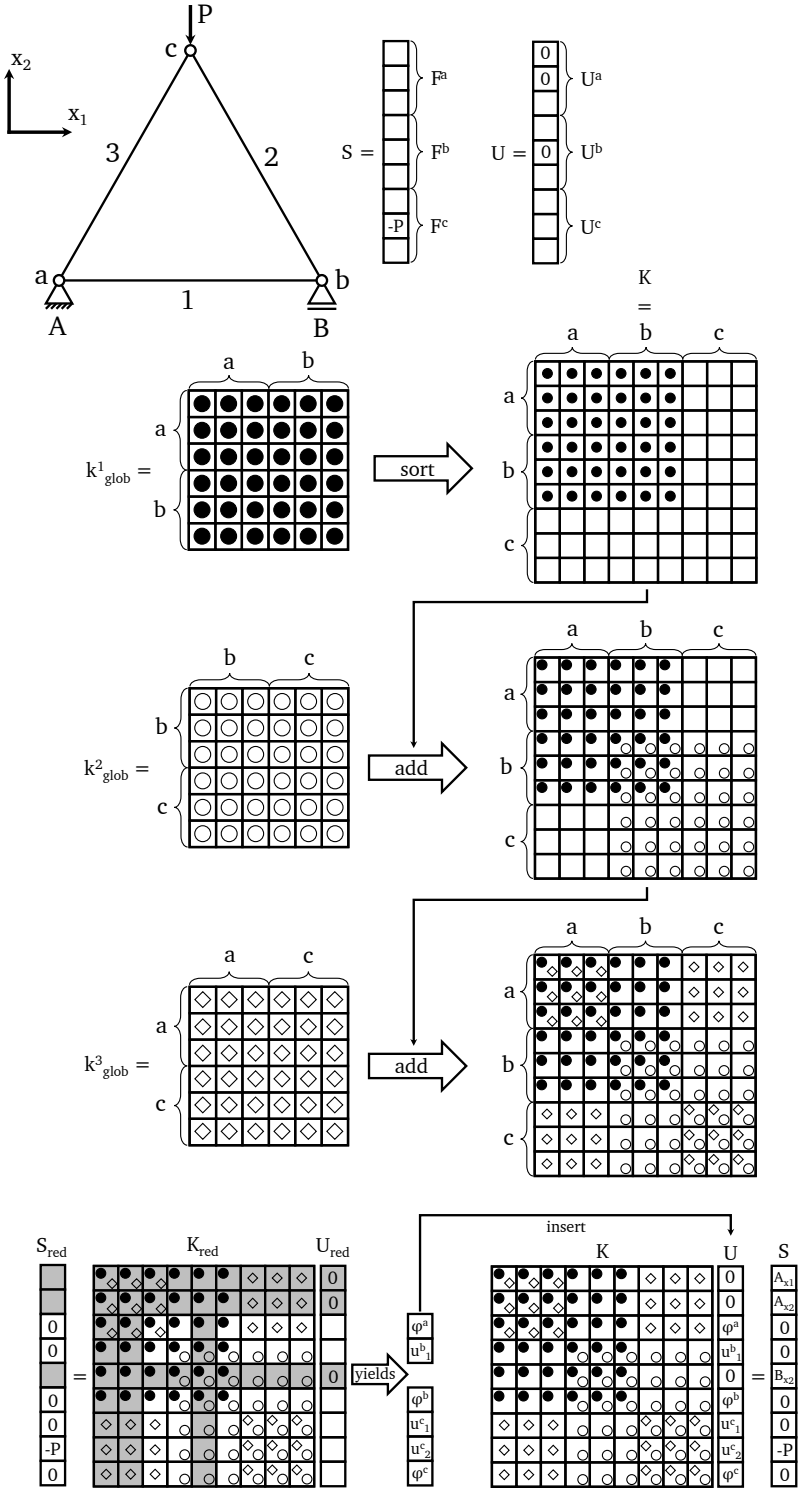

Fig. 2.14.: Construction of the system stiffness matrix K and calculation of reaction forces (adapted from [24])

3 Numerical Implementation and Operation

> *If at first you don't succeed, call it version 1.0*
>
> **— proverb**
> (exact origin unknown)

Solving the equations introduced in chapter 2 is not possible in an analytical way. A numerical solution is therefore required. The implementation of the numerical model uses in this thesis the scientific computing language MATLAB [26] resulting in an executable script, which went through a multitude of iterations, each with different approaches and stages of completeness. The only one of real importance for this documentation, however, is the last version which is used for the calculations in this thesis. In order for all readers to be able to use it, a short explanation on how to operate the main program and the multiple subfunctions as well as how to interpret the results will follow here. This chapter only serves as a general overview and an exact explanation of each line of code will be skipped as the basic mathematics have already been explained in chapter 2.

3.1 Running the script

The main program is the heart of the script. It is used to start the calculation and calls all subfunctions. For the most part, it guides the user through the process of the calculation by asking what kind of data input is desired. It is possible to choose between four different options:

1. A standard input set (lander on ground with a small slope is aligned and lowered a bit) the main purpose of which is showing how the results of the calculation are presented to the user (figure 2.7 shows a similar example).
2. Generating a "random" set of input variables for testing many different possible combination without the bias of manually chosen values. In this mode it is

possible to define the number of legs the lander shall have as well as the type of leg kinematics it shall have (Cantilever or Inverted Tripod). The slope of the ground is set randomly to a value of up to 15° with a random direction. The lengths of the legs primary struts are based on a standard input set but randomly vary by up to 0.1 m in order to simulate different amounts of crushing of the honeycomb dampeners. This mode is especially helpful for testing new parts of the calculation as it can quickly produce a working set of input variables and was mainly developed for debugging the code.

3. Reading in variables from a spreadsheet input file. This is probably the most useful mode for most situations as it allows the user to easily define the characteristics of the lander including dimensions, mass, and lengths of leg struts as well as some parameters of the calculation like the ground clearance or the number of intermediate steps between the tilted landing position and the final aligned and levelled position the program shall calculate. An overview output of the data also happens via a spreadsheet in order to get a quick understanding of the characteristics of a specific lander configuration without having to take a deep look into the raw data. How this works exactly is explained in section 3.2

3.2 Input of calculation parameters via a spreadsheet

As already mentioned, probably the most useful mode of operation is using the possibility to read in the contents of an input-file. This data input is handled by a spreadsheet, which in this thesis used MS Excel [27]. A template is set up where the user may choose all input values the calculation needs in order to properly function. It should be noted that it is still possible to choose values that might not work in a logical sense, e.g. by making the primary strut only a few centimetres in length or placing the CoG outside the perimeter of the lander itself.
Input parameters are split roughly into categories each of which will get a short explanation here. Figure 3.1 also shows an example of how a filled-in input file might look.

Lander Geometry, Mass, and Orientation Here, the user can specify physical properties of the lander as a whole. This includes the radius, height, and mass of the lander body as well as the number of landing legs it shall have. The number of legs is here limited to the range between three and six. Three legs is the absolute minimum

for a stable lander and even though the script can theoretically calculate as many legs as wanted, a limit was set to six as this keeps the spreadsheet less cluttered and most landers will not exceed this number of landing legs anyway. Additionally, roll and pitch (measured as explained in section 2.2.2.2) are defined in this section as well. Based on these angles, a first estimate of the ground angle is calculated and shown to the user. This makes choosing realistic angles for pitch and roll easier.

General Coordinates of Leg Interfaces and CoG The coordinates of the interfaces as defined in the body-coordinate-system (see also section 2.2.2.1) can be defined in this part. They are only defined for leg 1, as rotational symmetry of the lander is assumed and the other interface coordinates will be calculated based on the number of legs the lander shall have (as defined in the *Lander Geometry, Mass, and Orientation* part). The coordinates of the CoG are calculated automatically based on the landers height but can be changed if necessary.

Calculation Parameters The calculation parameters consist of two variables. The first is the number of calculation steps the script will do. Note that, when choosing five steps for example, step 0 will be the lander without any levelling or alignment operation while step 5 will be the lander in its fully levelled and aligned state, meaning that four in-between steps and a total of six lander states are calculated. The ground clearance specifies the closest distance of the lander body to the ground that shall be achieved during the levelling procedure. Setting this value to 0 for example would lead to the lander body touching the ground in the fully levelled state.

Strut Lengths The strut lengths are defined in this section. Usually, it is enough to define the lengths of each strut for leg 1 while the other legs will automatically be the same. If, for any reason, different legs shall have different lengths, they can of course be changed. The upper segment of the primary strut refers to the distance between the IF1 and the attachment point of the secondary struts. The lower segment is the distance below this attachment point to the footpad. These two values must (!) add up to the length of the primary strut.

Mechanical Properties of Struts The mechanical properties are used for the calculation of the forces acting on the lander and its legs under different misalignments. Most of these parameters are calculated based on the assumption of the struts being made up of solid tubes, which is why only four values have to be entered, while

the others are calculated based on these entries. Additionally, a standard input set is already present even in the empty version of the input spreadsheet, which makes the struts very stiff and only allows for little bending. All of the values can still be changed, although at own risk. One value one might want to change is the stiffness of the primary and secondary strut in axis direction. The reason for this is that this stiffness is mainly defined by the stiffness of the honeycomb cartridges (or other dampening systems that might be used) in the primary strut and the bending rods many secondary struts incorporate in their design. The material stiffness and geometric properties of a simple tube would therefore not represent the reality. It is advised not to change the stiffness of the structural struts as this might lead to unwanted deformation of the lander body.

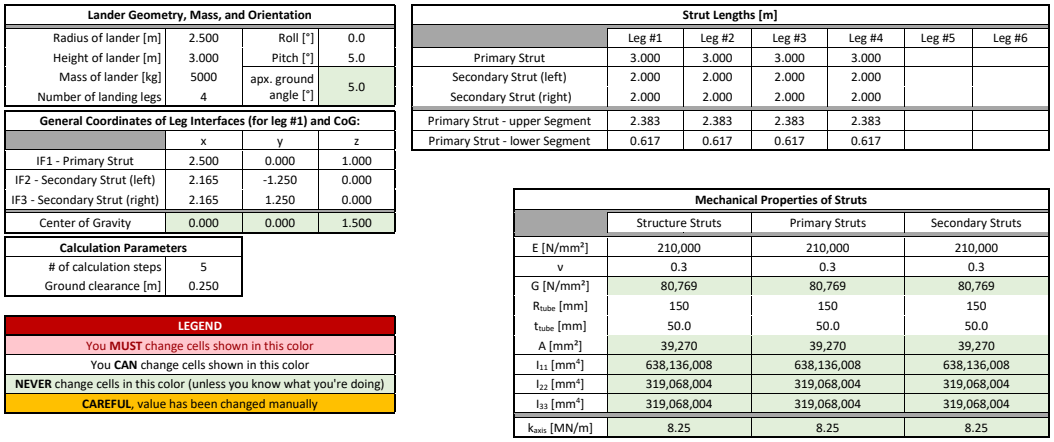

Lander Geometry, Mass, and Orientation			
Radius of lander [m]	2.500	Roll [°]	0.0
Height of lander [m]	3.000	Pitch [°]	5.0
Mass of lander [kg]	5000	apx. ground angle [°]	5.0
Number of landing legs	4		

General Coordinates of Leg Interfaces (for leg #1) and CoG:			
	x	y	z
IF1 - Primary Strut	2.500	0.000	1.000
IF2 - Secondary Strut (left)	2.165	-1.250	0.000
IF3 - Secondary Strut (right)	2.165	1.250	0.000
Center of Gravity	0.000	0.000	1.500

Calculation Parameters	
# of calculation steps	5
Ground clearance [m]	0.250

LEGEND
You **MUST** change cells shown in this color
You **CAN** change cells shown in this color
NEVER change cells in this color (unless you know what you're doing)
CAREFUL, value has been changed manually

Strut Lengths [m]						
	Leg #1	Leg #2	Leg #3	Leg #4	Leg #5	Leg #6
Primary Strut	3.000	3.000	3.000	3.000		
Secondary Strut (left)	2.000	2.000	2.000	2.000		
Secondary Strut (right)	2.000	2.000	2.000	2.000		
Primary Strut - upper Segment	2.383	2.383	2.383	2.383		
Primary Strut - lower Segment	0.617	0.617	0.617	0.617		

Mechanical Properties of Struts			
	Structure Struts	Primary Struts	Secondary Struts
E [N/mm²]	210,000	210,000	210,000
ν	0.3	0.3	0.3
G [N/mm²]	80,769	80,769	80,769
R_{tube} [mm]	150	150	150
t_{tube} [mm]	50.0	50.0	50.0
A [mm²]	39,270	39,270	39,270
I_{11} [mm⁴]	638,136,008	638,136,008	638,136,008
I_{22} [mm⁴]	319,068,004	319,068,004	319,068,004
I_{33} [mm⁴]	319,068,004	319,068,004	319,068,004
k_{axis} [MN/m]	8.25	8.25	8.25

Fig. 3.1.: Example of an MS Excel input spreadsheet for the MATLAB calculation

3.3 Processing

Once the input parameters of the calculation have been set, the code processing begins automatically. The equations explained in chapter 2 are utilised in a specific sequence to calculate the motion of and forces acting upon the lander.
There is a multitude of possible types of graphical code representation. The most common, however, are probably the so called *Nassi-Shneiderman diagram* and the *flowchart*. Here, the flowchart will be used to explain the code in a graphical way. It should be mentioned that only the sections relevant to understanding how the code works in general are going to be explained here. Other miscellaneous code parts (e.g. plotting of graphs or saving the output data) are left out on purpose in order to make understanding the core of the code easier. Additionally, for the most part no

equations will be explained here as all the basic equations used have already been explained in chapter 2.

3.3.1 Program overview

The flowchart shown in figure 3.2 includes all basic operations done by the program during operation in condensed form. It is necessary to explain parts of this flowchart in more detail, however, the general workflow can be understood well with this first depiction. Changes of a counter are depicted in green while decision blocks are depicted as a diamond shape and in yellow. The area encompassed by the dashed red line in the geometry calculation works slightly different depending on the state counter and is simplified here. This will be explained further in section 3.3.2.

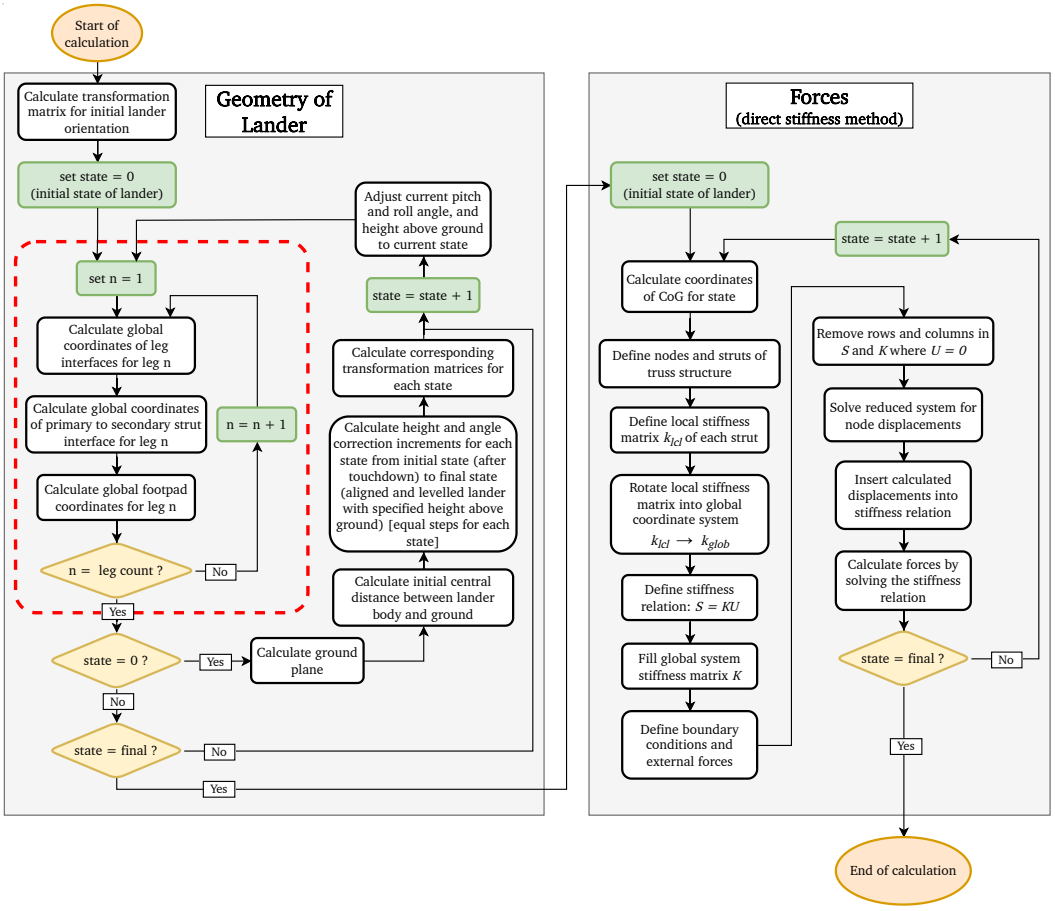

Fig. 3.2.: Overview flowchart of the script

3.3.2 Geometry computation

The first operation after starting the calculation is the computation of the initial transformation matrix for the position of the lander after touchdown. This initial state is set to *state 0* after which the coordinates of each point of the legs (interfaces to lander, intersection between primary and secondary strut, and footpad) are calculated for each leg. The intersection point and the footpad coordinates, however, require a slightly more difficult approach than simply rotating the coordinates based on the transformation matrix. The reason for this is that they are calculated based on the lengths of the struts, i.e. a technique similar to the operation of geopositioning satellites has to be utilised. The coordinates of the interfaces to the lander are set as anchor points with their known distance to the intersection between the struts as has already been explained graphically in section 2.3.2. As there are rounding errors and inaccuracies in the exact lengths of the struts and coordinates of the anchors, there might not be one exact intersection that can be calculated analytically.
However, by searching for local minima of a cost function f_{cost} based on a first guess of a point P, it is possible to calculate the position of the intersection between the struts iteratively. The cost function serves as a geometrical constraint function making sure only geometrically possible solutions are found. In the present case, the difference between the distance of a guessed position to the interfaces and the actual distance, based on the strut lengths, shall be minimized. To increase the accuracy, this difference is then squared and summed up for each of the interfaces. By varying the guess of P and iterating, a solution for a minimum of f_{cost} can be found.

$$f_{cost}(P) = \sum_{i=1}^{n} \left(\begin{vmatrix} \overrightarrow{IF1\,P} \\ \overrightarrow{IF2\,P} \\ \overrightarrow{IF3\,P} \end{vmatrix} - \begin{matrix} r_1 \\ r_2 \\ r_3 \end{matrix} \right)^{\circ 2 \text{ (denotes element wise squaring)}} \tag{3.1}$$

Even for inaccurate measurements, this method finds the coordinates of P for a local minimum, which is where the interface position $IF_{PS,SS}$ should be, provided the guess is close enough to the actual coordinates. Naturally, the calculation has to be repeated for each leg individually.
For the implementation into the script, optimisation techniques like the Nelder-Mead method have to be used. The *fminsearch*-function in MATLAB (a multidimensional unconstrained non-linear minimisation) can be applied for this purpose. By providing a guess and minimising the distance to the exact intersection through multiple iterations of the cost function 3.1, it is possible to get a result for the intersection. Figure 3.3 shows an representative example of the convergence of the *fminsearch*-function for the computation of the intersection coordinates. As can be seen, the

function converges very quickly early on and ends up at a function value of approximately 1e-10 after 77 iterations. Using vector addition afterwards, it is possible to calculate the footpad coordinates.

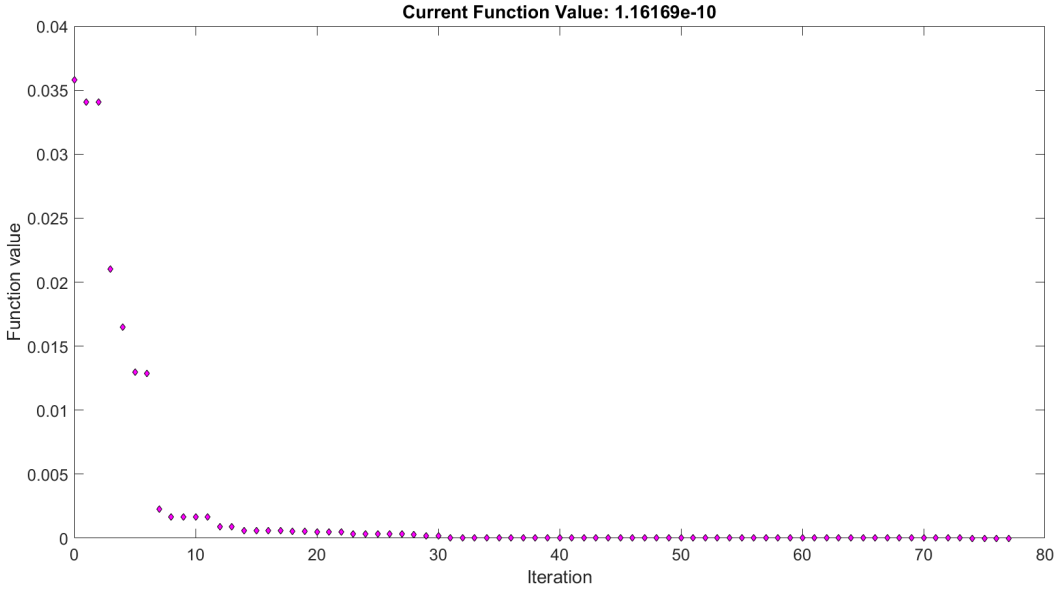

Fig. 3.3.: Exemplary convergence of the *fminsearch*-function

Once all of these initial points have been calculated, the initial ground plane is calculated from the footpad positions of the first three legs (each additional foot is assumed to also be on this plane). After calculating the distance between lander and ground plane, the difference between this height and the desired final height is divided into as many equal steps as defined during the input. The same is true for the pitch and roll angles which are also split into equal parts between the initial and the final (levelled) orientation. Based on the height and tilt angles of the lander for each state, the corresponding transformation matrices are computed.
The state counter is increased by 1 and the pitch and roll angle as well as the height above ground are adjusted based on the corresponding transformation matrix. The coordinates for all leg points are then calculated again, however, this time around it is necessary to use a slightly more advanced approach. As the position of IF1 for each of the legs has to be adapted to meet the boundary conditions set by the ground plane and the lander body position, additional iterations have to be made. Figure 3.4 shows the corresponding section encompassed by the red dashed line in more detail which was shown in a simplified version in figure 3.2. If in the first check of the state the answer whether the current state is state 0 is *No*, the coordinates for interfaces 2 and 3 are calculated as before by simply using the transformation matrix for the corresponding state. The vertical position of IF1 on the lander is then adapted slightly in order to change the geometry of the leg. Afterwards, the intersection and

the footpad coordinates are calculated as before using the positioning technique and the *fminsearch*-function. However, in every state other than state 0, the ground plane is set and can not be changed. Because of this, the footpad coordinates of this first iteration will most likely not correspond with a point on the ground plane. If the distance between the footpad and the ground exceeds 0.1 mm, the vertical position of IF1 is adapted again and a new coordinate calculation is made. Once the difference is smaller than a tenth of a millimetre, the coordinates are kept and the next leg is calculated until all legs are done. This way, it is possible to guarantee all legs stand solidly on the ground for each lander state and the position of all primary interfaces is correct for the orientation and height of the lander at each state. By calculating a large number of points it is possible to make the changes of angle and height arbitrarily small and therefore calculate the speed at which each of the legs interfaces have to move.

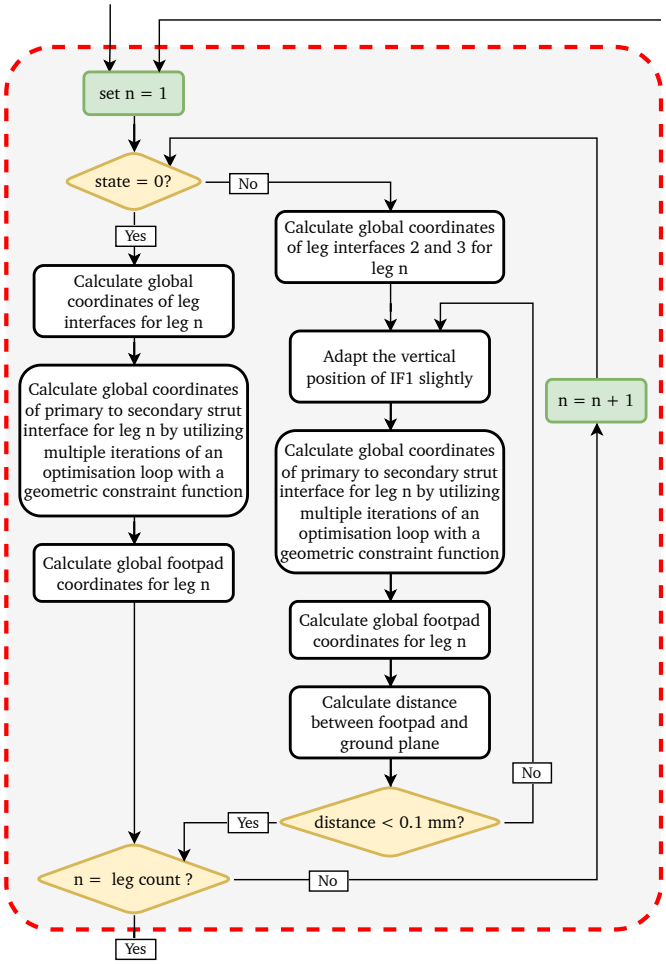

Fig. 3.4.: More detailed flowchart of the calculation of the interface coordinates of the lander

3.3.3 Force computation

The force computation is done using the direct stiffness method as explained in section 2.4.3.2. After calculating the coordinates of the centre of gravity for the current state, the nodes and struts of the lander are generated automatically based on the coordinates from the geometry calculation. For each strut, a local stiffness matrix k_{lcl} is defined including the geometric and material properties of each strut. The local stiffness matrices are then rotated into the global-coordinate-system using the known orientation of each strut. After defining the global stiffness relation $S = KU$, the parts of this relation can be filled with values. The global system stiffness matrix K is filled with the values of the global strut stiffness matrices k_{glob} of the single struts, while the boundary conditions and external forces are inserted into the U and S vectors, respectively. After temporarily removing the rows and columns from S and K that correspond to a 0 in the U vector and solving the reduced system, the calculated displacements are then inserted into the U vector. At this point, the system stiffness relation can be solved for the forces in the system. This operation is repeated for each state of the lander until the static forces for all the lander orientations are known.

3.4 Output of calculation results

After processing the inputs, the output of the calculation results is saved in multiple different ways. First, the MATLAB workspace is saved with all variables as a .mat-file for later use if needed. Additionally, some values are saved in an MS Excel spreadsheet to get a quick overview of the most important results of the calculation without needing to look through all of the generated data. This output spreadsheet looks very similar to the input spreadsheet with the difference of the mechanical properties of the struts section being replaced with some results of the calculation. First, there is the movement distance of IF1. Here, the distance each of the primary interfaces has to travel up or down is listed. It is possible to deduct the length of the linear actuator needed for movement from this. Below that, the maximum calculated forces on the footpads during levelling and alignment are split into normal force on the ground and downhill force in the direction of the ground slope (negative values here mean the force pushes more in the uphill direction which is only possible as the translational movement direction is locked for the lander, while it would most likely settle by sliding a bit downhill in reality). Additionally, the absolute friction on the ground disregarding direction is listed here as well. Going down

further, the maximum forces on the primary interface for each of the landing legs are listed in the body-coordinate-system (for explanation of this coordinate-system see section 2.2.2.1). These values may be used to choose an actuator as these maximum values are the forces the actuator has to overcome during levelling and alignment. It should be noted that it is assumed that only the force in the z-direction is transferred onto the actuator while any sideways force is transferred onto an additional guide rail. Figure 3.5 shows exemplary results for the input parameters from figure 3.1.

Date	Time
03.05.2023	11:23:05

Lander Geometry, Mass, and Orientation			
Radius of Lander [m]	2.500	Roll [°]	0.0
Height of Lander [m]	3.000	Pitch [°]	5.0
Mass of Lander [kg]	5000	ground angle [°]	5.0
Number of landing legs	4		

General Coordinates of Leg Interfaces (for leg #1) and CoG:			
	x	y	z
IF1 - Primary Strut	2.500	0.000	1.000
IF2 - Secondary Strut (left)	2.165	-1.250	0.000
IF3 - Secondary Strut (right)	2.165	1.250	0.000
Center of Gravity	0.000	0.000	1.500

Calculation Parameters	
# of calculation steps	5
Ground Clearance [m]	0.250

Mechanical Properties of Struts (for reference)			
	Structure	PS	SS
E [N/mm²]	210,000	210,000	210,000
v	0.3	0.3	0.3
G [N/mm²]	80,769	80,769	80,769
R_{tube} [mm]	150	150	150
t_{tube} [mm]	50.0	50.0	50.0
A [mm²]	39,270	39,270	39,270
I_{11} [mm⁴]	638,136,008	638,136,008	638,136,008
I_{22} [mm⁴]	319,068,004	319,068,004	319,068,004
I_{33} [mm⁴]	319,068,004	319,068,004	319,068,004
k_{axis} [MN/m]	8.25	8.25	8.25

Strut Lengths [m]						
	Leg #1	Leg #2	Leg #3	Leg #4	Leg #5	Leg #6
IF1 - Primary Strut	3.000	3.000	3.000	3.000		
IF2 - Secondary Strut (left)	2.000	2.000	2.000	2.000		
IF3 - Secondary Strut (right)	2.000	2.000	2.000	2.000		
Primary Strut - upper Segment	2.383	2.383	2.383	2.383		
Primary Strut - lower Segment	0.617	0.617	0.617	0.617		

Movement of IF1 [m]						
0.772	1.104	1.492	1.104			

maximum absolute Forces on Footpads [N]						
Normal Force on Ground	2417	2029	2031	2029		
Downhill Force on Ground	1856	159	-1375	158		
Absolute Friction on Ground	1856	1654	1375	1654		

maximum absolute Forces on IF1 (in body coordinate-system) [N]						
x	-1083	22	1037	22		
y	0	-1110	0	1110		
z	1874	1849	1814	1849		

Fig. 3.5.: Example of an MS Excel output spreadsheet for the MATLAB calculation

The output figures are a visual representation of the lander geometry in each calculation step (state), multiple of which can be seen in figure 2.7. Here, the user is able to check the state of travel of the lander during alignment and levelling. Parameters like ground interference (which theoretically should be impossible due to how the program is written) or whether the movement of IF1 goes beyond the height limits of the lander are the ones to look out for in these figures. Other than that they can be used to illustrate the movement.
Additionally, multiple force diagrams are generated. These include the forces on each of the footpads in normal and downhill direction as well as the total friction on the footpads and the forces acting on IF1, all of which are automatically saved alongside the MS Excel spreadsheets. The most interesting of these are by far the forces on IF1 as these dictate the design of the movement mechanism. Examples of these diagrams can be found in figure 4.3 and 4.5.

3.5 Validation of force computation

It is necessary to validate the results obtained through the direct stiffness method to make sure the results are correct within a small error margin. This is done by comparing the results achieved by the direct stiffness method in MATLAB with the results from an FEA program. Patran and MSC Nastran were utilised as pre/post-processor and solver, respectively [28]. The struts were implemented as one-dimensional beam elements, allowing for bending. Comparisons were made for multiple different slope angles up to 15° for the lander parameters as shown in figure 3.1 in section 3.2. The results for 0° and 15° pitch will be used as representative examples, however, multiple in-between values as well as roll angles, and combinations of roll and pitch have been tested as well. Above 15° no guarantee for accurate results can be given based on this validation.

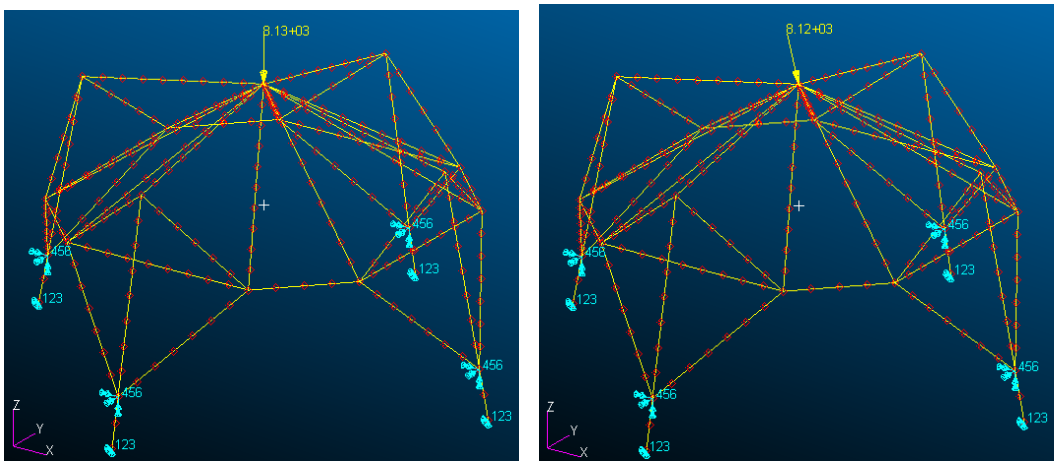

(a) level ground without slope **(b)** ground slope of 15°

Fig. 3.6.: Visual representation of lander in Patran

3.5.1 Validation - level ground

On a level ground, the largest difference between direct stiffness method (DSM) and the Patran/Nastran analysis has a magnitude of 8.1 N. This corresponds to a relative difference of approximately 1.2%, well inside the acceptable relative deviation. Most of the values are even exactly the same or differ only by about 0.1 N.
A visual representation of the lander in Patran can be seen in figure 3.6a and the full result comparison in table 3.1.

Tab. 3.1.: Comparison of results for force on the footpads in the inertial body-coordinate-system on a level ground without slope

0° pitch / 0° roll			leg 1	leg 2	leg 3	leg 4
x	DSM		-656.3 N	0.0 N	656.3 N	0.0 N
	Patran/Nastran		-648.2 N	0.0 N	648.2 N	0.0 N
	difference	abs.	-8.1 N	0.0 N	8.1 N	0.0 N
		rel.	1.2%	N/A	1.2%	N/A
y	DSM		0.0 N	-656.3 N	0.0 N	656.3 N
	Patran/Nastran		0.0 N	-648.2 N	0.0 N	648.2 N
	difference	abs.	0.0 N	-8.1	0.0 N	8.1 N
		rel.	N/A	1.2%	N/A	1.2%
z	DSM		2031.2 N	2031.2 N	2031.3 N	2031.3 N
	Patran/Nastran		2031.3 N	2031.3 N	2031.3 N	2031.3 N
	difference	abs.	-0.1 N	-0.1 N	0.0 N	0.0 N
		rel.	0.0%	0.0%	0.0%	0.0%

3.5.2 Validation - 15° ground slope

On a ground with a slope of 15° in the direction of leg 1, the largest difference between DSM and the Patran/Nastran analysis has a magnitude of 17.4 N. It should be noted that in this case this corresponds to a relative difference of 41%, but the absolute difference is small enough to disregard this. Especially since the leg in this case is the one with the smallest load overall. Additionally, all other results differ only by a maximum of approximately 10 N or about 2%.
A visual representation of the lander in Patran can be seen in figure 3.6b and the full result comparison in table 3.2.

Tab. 3.2.: Comparison of results for force on the footpads in the inertial body-coordinate-system for a ground slope of 15° in the direction of leg 1

	15° pitch / 0° roll		**leg 1**	**leg 2**	**leg 3**	**leg 4**
x	DSM		-1225.7 N	-459.7 N	42.0 N	-459.5 N
	Patran/Nastran		-1227.6 N	-449.9 N	24.6 N	-449.9 N
	difference	abs.	1.9 N	-9.8 N	17.4 N	-9.6 N
		rel.	0.2%	2.2%	41.4%	2.1%
y	DSM		-0.3 N	-633.7 N	0.0 N	633.9 N
	Patran/Nastran		0.0 N	-626.1 N	0.0 N	626.1 N
	difference	abs.	-0.3 N	-7.6 N	0.0 N	7.8 N
		rel.	N/A	1.2%	N/A	1.2%
z	DSM		3130.0 N	1961.8 N	794.1 N	1962.2 N
	Patran/Nastran		3129.9 N	1962.0 N	794.2 N	1962.0 N
	difference	abs.	0.1 N	-0.2 N	-0.1 N	0.2 N
		rel.	0.0%	0.0%	0.0%	0.0%

4 Motion and Forces of an Exemplary Lunar Lander

> *May the Force be with you!*[a]
>
> **— George Lucas**
> American filmmaker

[a] Star Wars: Episode IV – A New Hope [Film], 1977, 1:40:50 - 1:40:55

To be able to determine expected loads and forces on the actuation system of the Lunar lander, it is necessary to specify its associated hardware dimensions in a first step. From these characteristics, it is possible to choose the necessary landing configurations that have to be analysed. The results of this analysis are the forces on the primary interfaces. These forces can then be used to choose components which fulfil the force requirements based on the calculation.

4.1 Lunar lander characteristics and parameters

The characteristics and parameters of the lander used for the further calculation are based on the size and mass limitations specified for the planned European Lunar lander by the ESA [3], the information given in [29], and the CAD model provided by the department for *Landing and Exploration Technologies* of the *DLR Institute of Space Systems*, which can be seen in figure 4.1.
The lander features a total of four legs with primary struts at a length of a bit under 2 m and secondary struts at a length of a bit under 1.5 m. Attachment of the secondary strut is very close to the footpad with an Inverted Tripod design of the legs. The mass of the lander is composed of 1600 kg structural mass and a payload of 1500 kg totalling 3100 kg. The CoG is placed right in the centre of the octagonal body of the lander, which features an outer diameter of 4.5 m and a height of 6 m. This is largest possible size as defined by the ESA [3]. On a given ground slope, the CoG is shifted further from the centre the higher it is situated in the lander body. As the position of the CoG is assumed to be in the centre of the body by choosing the

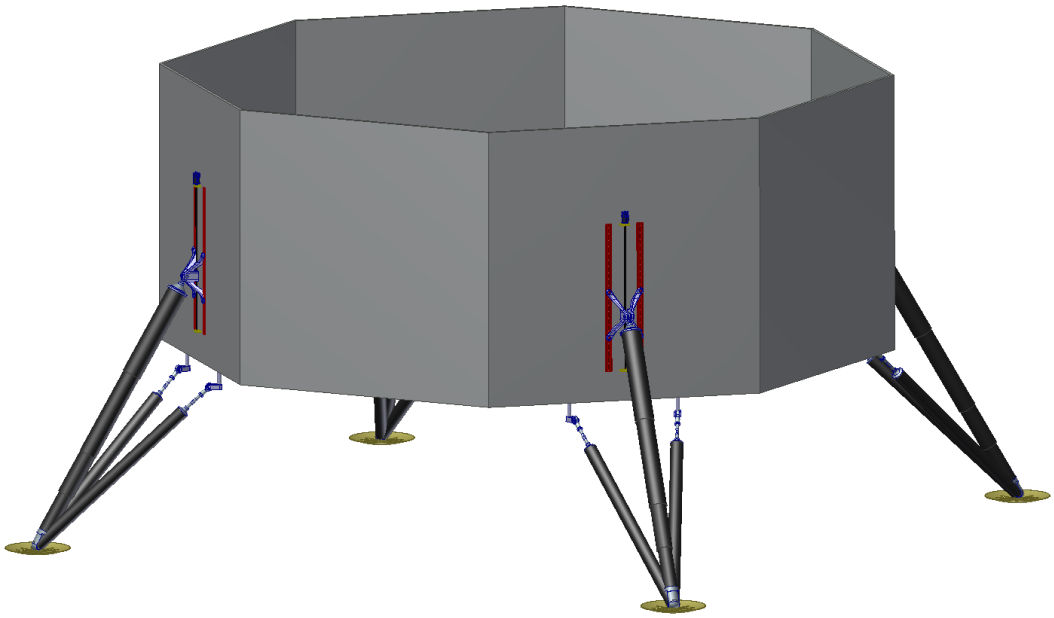

Fig. 4.1.: Original CAD model of the lander provided by the DLR

largest possible body size, the calculation will result in the highest loads. Having a CoG at a higher position than this would be unrealistic.
The minimal ground clearance is set to 0.25 m and the slope of the ground is to approximately 15°.
Material properties of the structural struts are set to represent a stiff steel tube in order to reduce effects of deformation and bending of the structure to which the legs are attached. This is necessary as the support structure is only a placeholder which connects the legs and the actual underlying structure that will be used is unknown at this point in time. The stiffness of the legs is also set to be represented by a steel tube. Even though CFRP (carbon fibre-reinforced plastic) is a far more likely choice to be used in an actual lander, for this first step this assumption is accurate enough. The material thickness is reduced, however, to allow for a bit more deformation of the structure under load. Additionally, the axial stiffness of the legs is set to represent the stiffness of the honeycomb crush elements for the primary strut and of the bending rod for the secondary strut. Values for these stiffnesses were taken from [14]. It should be noted that the material properties have a large influence onto the calculation results and for future optimisation, it is absolutely necessary to tweak these values carefully.
All important values are also listed in table 4.1. Figure 2.2 shows the dimensions of the lander and can be found in section 2.2.1.
The last important factor to take a look at is the configuration that will be considered for calculation. As we are dealing with a four legged lander, the most important

Tab. 4.1.: Parameters of exemplary Lunar lander

Symbol	Parameter	Value		
	Dimensions			
d_L	Lander diameter	4.500 m		
h_L	Lander height	6.000 m		
L_{S1}	Length of PS	1.925 m		
L_{S2}	Length of SS	1.440 m		
L_{S3}				
$L_{S1,seg1}$	Distance IF1 to SS attachment	1.875 m		
$L_{S1,seg2}$	Distance SS attachment to foot	0.050 m		
h_{CoG}	Height of CoG	3.000 m		
	Masses			
m_{struct}	Mass of structure	1600 kg		
$m_{P/L}$	Mass of payload	1500 kg		
m_{tot}	Total mass on the Moon	3100 kg		
	Ground slope			
α_{gnd}	Ground slope angle	15°		
	Properties of struts	**Structure**	**PS**	**SS**
E	Young's modulus	210 GPa	70 GPa	
ν	Poisson's ratio	0.3	0.2	
R_{tube}	Radius of tube	150 mm	60 mm	40 mm
t_{tube}	Wall thickness of tube	50 mm	5 mm	3 mm
	Alternative axial Stiffness			
$k_{axis,PS}$	PS axial stiffness	1.91 MN/m		
$k_{axis,SS}$	SS axial stiffness	0.35 MN/m		

configurations are the 1-2-1 configuration and the 2-2 configuration (illustrated in figure 2.9) which are the two extreme positions the lander can stand in. In the 1-2-1 configuration, one leg is positioned right in the direction of the ground slope with two parallel legs behind that and the last leg positioned opposed to the first one. A large share of the load is placed onto the downhill leg making this configuration the one with the highest load on a single leg. The 2-2 configuration is turned 45° from the 1-2-1 configuration, placing two parallel legs furthest down the slope and the other two opposed to them in the uphill direction. This configuration leads to the lowest load on a single leg, as the force is shared equally across the two downhill legs. Any rotational position between these two configuration can be considered as a combination of the two, i.e. when slowly turning from the 1-2-1 to the 2-2 configuration, the force on the downhill leg decreases as it is transitioned onto the second downhill leg. The results for force and movement distance of the primary strut interface will be used for the design of the kinematics in chapter 5.

4.2 1-2-1 configuration

In the 1-2-1 configuration, it is to be expected that the highest forces on a singular leg occur as the lander is leaning in the exact direction of that leg. As the alignment and levelling of the lander takes place, the force should slowly be shifted away from this leg onto the others.
The octagonal lander starts in the fully leaning position and ends up aligned horizontally and with the set clearance. Start and end state can be seen in figure 4.2. The input variables for this configuration were already shown in table 4.1, while the input spreadsheet can be found in the appendix in section A.1.1 in figure A.1.

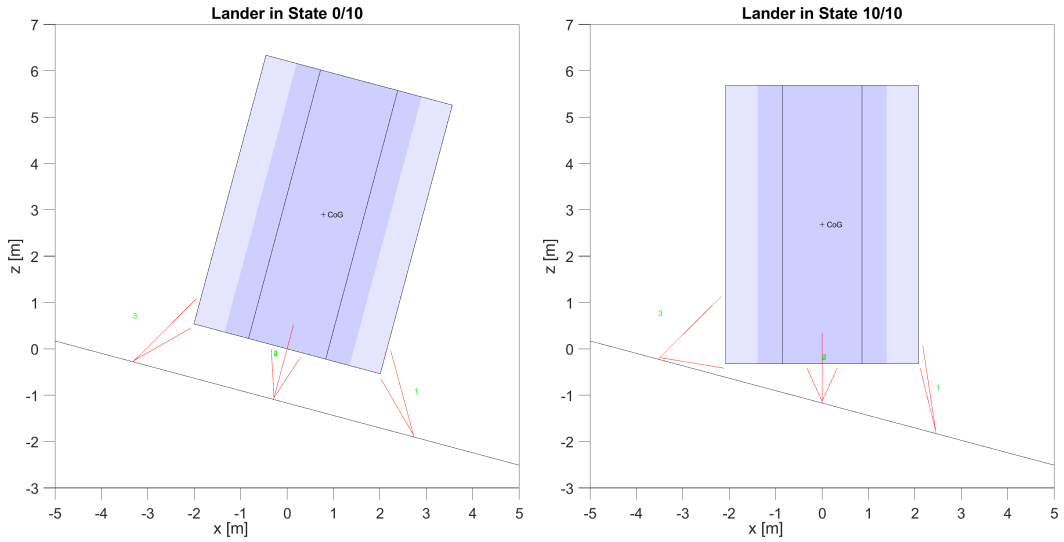

(a) State 0: *directly after landing* **(b)** State 10: *last state in this calculation*

Fig. 4.2.: MATLAB figure of exemplary lander in 1-2-1 configuration

This configuration results in a needed movement of the primary strut on leg 1 (downhill) of -0.142 m and on leg 3 (uphill) of 0.917 m for a total needed travel length of 1.059 m. The force maximum on IF1 in z-direction can be found on leg 1 in the first state right after landing with approximately 1304 N, just as expected. As the lander slowly aligns and levels itself from state 0 to state 10, the force is shifted from leg 1 onto the other 3 legs (see also figure 4.3). The force increase on leg 3 is the biggest here.
Another interesting fact that can be seen in the diagrams of leg 2 and leg 4 is that these legs are loaded equally during levelling. Even though the sign of the force values in the direction of the y-axis is opposite to those of leg 4, the absolute values are still equal (apart from small rounding errors). This confirms the assumption made earlier in section 2.4.2.2 that legs on an equal height on the slope experience

the same force. The complete output spreadsheet can be found in the appendix section A.1.1 in figure A.2.

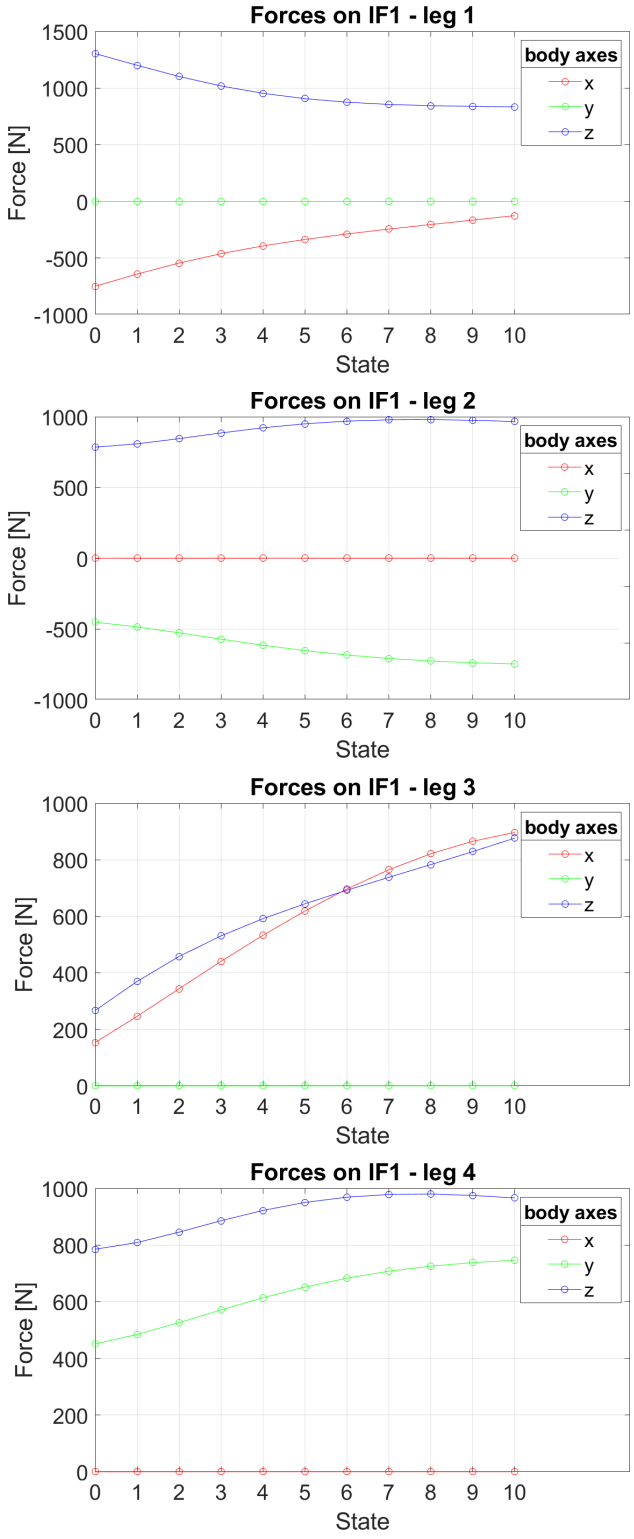

Fig. 4.3.: Force on IF1 in the 1-2-1 configuration

4.3 2-2 configuration

The 2-2 configuration features two pairs of similarly loaded legs. As the majority of the load is shared between two legs in this configuration, it is to be expected that the loads are smaller than in the 1-2-1 configuration. In fact, for a given lean angle these loads should be the smallest they become.
Start and end state of the alignment process can be seen in figure 4.4. The input variables are the same as in the 1-2-1 configuration only with a changed direction of the ground slope. The full input spreadsheet can be found in the appendix in section A.1.2 in figure A.3.

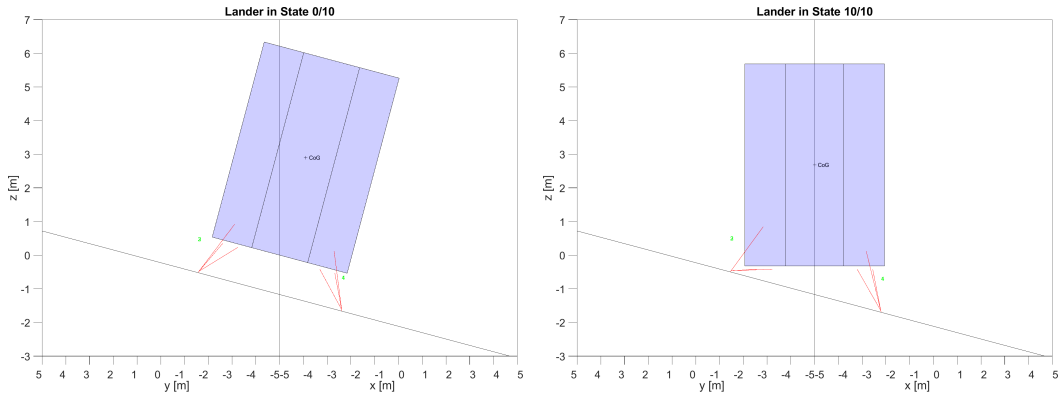

(a) State 0: *directly after landing* **(b)** State 10: *last state in this calculation*

Fig. 4.4.: MATLAB figure of exemplary lander in 2-2 configuration

The resulting needed travel length of 0.719 m is the sum of IF1 of legs 1 and 4 moving 0.095 m downwards and of legs 2 and 3 moving 0.624 m upwards. The maximal force on IF1 can be found on legs 1 and 4 in the state right after landing, just as in the 1-2-1 configuration. The magnitude of the force is lower, however, with a maximum of 1151 N of force in the vertical lander direction. The absolute forces on legs 1 and 4 as well as legs 2 and 3 are the same, just as expected. Again, the force is slowly shifted onto the uphill legs as the lander aligns and levels itself (see also figure 4.5). The complete output spreadsheet can be found in the appendix section A.1.2 in figure A.4.
One point to note here is that the difference between the expected force maximum for the 1-2-1 and the 2-2 configuration is only 153 N (1304 N to 1151 N) or around 13%.

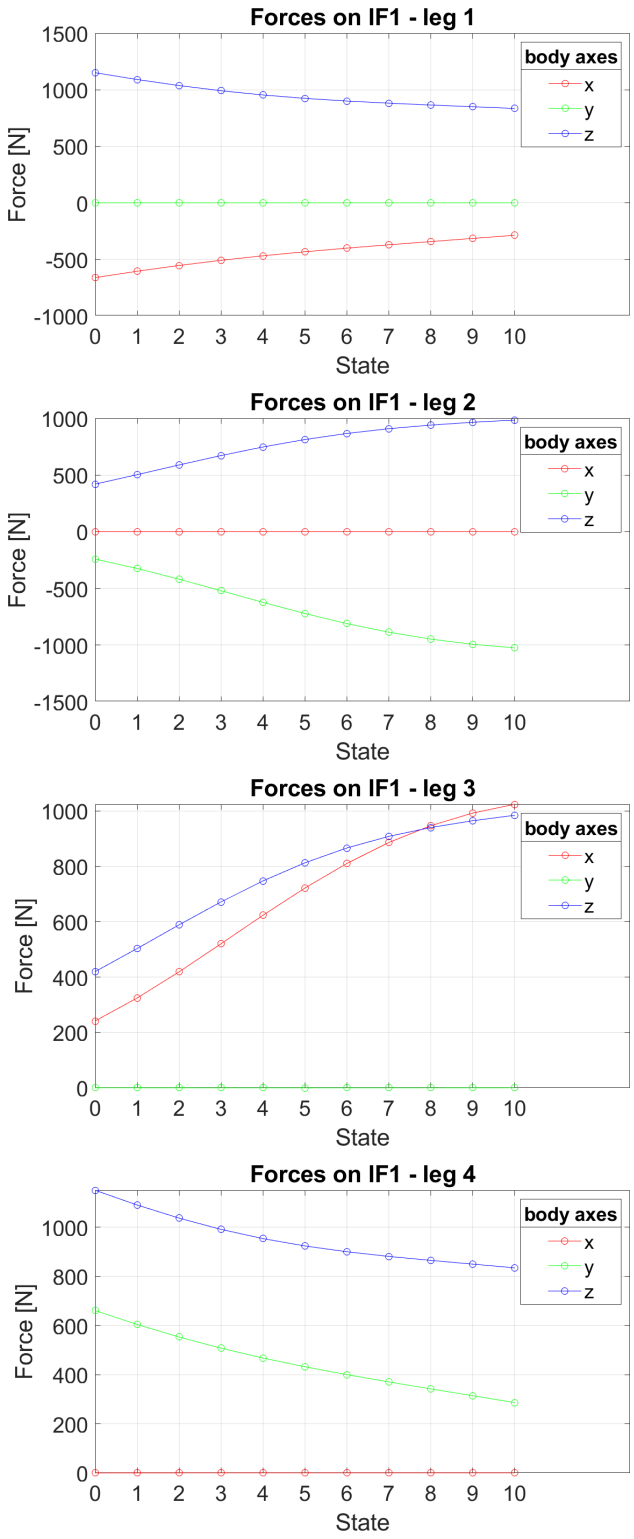

Fig. 4.5.: Force on IF1 in the 2-2 configuration

4.4 Key design drivers

The results from the two configurations show that the force exerted in the vertical direction on IF1 has a similar magnitude regardless of which way the lander is facing. This might not hold true for other landing leg configurations, be it other lengths of the struts or using a Cantilever setup instead of an Inverted Tripod.
For the design of the mechanism in section 5, it is absolutely necessary to have fixed value ranges for the drive length and the force on the mechanism. Both, the largest drive length range and the highest force were calculated for the 1-2-1 configuration. The length of drivable distance of the linear actuator has to be at least 1.059 m. In order to allow for a minimum distance to the end stop of the linear drive, be able to offset the length change of the struts due to crushing (which was left out for this calculation), or even increase the drivable length slightly in order to account for the ruggedness of the Lunar terrain, this length should be increased. A minimal length of 1.4 m was chosen to allow for 17 cm of space to the end stop in the lowest and highest calculated position. This way, around 75% of the length are used according to the calculation of the 1-2-1 configuration in section 4.2.
As it is reasonable to assume that the specification for the lander might change during design as launchers get more powerful or e.g. margins on residual propellants are reduced, i.e. payload masses could increase, the force values used for the design should be adapted. A possible mass increase of approximately 30% will be assumed, bringing the mass of the lander to 4000 kg. The force exerted on IF1 increases likewise to 1682 N.
Additionally, in compliance with the *European Cooperation for Space Standardization (ECSS)*, there are factors of safety (FOS) that have to be applied to force results. The space engineering standard for *Mechanisms* ECSS-E-ST-33-01C-Rev.2(1March2019) lists the FOS for buckling in section 4.7.5.2.6 b for standard metallic materials as 2.0 [30]. Other FOS come from the space engineering standard for *Structural factors of safety for spaceflight hardware* ECSS-E-ST-32-10C-Rev.2(15May2019) from table 4.3 in section 4.3.2.1, where the higher values for metallic where chosen due to the early development stage. They are listed here as 1.25 for yield stress and 2.00 for ultimate stress [31]. Table 4.2 lists the used FOS.

Tab. 4.2.: Factors of safety from ECSS standards

Type	FOS	Reference
yield stress	1.25	ECSS-E-ST-32-10C-Rev.2(15May2019) [31]
ultimate stress	2.00	ECSS-E-ST-32-10C-Rev.2(15May2019) [31]
buckling	2.00	ECSS-E-ST-33-01C-Rev.2(1March2019) [30]

Additionally, even though the forces on the lander are assumed to be quasi-static once it sits safely on the ground and the main force path during touchdown is planned to be decoupled from the movement mechanism, it is advisable to implement at least a small factor of safety regarding the dynamic part of touchdown. A peak load of 2.00 times the calculated static load will be assumed here.
Sideways forces are highest in the load case of an even ground without slope with a maximum of 1635 N (without safety) in radial direction to the lander body. These sideways forces shall be absorbed by a linear guide rail an not by the movement mechanism (more on the guide rail will follow in section 5.3.3).
Table 4.3 summarises the key design drivers discussed in this section. The largest values (6728 N vertical and 6540 N horizontal) in the table are the ones which have to be considered when sizing the components later. The vertical force has to be absorbed by the movement-mechanism, while the horizontal force in radial direction to the lander body has to be absorbed by some form of guide rail.

Tab. 4.3.: Summary of design driving forces on IF1

direction	**force w/o FOS**	**stress type**	**FOS**	**force with FOS**	**FOS_{dyn}**	**force with FOS_{dyn}**
vertical (axial)	1682 N	yield	1.25	2102.5 N	2.00	4205 N
		ultimate	2.00	3364 N		6728 N
		buckling	2.00			
horizontal (radial)	1635 N	yield	1.25	2043.75 N	2.00	4087.5 N
		ultimate	2.00	3270 N		6540 N

Construction and Design

5

> *We cannot direct the wind, but we can adjust the sails.*
>
> **— proverb**
> (exact origin unknown)

As already mentioned in the introduction to this thesis, most landers, at least those designed for landing on celestial bodies with a large mass and therefore gravitational acceleration, use a form of passive shock absorbent like a honeycomb crush cartridge or other dampening mechanisms. Examples for these soft landing vehicles include Lunar landers like the Surveyor spacecraft [4] or the Lunar Modules from the Apollo program [15], Martian landers like Viking [16], as well as spacecraft designed for other planets or moons in the solar system, or even ESA's Rosetta mission with its lander Philae which targeted the comet 67P/Churyumov-Gerasimenko [4].
Once landed, however, most of them do not have the ability to align or level themselves in any way, shape, or form. If, for example, the slope at the landing site is very steep, this might lead to problems regarding the payload. It might be some form of sensitive observatory that has to be aligned horizontally to function properly, or the lander might include an ascent stage that can not launch at too steep of an angle. In order to be able to adapt to these outer influences that can not br influenced directly, the geometry of the lander has to be adjusted to adapt to the environment. To allow landers to do exactly that, some form of mechanism is needed, which moves the legs in some way and by that reorients the lander after touchdown.
First, it is necessary to formulate requirements, which have to be fulfilled by the mechanism which will be designed after a type of movement mechanism that has been chosen from the many possible candidates.

5.1 Requirements for the movement mechanism

There are a few requirements that have to be fulfilled by the movement mechanism that shall be designed. The main categories here are the complexity of the system

(i.e.: How many parts is the mechanism comprised of? Are there multiple moving parts? Is lubrication needed? Does it need additional sub-mechanisms to function correctly like a locking mechanism to prevent back-driving?), suitability to the expected environment (i.e.: Are there possible problems due to exposure to the vacuum of space, or the thermal environment on the Lunar surface, or during transit?), the efficiency (i.e.: Is there a large amount of friction to overcome? How efficiently can the input torque be transferred? How much torque is needed? How large is the power requirement?), as well as supportable load, accuracy, cycle life, and movement speed.

It should be noted that no sideward forces or impact shocks are expected to be absorbed by the driving mechanism as additional guide rails and frangible bolts will be used for this purpose. Additionally, not all these requirements are to be weighted equally. As the expected loads are comparably low (especially because of the Lunar gravity), most mechanisms have a high enough inherent accuracy, only one time movement is needed and a fast movement speed is not critical, there is basically no mechanism type not capable to fulfil the requirements. A high efficiency is not as important as the mechanism consisting of few moving parts and not needing an additional locking mechanism or brake. Every additional part and sub-mechanism increases the risk of system failure exponentially as each additional part could theoretically fail, which is especially problematic when using it on another celestial body like the Moon. At the same time, a worse efficiency might make the system slightly heavier and require slightly more power, however, it can not lead to a critical system failure making this factor inherently not as important.

With all of that in mind, the requirements can be formulated (note that some are only qualitative requirements and are not quantified yet).

Requirements

1. The mechanism shall consist of few moving parts.
2. The mechanism shall not be susceptible to jamming.
3. The mechanism should be self-locking, without relying on additional sub-mechanisms or actuators other than the drive motor itself.
4. The mechanism should not rely on lubrication to execute its function.
5. The mechanism shall be be able to withstand the harsh environment on the Lunar surface (vacuum, temperature, solar radiation, etc.).

6. The mechanism shall support low friction to increase efficiency and decrease power consumption.
7. The mechanism shall be able to withstand the loads it is exposed to and which have been calculated in chapter 4.
8. The mechanism shall have a positioning accuracy of less than 1 mm.
9. The mechanism shall have a cycle life of at least 10 drive cycles to accommodate for qualification.
10. The mechanism shall be able to level the lander in less than 6 hours.

5.2 Linear movement

Possible approaches to achieve the requirements have already shortly been mentioned in the introduction of this thesis. They include i) questionable active systems, ii) changing the length of the legs after touchdown by including some form of mechanism inside of them, and iii) moving the interface of each primary strut to change the geometry of the lander. This thesis focuses on moving the primary strut interface in a translational way up and down the lander body.
There is a number of possible approaches to move the interface of the primary strut on a straight line up and down the side of the lander, each with its own advantages and disadvantages. Aside from hydraulic solutions which always come with the risk of leakage (especially in the vacuum of space [5][32]), electromechanical solutions using electric motors are conceivable. Probably the most widely recognised possible mechanisms include:

- Electromagnetic drive
- Belt drive/Chain drive
- Pinion gear and rack
- Worm drive
- Lead screw
- Ball screw
- Planetary roller screw

Lead screws, unlike any of the other listed candidates, offer self locking capabilities, depending on the lead angle, which makes them seem like the obvious choice by default as self-locking is absolutely required to reduce the power consumption of the system. Without self-locking the system would be back-drivable, i.e. power is needed constantly to hold the system in its current position. The other drives would be out of the picture because of this, however, it is possible to combine a back-drivable mechanism with one that locks it in place. By using springs to lock the mechanism this setup is also fail-safe even if the power should be cut off because of a failure. Additionally, lead screw mechanisms are usually less efficient than other mechanisms because of their higher friction coefficient (e.g. the friction coefficient of a lead screw is approximately one order of magnitude larger than that of a ball screw) making them undesirable for the lander. [33]
Electromagnetic drives require magnetic tracks to function properly making them relatively complex when compared to the other listed options. The coil would have to be mounted on the moving part meaning additional power transfer to the moving interface and the induced moving magnetic field could theoretically damage sensitive equipment on board. Belt and chain drives have the disadvantage of needing some slack in their mounting making them inaccurate in their positioning. Additionally, over time, their length may increase due to the load and strain put onto them decreasing their accuracy even further. Chain drives also have the added disadvantage of needing lubrication. Pinion gear and rack basically fulfil the same requirements as a lead screw with the disadvantage of providing less guidance in this vertical setup as well as possibly having a looser fit and therefore decreasing accuracy. They basically offer no advantages over lead screws for this particular use case but add disadvantages. Using a worm drive (combined with a rack) would require the motor to be mounted on the moving interface, just as with the electromagnetic drive, which is less than ideal, without adding any real advantages. This leads to the finding that out of the above list the only other viable alternatives to the lead screw are the ball screw and the planetary roller screw.

5.2.1 Screw drive explanation and comparison

As explained, only screw drives are an actual conceivable option at this point. This section will shortly explain the different types of screw drives and compares them based on the requirements defined in section 5.1.

Lead screw Probably the most obvious and simple solution for linear movement is the lead screw drive. Here, the screw features a standard trapezoidal or Acme thread

with corresponding lead nut. By attaching the lead nut to the primary interface and rotating the lead screw, which is attached to the lander, the nut, and therefore the interface, can be moved up and down.
An additional main feature of this linear actuator is its self-locking capability. By having a lead angle of the screw which is smaller than the friction angle, depending on the friction coefficient between nut and screw material, the screw can not back-drive on its own but stays in place under translational load. Generally speaking, for most technical cases with metallic materials, this means the screw lead angle has to be smaller than 5°. Another advantage of small lead angles is a higher translational accuracy as each rotation of the screw leads to a smaller translational movement than with a higher lead angle.
Lead screws are cheap and do not require any maintenance as they generally use bronze nuts and are therefore self lubricating. As they do not have any moving parts except for the nut, they are also suited for harsh environments. They are, however, not as efficient as ball or roller screws as they have a higher friction, meaning they are also not suited for very high cycle lives. Additionally, lead screws can only be used in low to medium load applications.

Ball screw One alternative to the lead screw is the ball screw which features recirculating balls that roll around a special thread. It is comparable to a ball bearing, however, the balls are arranged in a helical shape as they roll around the thread. An example for such a screw can be seen in figure 5.1a. The main advantages of ball screws over lead screws include their higher efficiency due to lower friction, higher force/load tolerance with a longer life, and higher accuracy. At the same time, they have the disadvantage of being able to be back-driven as they are not self-locking, meaning an additional break or locking mechanism has to be installed. Especially in the vertical configuration, this actuator is intended to be used in. They also need lubrication and are more expensive.

Planetary roller screw Another possible alternative to lead and ball screws is the planetary roller screw. Here, the nut is made up of multiple small rollers that have threads themselves and revolve around the central thread as the nut is moved. The internal working of such a screw can be seen in the cutaway image in figure 5.1b. Planetary roller screws offer even greater load capabilities than ball screws, i.e. they can withstand higher forces as they have a significantly increased contact area. Additionally, they have a greater impact tolerance and a significantly increased cycle life. They are, however, more expensive than both, lead and ball screws.

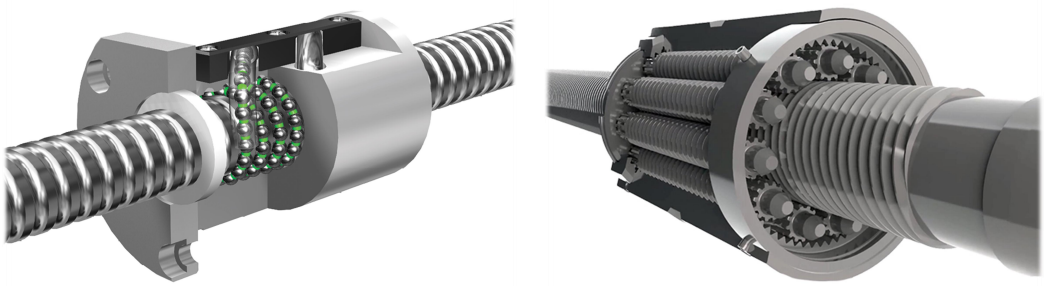

(a) Cutaway drawing of a ball screw (courtesy of *THK LM SYSTEM Pte. Ltd.*)

(b) Cutaway drawing of a roller screw (courtesy of *Tolomatic, Inc.*)

Fig. 5.1.: Cutaway examples of a ball screw and a planetary roller screw

5.2.2 Comparison of screw drives

In order to select one of the three possible actuators as the best suited option for the task at hand, they have to be compared. Unfortunately, it is almost impossible to quantitatively compare them regarding characteristics like weight, power consumption, or cost, because there are too many factors affecting these characteristics. Trying to do so regardless would only result in a comparison between a detailed design of one mechanism and another detailed design of another one while failing to compare the base mechanisms behind these detailed designs. Therefore, it is necessary to make a qualitative comparison based on the requirements defined in section 5.1. Table 5.1 shows this comparison of the drive types for each of the requirements formulated earlier.

Tab. 5.1.: Comparison between lead screw, ball screw, and planetary roller screw: *The winner of each requirement is marked in green*

requirement	lead screw	ball screw	roller screw
1. number of moving parts	few	many	many
2. susceptible to jamming	no	yes	yes
3. self-locking	yes	no	usually no
4. needs lubrication	no	yes	yes
5. harsh environments	yes	yes	yes
6. efficiency	≈ 0.3	≈ 0.9	≈ 0.8
7. force	low to medium	medium to high	high
8. accuracy	medium	medium to high	high
9. cycle life	low	medium	high
10. speed	slow to medium	high	high

The lead screw wins the comparison for the specific kinematic that is to be designed in this thesis. Mainly in the first four requirements number of moving parts, jamming-susceptibility, self-locking capability, and lubrication need it is a clear win for the lead screw. The suitability for harsh environments is a tie between all three options. The categories in which the lead screw falls behind the other two options are arguably not as important as the ones in which it wins. Even though the lead screw shows a lower efficiency and therefore higher power demand, it should be noted that the expected number of cycles driven by this mechanism is only one, right after initial touchdown. So even with a higher power demand, only one cycle has to be driven which should not be a problem for the power supply. Also, the increased torque needed because of the lower efficiency might increase motor weight slightly, however, most likely it will be possible to counteract this effect by simply using a higher gear ratio in the gearbox of the motor assembly. As the lander is not intended to be reused, the cycle life also does not have to be high. For future missions or different requirements of other landers this might be of greater concern. Speed is also not important as we do not care about a high speed alignment but rather about an accurate one. Here, the medium accuracy of a lead screw mechanism should suffice as it is still usually in the sub-millimetre range. The final disadvantage of the lead screw is the smaller load capacity when compared to ball and roller screws. Even so, the mechanism only has to deal with Lunar gravity and the available lead screws offer plenty load capability for the expected force.
For other requirements, this result might have looked very different. Considering possible reusability for example would require the longevity of ball or roller screws and implementing the mechanism into the primary strut, i.e. it would be exposed to the landing shock, would require the impact tolerance of roller screws. For the task at hand, however, the lead screw offers the best cost-benefit-ratio of the three options. Based on this decision to go with the standard lead screw, a design can be made.

5.3 Dimensioning and off-the-shelf component selection

Before designing the geometry of the overall mechanism using CAD software, the components have to be dimensioned mechanically. Minimal dimensions and performance capabilities of components have to be defined or calculated. This includes choosing possible components that work in combination with each other. It should be noted that none of the selected or designed components are likely to be the optimal

choice but rather serve as a preliminary design example of a possible combination of components. The selection is made to get an understanding of the interactions between the components and of the expected mass and other characteristics of the proposed mechanism.
That being said, the components that have to be designed or can be selected as commercially available off-the-shelf (COTS) components, according to the requirements, are:

- Trapezoidal lead screw
- Bearings
- Linear guide rail
- Motor-gearhead assembly
- Other (e.g. screws, washers, etc.)

5.3.1 Trapezoidal lead screw

Most trapezoidal lead screws are made of steel, however, materials such as titanium or aluminium are also available although they are not as common as they can not be rolled in most cases and therefore have to be cut. As yield and ultimate strength of the screw as well as the Young's modulus depend on the choice of material, it is important to compare the results for each material and make a choice based on factors such as weight in the end.
Values for properties of commonly used materials, i.e. stainless steel (1.4301 & 1.4404), titanium Ti-6Al-4V (Grade 5), and aluminium 7075-T6, were taken from material data sheets by the thyssenkrupp AG [34] and are listed in table 5.2.

Tab. 5.2.: Material properties of common metals

material	**Young's modulus** E **[MPa]**	**yield strength** σ_y **[MPa]**	**ultimate strength** σ_u **[MPa]**
1.4301 & 1.4404	200,000	≈ 195	600
Ti-6Al-4V (Grade 5)	114,000	910	1000
EN AW 7075-T6	72,000	480	540

Yield and ultimate strength of the screw of course have to exceed the expected forces including the safety factors already explained in section 4.4 and possible peak loads due to dynamic forces during touchdown. The values used for the calculation were explained in section 4.4.

The root diameter of the screw needed to withstand the expected forces can be calculated using equation 5.1 with the respective factors.

$$d_{root} = \sqrt{\frac{4 \cdot A_{root}}{\pi}} = \sqrt{\frac{4 \cdot F_{max} \cdot FoS}{\pi \cdot \sigma}} \tag{5.1}$$

where:

d_{root} = root diameter of lead screw [mm]
A_{root} = root area of lead screw [mm²]
F_{max} = force maximum on screw [N]
FoS = factor of safety
$\sigma_{y/u}$ = yield/ultimate strength of material [MPa]

Usually, the most critical failure mode for long slender parts that are compression loaded is buckling. The needed root diameter to withstand buckling can be calculated using equation 5.2. The column buckling end-condition factor f_c will be set to 2 for one fixed and one pinned end as this configuration is best comparable with the actual linear actuator.

$$d_{root} = \sqrt[4]{\frac{F_{max} \cdot L^2 \cdot 64}{f_c \cdot \pi^3 \cdot E}} \tag{5.2}$$

where:

L = length of screw [mm]
E = Young's modulus [MPa]
f_c = column buckling end-condition factor (depending on bearing type)

The results for the minimum root diameter needed for each material and failure mode are listed in table 5.3. It should be noted that the largest of the listed diameters for each material is the one that has to be used for further consideration because using a smaller diameter would lead to failure in that load case. As expected, the critical failure mode with the largest needed root diameters is buckling.

Tab. 5.3.: Minimal root diameter needed to withstand failure mode for different materials

material	**root diameter d_{root} [mm]**		
	yield	**ultimate**	**buckling**
1.4301 & 1.4404	5.24	3.78	16.15
Ti-6Al-4V (Grade 5)	2.43	2.93	18.59
EN AW 7075-T6	3.34	3.98	20.85

At this point it is very obvious that continuing with these results will lead to a very large and heavy screw and therefore an overall heavy system. As the root diameter needed to withstand the buckling requirement is between three and almost seven times higher than those required to withstand yield and ultimate stress, the mass would increase between nine- and 49-fold as the diameter is squared for the cross sectional area calculation. Because of this, it is necessary to adapt the design and to eliminate buckling altogether. By changing the upper attachment point such that it only features a floating bearing instead of a fixed one, no buckling can occur as the screw will only be exposed to tension. Figure 5.2 shows the power flow/load path through the primary strut into the trapezoidal lead screw. Design a) has the fixed bearing located on the top leading to the risk of buckling in the screw part that is above IF1. In design b), where the fixed bearing is located at the bottom, the screw is only exposed to tension. It is important to note that all lateral forces would be transferred via a guide rail system onto the lander in order to remove all off-axis loading from the screws. This planned guide rail system was left out in the figure for clarity.

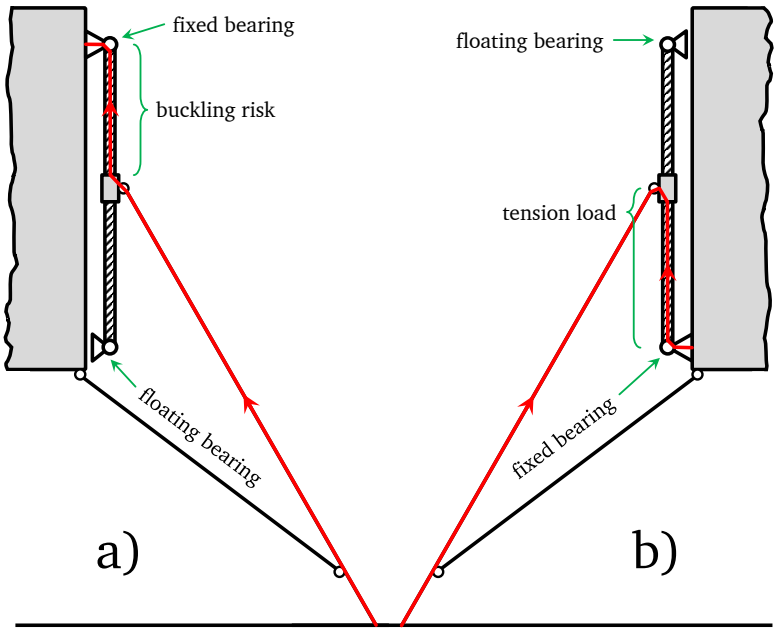

Fig. 5.2.: Load path diagram through primary strut and lead screw: *red lines show the power flow; planned linear guide rail left out for simplicity.*

Because of the largely increased root diameter when using the left design, and as there is a simple solution fixing this problem, the right design will be used for further consideration and all buckling forces can be neglected. The low root diameters would in this case, however, also mean that the screws would only feature outer

diameters in the range of 4 mm to 6 mm. There are very few manufacturers that only recently started offering trapezoidal lead screws with these small diameters and even the norm classifying their dimensions (DIN 103/ISO 2904) only starts at an outer diameter of 8 mm. Additionally, with smaller diameters also come problems like being able to withstand launch loads, especially for these long unsupported lengths, or integrability on Earth where the allowed load would be surpassed because of theh igher gravity of the Earth. Especially for these long slender parts, this can quickly become a problem when the higher gravity bends them, making the test setup more elaborate and complicated. Furthermore, not only the screw but also the bearings have to withstand the forces (more on the bearing selection in section 5.3.2) and the drive shaft usually decreases in diameter at this point which is necessary to be able to integrate the system. In order to cope with these problems, a minimal outer screw diameter of 10 mm will be assumed. This does increase the mass of the screw over the theoretically needed value, but allows for an easier design with fewer of the aforementioned challenges. Furthermore, as the overall design does not change drastically with different screw sizes, an adaptation of the size in later stages of an actual project is still easily implementable.
A TR 10x2 screw features a core diameter of 6.89 mm, easily surpassing the needed minimum root diameter for all materials as listed in table 5.3 (when neglecting the buckling column). Because of this, the aluminium screw is easily the lightest options because of its low density at a specific weight of approximately 0.177 kg/m. However, even the steel variant only comes to about 0.503 kg/m which is still very light when compared to the size of screws that would have been needed to compensate buckling. This screw size also has a very small lead angle at only 4° 2’ ensuring self-locking of the screw as long as the friction angle between screw and nut material is larger, which is the case for most if not all metal combinations.

5.3.2 Shaft bearings

As has been mentioned in the previous section, the bearing selection is not trivial as they have to fit the size of the main shaft while being able to withstand the expected loads. The bearing selection therefore also influences the shaft size.
The bearing selection was based on larger lead screw/bearing-combinations (diameter of 18 mm and larger) from the company *Thomson Industries, Inc.* which was chosen as it offers a wide variety of screws with extensive documentation, characteristics, and parameters and these characteristics of the screws should not vary much across the industry.
In combination with the bearings used for larger screws and based on the load

of 6728 N (including safety), which was the result of the exemplary calculation listed in table 4.3, smaller variants of the same bearings used by *Thomson Industries, Inc.* were selected. The axial angular contact ball bearing *ZKLFA0640-2RS*, which features a 6900 N dynamic axial load rating [35], was chosen as the fixed bearing on the bottom. For the floating bearing at the top, the deep groove ball bearing *W606-2RS1* [36] was selected based on its size and load carrying capability. Exemplary depictions of the bearings can be seen in figure 5.3.

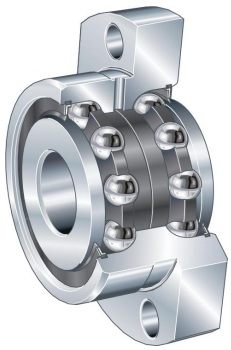

(a) Double row axial angular contact ball bearing with flange: *ZKLFA0640-2RS* (courtesy of *Schaeffler Technologies AG & Co. KG*)

(b) Deep groove ball bearing: *W606-2RS1* (courtesy of *AB SKF*)

Fig. 5.3.: Cutaway depictions of bearings

5.3.3 Linear guide rail

A linear-motion bearing is used to transfer the forces that are off-axis from the main lead screw onto the body of the lander in order to minimise stress on the screw and to provide a guide rail along which the primary interface may move. In order to minimise the number of moving components, roller slides are out of question. A plain bearing (more commonly known as a sliding contact bearing) shall be utilized. The *igus® GmbH* offers a solution of W-shaped profile guides under the registered trademark name *drylin®*. These guides consist of a double rail of round, hard-anodised aluminium and can be combined with a guide carriage that can be fitted with different liner materials in order to be suitable for a multitude of different environments and requirements.
In order to be able to withstand the calculated force of 6540 N (including safety), the relatively large *WW-16-60-10* carriage has to be utilized, which features round guide rails with a diameter of 16 mm at a distance of 60 mm and a length of 10 cm, weighing 0.71 kg [37]. The corresponding *WS-16-60* guide rail weighs in at 1.96 kg/m [38]. Both components are depicted in figure 5.4.

(a) drylin® W profile guide - assembled guide carriage: *WW-16-60-10* (courtesy of *igus® GmbH*)

(b) drylin® W profile guide - double rail: *WS-16-60* (courtesy of *igus® GmbH*)

Fig. 5.4.: Exemplary depictions of linear guide rail components

5.3.4 Electrical motor-gearhead combination

Many different combinations of electrical motors and gearheads are conceivable. To get a first understanding of the approximate mass, the drive system adds to the assembly a few assumptions have to be made to select one of the possible candidates.

5.3.4.1. Required torque calculation

First, the torque needed to raise and lower the carrier nut on the TR 10x2 screw has to be determined. This can be done using equations 5.3a and 5.3b to calculate the torque needed to raise and lower the load, respectively. An assumption has to be made for the coefficient of friction as the materials of screw and nut might still change in the future. According to both, the space engineering handbook ECSS-E-HB-32-23A(16April2010) (*Threaded fasteners handbook*) [39] and the US military handbook *MIL-HDBK-60: Threaded Fasteners - Tightening to Proper Tension* [40], the most common metal material combinations show friction coefficients between 0.07 and 0.28 without lubrication. A friction coefficient of 0.21 will be assumed which approximately corresponds to an aluminium-aluminium material combination (table C-2 from [39]).

$$T_{raise} = \frac{F \cdot d_m}{2} \cdot \left(\frac{l + \pi \cdot \mu \cdot d_m \cdot \sec \alpha}{\pi \cdot d_m - \mu \cdot l \cdot \sec \alpha} \right) \tag{5.3a}$$

$$T_{lower} = \frac{F \cdot d_m}{2} \cdot \left(\frac{\pi \cdot \mu \cdot d_m \cdot \sec \alpha - l}{\pi \cdot d_m + \mu \cdot l \cdot \sec \alpha} \right) \tag{5.3b}$$

where:

T = torque [Nm]
F = load on the screw [N]
d_m = mean diameter [m] (here: $d_m \approx$ 8.8 mm)
μ = coefficient of friction
l = screw lead [m] (here: l = 2 mm)
α = one half of thread angle [°] (here: α = 15°)

The resulting torque required is 2.18 Nm for raising and 1.06 Nm for lowering the carrier at a load of 1682 N. According to the ECSS standard for *Mechanisms* ECSS-E-ST-33-01C-Rev.2(1March2019), the minimum actuation torque T_{min} including margins shall be derived using equation 5.4 [30].

$$T_{min} = 2 \cdot (1.1 \cdot I + 1.2 \cdot S + 1.5 \cdot H_M + 3 \cdot F_R + 3 \cdot H_Y + 3 \cdot H_A + 3 \cdot H_D) + 1.25 \cdot T_D + T_L \quad (5.4)$$

The resistive inertial torque applied to a mechanism subjected to acceleration in an inertial frame of reference I can be neglected as the mechanism is not subjected to any acceleration of this kind (e.g. a spinning spacecraft) during actuation. Likewise, the factors for torque needed to overcome spring forces S, magnetic effects H_M, hysteresis effects (e.g. elasticity) H_Y, and adhesion H_D can be neglected as there are no springs in the mechanism that have to be compressed or tensioned, the work environment is not magnetic, there are no elastic effects, nor is there adhesion that has to be overcome.
The deliverable output torque T_L and the torque needed to overcome friction F_R are the result of equations 5.3a and 5.3b. Here, the friction is directly included into the resulting torque. To calculate the correct margin, however, it is necessary to split this result into a frictionless torque that only represents the work needed to raise or lower the interface and the friction itself. By setting μ to 0, equation 5.3a can be simplified to equation 5.5 and the result is the torque needed to move the mechanism if there were no friction present (equation 5.3b can be neglected here as it will always have the same value, although negative instead of positive, and only the maximum possible torque is needed to calculate T_{min}). This part is T_L and for the present case equal to approximately 0.54 Nm.

$$T_L = \frac{F \cdot l}{2 \cdot \pi} \quad (5.5)$$

The maximum difference between this result and the results of equations 5.3a and 5.3b is the friction portion F_R, which in this case is approximately 1.64 Nm.
The H_A fraction or also simply called the "other" factors in this case consist of

friction in the bearings as well as friction due to the radial force fraction pushing the whole mechanism against the linear guide rail. With the frictional torque of the fixed double row axial angular contact ball bearing, selected in section 5.3.2, readily available in the data sheet at 0.04 Nm, the frictional torque of the floating deep groove ball bearing is estimated to approximately 0.02 Nm. Here, no easily researchable data was available and an estimation of half the torque for one instead of two rows of balls seems reasonable (especially since these values are so low they do not have a big influence on the overall results). The frictional torque needed to overcome the friction against the linear guide rail can be calculated using the same equations 5.3a and 5.3b by replacing F with the frictional force. This frictional force is equal to the maximum radial force at 1635 N times the friction coefficient of the plain bearing which, depending on material combination and other influence factors, may fall anywhere between approximately 0.05 and 0.3. The worst case scenario will be assumed here, i.e. the additional force that has to be lifted is equal to approximately 490.5 N. This force is then inserted into equation 5.3a, as it increases the force that has to be lifted, resulting in an additional needed torque of 0.64 Nm. Overall, the other factor H_A increases the torque by 0.7 Nm.
Lastly, there is the inertial resistance torque caused by initial acceleration of the system T_D. It can be calculated using following equation

$$T_D = I \cdot \ddot{\phi} = I \cdot \dot{\vec{\omega}} \tag{5.6}$$

where:

I = principal moment of inertia [kg·m²]
ϕ = angle/angular position [rad]
$\vec{\omega}$ = angular velocity [rad/s]

The moment of inertia for the trapezoidal lead screw was estimated at 3.08 kg mm² using CAD-software. For $\vec{\omega}$, an angular velocity of approximately 12.6 rad/s, or 120 min^{-1}, will be assumed. This corresponds to a relatively high estimate judging by a first look at possible motor-gearbox combinations, most of which are more in the realm between 20 min^{-1} and 90 min^{-1}. The important factor here is the spin-up time of the motor, which for most electrical motors is only a few milliseconds. For this calculation, T_D is assumed at 5 ms. This results in a T_D of 7.7 mNm, which could almost be neglected.
Multiplying all of these results by their respective safety factors and adding them up, according to equation 5.4, yields a required minimal torque T_{min} of approximately 14.58 Nm. Based on this value, a motor-gearhead combination can be selected.

5.3.4.2. Component selection

Typical manufacturers for electrical motors and gearheads for space applications are the companies *maxon motor AG* and *Dr. Fritz Faulhaber GmbH & Co. KG*. As Faulhaber offers a more intuitive configurator, it was used for this calculation. A multitude of possible combinations are conceivable, none of which seems to have a clear advantage over the others. One of the lighter variants was chosen consisting of the planetary gearhead *42GPT 196:1* with a 196:1 reduction and the for this gearhead recommended DC motor *3863X048CR*. Depictions of motor and gearhead can be seen in figure 5.5. This setup weighs in at a total mass of 920 g (530 g for the gearhead and 390 g for the motor). As the motor does not contain sensors nor a controller, these components would add additional weight to the system which will be estimated at 150 g, based on a few of the possible sensors and controllers recommended by Faulhaber.
At the wanted output torque of approximately 15 Nm and with the present reduction of 196:1, an input torque to the gearhead of 107.6 mNm is required which the chosen motor offers at a nominal voltage of 28 V and a nominal current of 1.35 A, i.e. approximately 37.8 W of power. At this power input and with a load of 15 Nm, the motor outputs 2955.5 min^{-1}, i.e. the output speed of the gearhead lies at 15.08 min^{-1}. 1 m of travel (a bit more than the expected travel of 0.917 m needed to level the lander on a ground slope of 15° in the 1-2-1 configuration [see section 4.2]) of IF1 should therefore take around 33:09 min as one rotation moves the interface by 2 mm. [41]–[43]

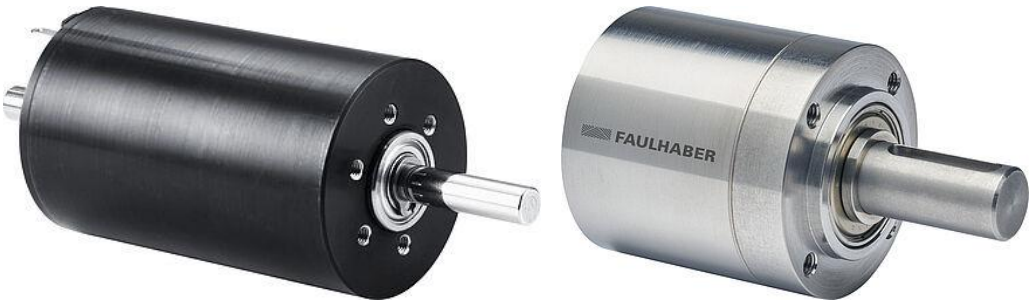

(a) DC-Micromotor: *3863X048CR* (courtesy of *Dr. Fritz Faulhaber GmbH & Co. KG*)

(b) Planetary Gearhead: *42GPT 196:1* (courtesy of *Dr. Fritz Faulhaber GmbH & Co. KG*)

Fig. 5.5.: Depiction of electrical motor-gearhead combination

5.3.5 Summary of off-the-shelf components

This subsection will give a quick summary of the specifications of the results of the sizing and the COTS components selected, without further explanation, in order to provide a simple and fast overview of the system characteristics. Most of them are also available in a more sturdy, albeit heavier variant should the need for a more performant design arise in the future.

Trapezoidal lead screw

- based on DIN 103/ISO 2904 for metric trapezoidal threads in the size TR 10x2
- outer diameter: 10 mm
- inner diameter: 6.89 mm
- lead: 2 mm
- lead angle: 4° 2’
- length: 1.4 m
- manufactured from EN AW 7075-T6 aluminium
- mass: approximately 0.25 kg

Bearings

- ZKLFA 0640-2RS double row axial angular contact ball bearing with flange (fixed bearing at lower end of lead screw)
- S606-2RS deep groove ball bearing (floating bearing at upper end of lead screw)

Linear guide rail

- plain bearing by igus®
- drylin® profile guide rail WS-16-60 made from aluminium (approximately 2.75 kg at a length of 1.4 m)
- drylin® carriage WW-16-60-10 (weighing in at 0.71 kg)

Electrical motor-gearhead combination

- Faulhaber DC motor 3863X048CR with 42GPT 196:1 planetary gearhead
- total mass: 0.92 kg
- output torque: up to 15 Nm
- supply voltage: 28 V
- power usage: approximately 37.8 W
- rotational frequency: approximately 15 min^{-1}
- levelling time: approximately 30 min (maximum at 15° initial angle in a 1-2-1 configuration)

Additional required off-the-shelf components

- motor sensor and controller
- coupling
- screws, washers, and nuts
- pin puller (see also section 5.4.2 for further explanation)

5.4 CAD design of custom components

The components that where discussed in section 5.3 were all, except for the trapezoidal lead screw, COTS components. Additional manufactured parts connecting everything are, however, also needed. This includes the bearing brackets as well as the so called carrier which connects the linear guide, trapezoidal lead nut, an IF1 of each leg to one another. This carrier also provides a means of securing the interface during initial touchdown without overloading the lead screw in the form of a pin puller. All of these components have to be designed in CAD-software as they are not COTS in the form they are needed here.
This section will introduce possible solutions for the needed parts, which can be used to get a first estimate of their mass. All custom manufactured components are assumed to be made from EN AW 7075-T6 aluminium. The design might have to be improved or changed later on in the design process.

Figure 5.6 shows the complete mechanism in a side view giving an idea of the scale of the components. Overall length of everything is approximately 1.67 m.

Fig. 5.6.: Overview of entire mechanism CAD model

5.4.1 Shaft ends of trapezoidal lead screw

Although the lead screw can generally be purchased as a commercially available component, the special material selection and end configuration might mean, it has to be custom manufactured. The shafts on either side have to be designed according to the specifications of the bearings as well as applicable norms.
Figure 5.7 shows a short section of the trapezoidal lead screw with the entire shaft on each end. The right side in the figure is the top end of the screw.

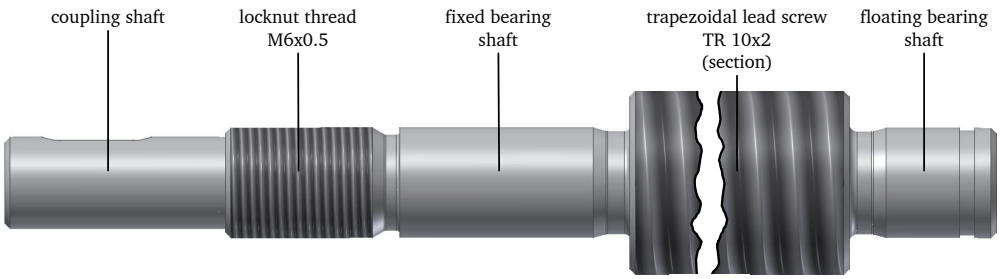

Fig. 5.7.: CAD model of lead screw (short section) with shaft on either side

5.4.2 Carrier

As already mentioned, the carrier connects IF1 to the trapezoidal lead nut and the linear guide. It is, in its current form, loosely based on the primary interface of CALLISTO (a reusable demonstrator for a vertical take-off and vertical landing (VTVL) rocket stage currently in development by DLR, CNES, and JAXA). The reason for this is that the CAD data for this was readily available in the department this thesis was written in. It is designed to secure the swivel head ball joint atop the primary strut.
The lead nut, connecting the carrier to the lead screw, is designed as a separate part. This simplifies integration immensely while also allowing for a relatively easy change

of the screw size during testing without needing to manufacture the complicated carrier in many different variations. By simply swapping the nut, different sizes can be tested.
The carrier is connected to the linear guide using four screws allowing for translation of force in radial direction to the lander body.
At its lower end, the carrier features an extension with a hole in it. This hole is intended to prevent the interface from moving during initial touchdown of the lander via a metal bolt. Initially, the so called *TiNi™Frangibolt®* by the company *EBAD (Ensign-Bickford Aerospace & Defense)* were intended to be used here. After talking to engineers of EBAD, this idea was discarded as these bolts are only designed to support tension loading but not sheer.
Instead, a bolt has to be designed, capable of withstanding the high shock during touchdown and interlocking with the carrier in the aforementioned hole. This bolt is then retracted into the lander using the largest *TiNi™Pin Puller* EBAD has to offer, called *P1000*. Unfortunately, it was not possible to get images of the P1000 as this pin puller variant is custom made for the exact application for each customer and currently under revision according to EBAD. Figure 5.8, however, shows an example for the bolt attached to the slightly smaller *P100* variant of the pin puller. This design will have to be edited and improved later on to make it structurally feasible. This depiction is only meant to explain the idea of this touchdown lock mechanism.

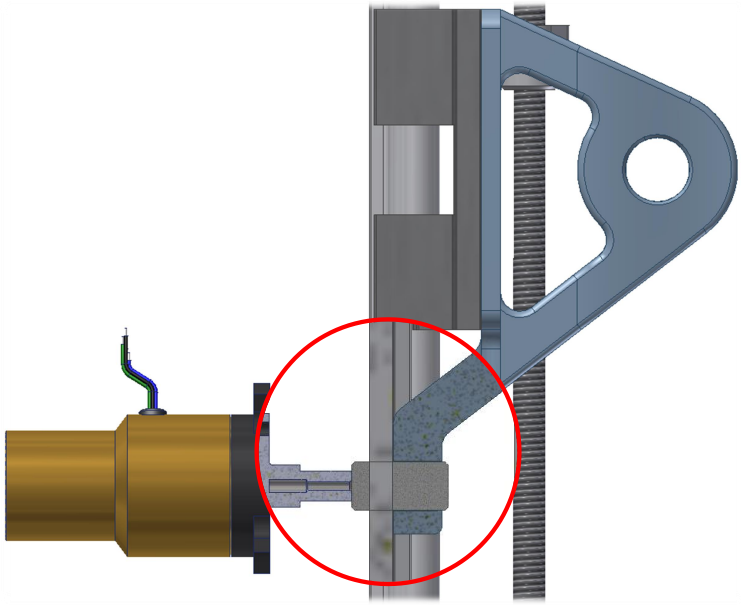

Fig. 5.8.: CAD Model of EBADs P100 TiNi™Pin Puller with cut-out showing the safety bolt

According to the data sheet, it is capable of activating under a side load of 6675 N with a pull force of almost 4.5 kN, easily enough to overcome the static forces on

the interface after touchdown. This will retract the bolt approximately 18.4 mm, releasing the carrier to be moved by the lead screw once the landing is complete and the touchdown shock has been diverted from the movement mechanism. [44] With this design, the carrier comes to a mass of approximately 654 g and the nut weighs in at 19 g.
Figure 5.9 shows the carrier, the linear guide carriage and rail, the lead nut, the lead screw, and the dome of the primary strut.

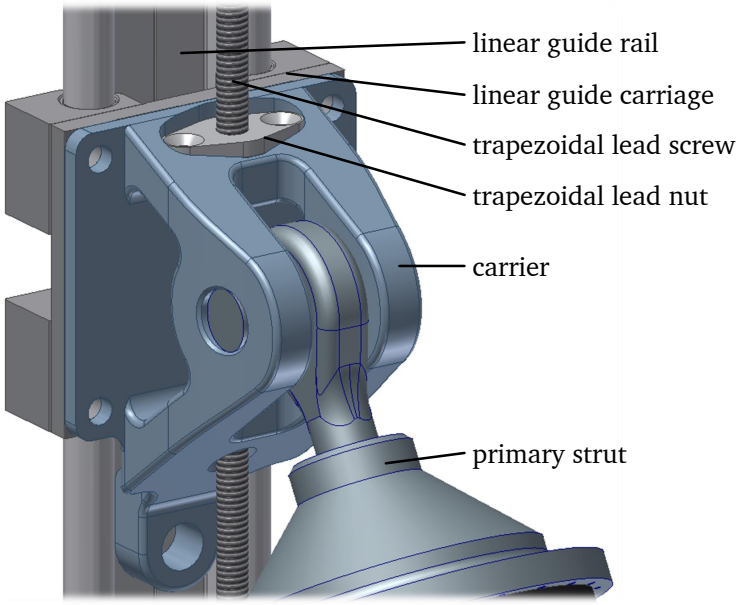

Fig. 5.9.: CAD model of carrier connecting IF1, linear guide, and lead nut

5.4.3 Bearing brackets

Both, the upper and lower bearing need brackets to hold them in place. The upper bearing also has to be able to move in its axis direction in order to compensate for expansion and contraction of the lead screw. The lower bracket needs an additional attachment to hold the motor-gearhead assembly which powers the whole mechanism.

5.4.3.1. Upper bearing bracket

As mentioned, the upper bearing is designed as a floating bearing, capable of movement in the axis direction. Figure 5.10 shows a cutaway of an example for a bracket, capable of providing this exact property. The bearing is inserted into the

bracket from the top and restricted from too much movement by a locking plate. The bearing is prohibited from moving in its plane while axial a small amount movement is still possible.

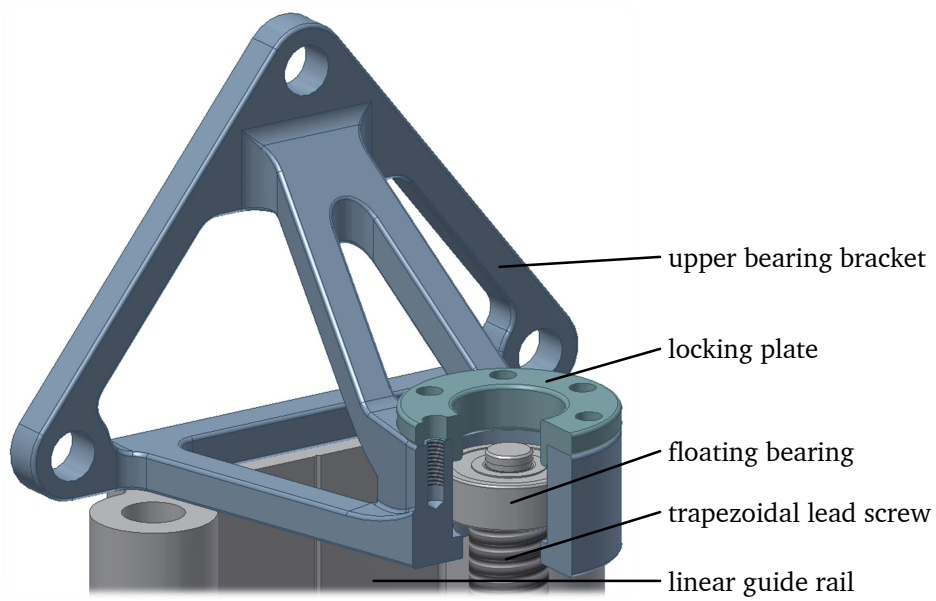

Fig. 5.10.: Cutaway CAD model of upper bearing bracket with locking plate

As for all the parts, this is a preliminary design that most likely would have to be adapted for a future version, however, a mass estimate is possible using this design. The bracket itself has a mass of approximately 45 g plus an additional 3 g for the locking plate.

5.4.3.2. Lower bearing bracket

The lower bearing bracket does not only have to house the fixed lower bearing but also provide an attachment point for the motor-gearhead assembly. Of course, attaching the motor at the top would also be an option. It was decided against this because any thermal expansion has to be compensated at the floating bearing which is located at the top end of the lead screw in this design. Attaching the motor at the top would therefore require the coupling to be able to compensate for the possible length change of the screw, increasing complexity.
Figure 5.11 shows the exemplary design of the lower bearing bracket. It has a mass of approximately 132 g with this design.

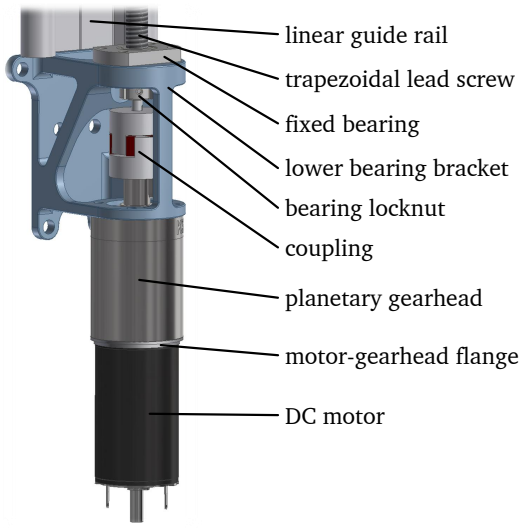

Fig. 5.11.: CAD model of lower bearing bracket including motor-gearhead assembly and coupling

5.5 Mass estimate

With all COTS and custom components defined, a first estimate for the mass of the entire system can be made. For this, all parts are assembled and attached to the lander in the CAD program (which can be seen in figure 5.12) and the mass estimate can be based on the masses in the CAD program and on the data sheets of the COTS components.

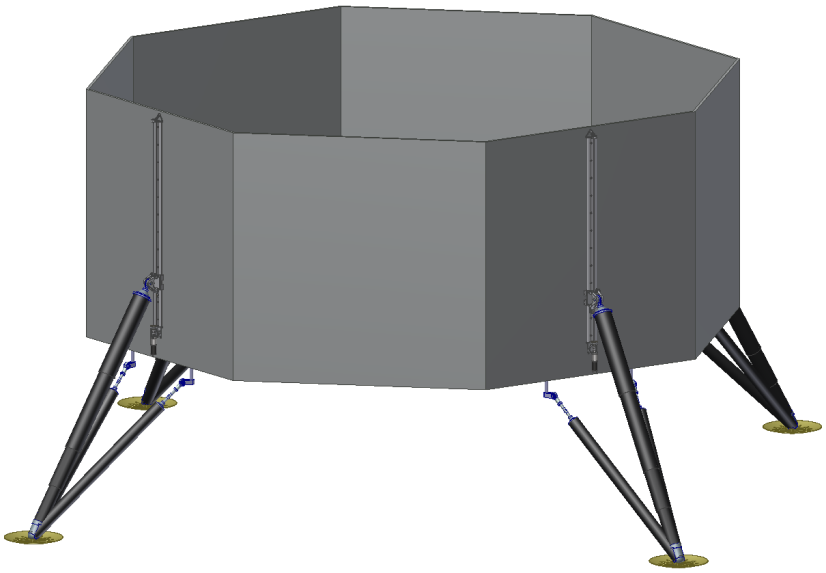

Fig. 5.12.: Final CAD model of a lander with the new alignment and levelling kinematic

Included in this estimate besides all mentioned COTS and custom components are an additional 250 g for screws and washers plus another 250 g for additional hardware like covers and cables. Based on the space engineering technical memoranda *Engineering design model data exchange (CDF)* ECSS-E-TM-10-25A(20October2010), mass margins have to be applied for each part based on its technical maturity. Fully developed items (COTS components) get a design margin of 5%, items that are mainly COTS but have to be modified get a 10% margin, and new developments get a 20% margin on their nominal mass [45].
Based on the data sheets, the CAD mass data, and the mass margins, it is possible to calculate the masses of each of the parts. Figure 5.13 shows these masses in a list sorted by part category. Aside from the nominal mass, minimum and maximum estimates can be found here as well.

System	Subsystem	Assembly	Part Category	Part	Part Name	Quantity [-]	Nominal Mass [kg]	Margin	Mass (min) [kg]	Mass (max) [kg]	Comment	Material
					Lander System	1	26.868	7%	25.037	28.700		
					Landing Leg	4	26.868	7%	25.037	28.700		
					Alignment & Levelling Kinematic (ALK)	1	6.717	7%	6.259	7.175		
					Carrier	1	0.672	20%	0.538	0.806		EN AW 7075-T6
					Screws & Washers	1	0.250	20%	0.200	0.300		TBD
					Additional Hardware	1	0.250	20%	0.200	0.040	e.g. covers; cables	various
					Trapezoidal Lead Screw Assembly	1	0.269	10%	0.242	0.296		
					Trapezoidal Lead Screw	1	0.250	10%	0.225	0.275	TR 10x2 - L = 1400	EN AW 7075-T6
					Trapezoidal Lead Nut	1	0.019	10%	0.017	0.021	TR 10x2	EN AW 7075-T6
					Linear Guide Assembly	1	3.454	5%	3.281	3.627		
					Linear Guide Rail	1	2.744	5%	2.607	2.881	igus® drylin® WS-16-60-1400	Aluminium
					Linear Guide Carriage	1	0.710	5%	0.675	0.746	igus® drylin® WW-16-60-10	various
					Electric Drive Assembly	1	1.150	7%	1.070	1.230		
					Motor	1	0.390	5%	0.371	0.410	Faulhaber 3863X048CR	various
					Planetary Gearhead	1	0.530	5%	0.504	0.557	Faulhaber 42GPT 196:1	various
					Flange	1	0.040	5%	0.038	0.042		steel
					Coupling	1	0.040	5%	0.038	0.042		various
					Motor Sensors and Controller	1	0.150	20%	0.120	0.180	most likely own development	various
					Bearings and Brackets	1	0.280	15%	0.238	0.322		
					Lower Bracket	1	0.132	20%	0.106	0.158		EN AW 7075-T6
					Fixed Bearing	1	0.080	5%	0.076	0.084	ZKLFA 0640-2RS	steel
					Lower Bearing Locknut	1	0.008	5%	0.008	0.009	ZM06	steel
					Upper Bracket	1	0.049	20%	0.039	0.059		EN AW 7075-T6
					Upper Bearing Locking Plate	1	0.004	20%	0.003	0.005		EN AW 7075-T6
					Floating Bearing	1	0.007	5%	0.007	0.007	S606-2RS	steel
					Touchdown Locking Mechanism	1	0.522	6%	0.490	0.554		
					Pin Puller	1	0.482	5%	0.458	0.506	EBAD TiNi™Pin Puller	various
					Locking Bolt	1	0.040	20%	0.032	0.048	for locking during touchdown	steel

Fig. 5.13.: Mass budget of the proposed mechanism including margins

With the current design, the nominal mass per mechanism measures approximately 6.72 kg for a total of 26.87 kg in a system with four legs. For the 4000 kg lander this alignment and levelling kinematic was designed for, this is less than 0.7 % of the entire system mass including payload. Even in the case of a massive increase of the kinematics mass in later design stages by 50% (from 6.72 kg up to 10 kg per unit or 40 kg for all four legs), it would still only account for 1% of the total mass of the lander.

In this mass fraction, the linear guide rail is by far the heaviest component of the current design making up almost 41% of the overall kinematics mass. Together with the guide carriage, this part of the design makes up more than half of the entire mass. Judging by the fact that these are unmodified COTS components, it will most likely be possible to design lighter custom components tailored specifically to the requirements of the system.

5.6 Power estimate

Based on the characteristics of the motor-gearhead assembly and the pin puller, it is possible to get a first estimate of the power the alignment and levelling kinematic would need to operate.
First, the motor power consumption is calculated based on the motor characteristics, the lead screw characteristics, and the travel distance of IF1 calculated earlier. The motor operates at a supply voltage of 28 V with a load current of 1.35 A, or 37.8 W of power with an output speed 15.08 revolutions per minute. The trapezoidal lead screw has a pitch of 2 mm, leading to a travel distance of 30.16 mm/min. For the total maximum needed travel distance in this configuration of 0.917 m, the motor has to operate for approximately 30 minutes and 25 seconds or 0.507 hours, leading to a total power consumption of 19.15 Wh per leg or 76.6 Wh for all four legs.
For the pin puller, it was not possible to find a supply voltage or power rating, however, the selected P1000 from EBAD has a function time of 75 ms at a current of 4 A. At this short operating time, the power consumption is negligibly small especially considering the smaller variants of the pin puller operate with a supply voltage of 2 V to 5 V. It will therefore be assumed that the activation of the pin pullers will not overload the system and consume a negligibly small amount of power that does not have to be considered for the overall power consumption.
Referring to ECSS-E-TM-10-25A(20October2010) again for a power margin and considering all of the electrical components here are COTS components, a margin of 5% has to be included [45]. This results in an overall power consumption of 80.45 Wh with a peak load of approximately 151.2 W for all four legs combined. Most likely, the actual consumption be smaller as this calculation assumes the maximum travel distance for all four legs.

Conclusion

6

> *I seem to have been only like a boy playing on the seashore, and diverting myself in now and then finding a smoother pebble or a prettier shell than ordinary, whilst the great ocean of truth lay all undiscovered before me.*
>
> **— Isaac Newton**
> Mathematician, Physicist, Astronomer

6.1 Summary and Conclusions

While still at an early stage of development, this thesis explored the possibility of a novel type of leg movement kinematic able to align and level a legged lander after touchdown on a celestial body. The specific kinematic that was considered is a linear drive which moves the interface of the primary strut vertically along the lander body. Thereby changing the geometry of the lander as a whole allowing for adaption to the soil and uneven surface beneath the lander's footpads. By doing this, it is possible to use landing sites with higher ground inclinations than before while still providing a level platform for experiments, sensors, and equipment. Additionally, it allows for easy access by astronauts for future crewed missions to the Moon. The main research question this thesis sought to answer was whether such a system is possible and a viable addition to landers. Especially regarding its added expense in regard of mass, power, and complexity.

The mathematical foundation this idea is based on are parallel manipulators and inverse kinematics similar to the way hexapods operate. By knowing the final desired position of the lander, it is possible to calculate how the kinematics have to be moved to get there. After defining the needed coordinate-systems, known parameters, and assumptions, the basic equations were explained. This includes, inter alia, transformation matrices, positioning of points in three-dimensional space, and the computation of intermediate positions between the initial orientation of the lander after touchdown and the final aligned and levelled position. Once the geometry of

intermediate positions was solved, the forces and loads could be calculated using the direct stiffness method with the approach of a quasi static load case in each position. This assumption was possible as the alignment shall happen very slowly. The computation was done using MATLAB with a MS Excel spreadsheet as input and output. A validation of the force results was conducted using Patran and MSC Nastran. With this tool, it is now possible to enter the dimensions and mass of any lander into the input spreadsheet, define calculation parameters, and solve for a possible motion path of the landing platform. The results could directly be used to generate commands for the motors allowing for an automatic operation without the need for human intervention.

To get an understanding of the complexity, power demand, and additional mass such a system would add to a hypothetical lander, an exemplary CAD design was made. Based on the proposed characteristics of a future European Lunar lander combined with interface positions of a first design of such a lander, provided by the *DLR Institute of Space Systems*, the motion and expected loads were calculated. The results were the track length for the linear drive and forces including safety margins on the primary interfaces. The final design that was proposed consists of a trapezoidal lead screw powered by an electrical motor-gearhead combination. By rotating the screw, a carrier can be moved up and down the side of the lander. Attached to this carrier is the primary interface. The mechanism also includes a linear guide rail to reduce the lateral loads on the screw to basically zero while also providing additional stability. During initial touchdown, the carrier is fixed to the lander body using a pin, which is later retracted using a pin puller. This allows the screw itself to be a lot smaller as the dynamic loads during touchdown can be neglected for the mechanical dimensioning of the screw. At an overall weight of approximately 6.72 kg per leg or 26.87 kg for a four legged lander, the system makes up less than 1% of the overall mass of a 4000 kg lander, which it was designed for. The power consumption lies at a conservatively estimated 80.45 Wh for all four legs with an operation time of approximately 30 minutes. At a bus voltage of 28 V, this corresponds to only about 2.87 Ah or approximately two thirds of the electric charge of a typical modern smartphone battery, making it very energy efficient.

As a final assessment, it is possible to say that this type of kinematic is definitely feasible with the right kind of hardware and does not add a lot of mass or power demand to the lander system as a whole. Even though this is still an early design, it was shown that with only few additional components the versatility of a landing system can be increased significantly. Considering this added operational capability of the landing system, such an alignment an levelling kinematic should be pursued further for the design of future landers.

6.2 Outlook and Future Work

This thesis proposed a novel type of linear actuator for a Lunar lander. To fit into the envelope of a master thesis, it was necessary to simplify some problems and make assumptions that will likely have to be corrected for future work on this topic. Including the fact that only 3 DOF were considered while in reality a lander moves in 6 DOF. Considering these additional 3 DOF, namely translational movement in the horizontal plane and rotation around the vertical axis, requires the introduction of so called parasitic motion. This undesired motion happens when a movement in one dimension also moves the platform in one ore more other dimensions because of geometric constraints in the system. This is a non-trivial problem for which multiple PhD dissertations have been written already. To fully explain the realistic motion of the landing platform, however, it is necessary to consider this parasitic motion as well. Additionally, the ground plane was only considered as an even and solid surface. For a more realistic approach, the uneven and soft nature of the Lunar soil has to be included. This might increase the friction experienced by the footpads, therefore increasing forces and power required by the motor.

The computation could be improved by using a more powerful programming language. Another benefit of this would be the possibility to directly implement this code into the computer of a lander to control the kinematics. At the same time, a continuous calculation over the motion could increase the accuracy contrary to the stepwise approach used in this thesis.

Aside from mathematical assumptions and implementation into MATLAB, the design of the mechanism has room for future improvements as well. It might be beneficial to use a larger but hollow lead screw to decrease weight and/or increase strength. The pin puller mechanism which is supposed to take the dynamic forces during touchdown is also designed very crudely at the current time. A more in depth analysis is needed to size it correctly. Furthermore, a completely different design in which the screw is directly integrated into the primary strut, changing the length of the strut after touchdown, might also be an interesting approach to take a look at.

Apart from all of these theoretical improvements, a first prototype will increase the understanding of the mechanism and areas which need further refinement immensely, while at the same time proving that the design works. The next step should therefore be building a first prototype to test the theory laid out in this thesis, measure and compare forces to the results of the calculation, and see whether a mechanism like this also makes sense in reality and not just on paper.

Bibliography

[1] NASA. "Artemis program." S. Loff, Ed. (Jun. 1, 2021), [Online]. Available: https://www.nasa.gov/artemisprogram (visited on Mar. 29, 2023) (cit. on p. 1).

[2] European Space Agency. "Human spaceflight and robotic exploration programmes." (2016), [Online]. Available: https://www.esa.int/About_Us/Ministerial_Council_2016/Human_Spaceflight_and_Robotic_Exploration_Programmes (visited on Mar. 29, 2023) (cit. on p. 1).

[3] European Space Agency. "Argonaut – european large logistics lander." (2020), [Online]. Available: https://www.esa.int/Science_Exploration/Human_and_Robotic_Exploration/Exploration/Argonaut_European_Large_Logistics_Lander (visited on Mar. 29, 2023) (cit. on pp. 1, 2, 47).

[4] A. Ball, J. Garry, R. Lorenz, and V. Kerzhanovich, *Planetary Landers and Entry Probes*. Cambridge University Press, May 2007 (cit. on pp. 2, 3, 5, 57).

[5] T. Maeda, R. Kajiwara, M. Otsuki, and T. Hashimoto, "Proposal of an actively controllable landing leg for lunar-planetary lander," in *2013 6th International Conference on Recent Advances in Space Technologies (RAST)*, IEEE, Jun. 2013 (cit. on pp. 2, 59).

[6] C. Bai, J. Guo, and H. Zheng, "Optimal guidance for planetary landing in hazardous terrains," *IEEE Transactions on Aerospace and Electronic Systems*, vol. 56, no. 4, pp. 2896–2909, Aug. 7, 2020 (cit. on p. 2).

[7] Y.-B. Kim, H.-J. Jeong, S.-M. Park, J. H. Lim, and H.-H. Lee, "Prediction and validation of landing stability of a lunar lander by a classification map based on touchdown landing dynamics' simulation considering soft ground," *Aerospace*, vol. 8, no. 12, p. 380, Dec. 2021 (cit. on p. 2).

[8] National Research Council, *Vision and Voyages for Planetary Science in the Decade 2013-2022*. Washington, DC: National Academies Press, Dec. 2011 (cit. on p. 2).

[9] S. Shigeto, H. Fujimoto, Y. Hori, M. Otsuki, and T. Hashimoto, "Fundamental research on reduction of impact forces using actively controlled landing gear in lunar/planetary landers," *IEEJ Transactions on Industry Applications*, vol. 133, no. 3, pp. 335–341, 2013 (cit. on p. 2).

[10] T. Maeda, T. Ozaki, S. Hara, and S. Matsui, "Touchdown dynamics of planetary lander with translation–rotation motion conversion mechanism," *Journal of Spacecraft and Rockets*, vol. 54, no. 4, pp. 973–980, Jul. 2017 (cit. on p. 2).

[11] M. Huang, "Analysis of rocket modelling accuracy and capsule landing safety," *International Journal of Aeronautical and Space Sciences*, vol. 23, no. 2, pp. 392–405, Jan. 2022 (cit. on p. 2).

[12] M. Huang, H. Nie, M. Zhang, X. Wei, and S. Yue, "Design of mission adaptive landing gear for near space travel lander," *Journal of Vibroengineering*, vol. 18, no. 8, pp. 4949–4963, Dec. 2016 (cit. on p. 2).

[13] R. Manca, M. Puliti, S. Circosta, *et al.*, "Design and optimization of an active leveling system actuator for lunar lander application," *Actuators*, vol. 11, no. 9, p. 263, Sep. 2022 (cit. on p. 3).

[14] L. Witte, "Touchdown dynamics and the probability of terrain related failure of planetary landing systems - a contribution to the landing safety assessment process," Doctoral Thesis, University of Bremen, Nov. 2015 (cit. on pp. 4, 48).

[15] W. F. Rogers, "Apollo experience report: Lunar module landing gear subsystem," NASA Lyndon B. Johnson Space Center (Manned Spacecraft Center), Houston, TX, United States, Tech. Rep. NASA-TN-D-6850, Jun. 1972 (cit. on pp. 4, 57).

[16] N. A. Holmberg, R. P. Faust, and H. M. Holt, *Viking '75 spacecraft design and test summary. volume 1: Lander design*, in *NASA Reference Publication 1027*, Nov. 1980 (cit. on pp. 4, 57).

[17] J. Mareczek, *Grundlagen der Roboter-Manipulatoren – Band 1*. Springer Berlin Heidelberg, 2020 (cit. on pp. 9–11).

[18] F. C. Park, "Parallel robots," in *Encyclopedia of Systems and Control*, J. Baillieul and T. Samad, Eds. Cham: Springer International Publishing, Aug. 4, 2021, pp. 1661–1666 (cit. on p. 10).

[19] M. Bottin, S. Cocuzza, N. Comand, and A. Doria, "Modeling and identification of an industrial robot with a selective modal approach," *Applied Sciences*, vol. 10, no. 13, Jul. 3, 2020 (cit. on p. 10).

[20] D. Silva, J. Garrido, and E. Riveiro, "Stewart platform motion control automation with industrial resources to perform cycloidal and oceanic wave trajectories," *Machines*, vol. 10, no. 8, Aug. 19, 2022 (cit. on p. 10).

[21] H. Nigatu, Y. H. Choi, and D. Kim, "Analysis of parasitic motion with the constraint embedded jacobian for a 3-PRS parallel manipulator," *Mechanism and Machine Theory*, vol. 164, no. 104409, Oct. 2021 (cit. on p. 10).

[22] R. Lin, W. Guo, and F. Gao, "On parasitic motion of parallel mechanisms," in *Volume 5B: 40th Mechanisms and Robotics Conference*, American Society of Mechanical Engineers, Aug. 2016 (cit. on p. 10).

[23] W. B. Krätzig, R. Harte, C. Könke, and Y. S. Petryna, *Tragwerke 2, Theorie und Berechnungsmethodenstatisch unbestimmter Stabtragwerke*. Springer Vieweg, 2019, vol. 5 (cit. on pp. 26, 28–30).

[24] C. Krämer, "Gewichtsvergleich verschiedener Bauweisen einer Mondstation auf Basis des Strukturkennwerts," M.S. thesis, Institut für Strukturmechanik und Leichtbau (SLA) - RWTH Aachen, Jul. 2021 (cit. on pp. 26, 28–30, 32).

[25] S. Patnaik, "An integrated force method for discrete analysis," *International Journal for Numerical Methods in Engineering*, vol. 6, no. 2, pp. 237–251, Jan. 1973 (cit. on p. 26).

[26] The MathWorks Inc., *MATLAB*, version 9.6.0.1472908 (R2019a) Update 9, Natick, Massachusetts, United States, 2019 (cit. on p. 33).

[27] Microsoft Corporation, *Microsoft Excel*, version 2019 MSO (16.0.10400.20007) 64-Bit (cit. on p. 34).

[28] MacNeal-Schwendler Corporation (MSC), *Patran/MSC Nastran*, version 2018, 2018 (cit. on p. 43).

[29] M. Kinnersley and B. Bischof, "A lunar logistic lander for europe," in *AIAA SPACE 2009 Conference & Exposition*, American Institute of Aeronautics and Astronautics, Jun. 2009 (cit. on p. 47).

[30] "ECSS-E-ST-33-01C-Rev.2(1March2019) - Mechanisms," European Cooperation for Space Standardization, Standard, Mar. 1, 2019 (cit. on pp. 54, 70).

[31] "ECSS-E-ST-32-10C-Rev.2(15May2019) - Structural factors of safety for spaceflight hardware," European Cooperation for Space Standardization, Standard, May 15, 2019 (cit. on p. 54).

[32] P. Arm, R. Zenkl, P. Barton, *et al.*, "SpaceBok: A dynamic legged robot for space exploration," in *2019 International Conference on Robotics and Automation (ICRA)*, IEEE, May 2019, pp. 6288–6294 (cit. on p. 59).

[33] D. B. Doman, M. W. Oppenheimer, and W. Rone, "Selective self-locking actuator and control allocation approach for thermal load minimization," *Journal of Guidance, Control, and Dynamics*, vol. 38, no. 6, pp. 1110–1118, Jun. 2015 (cit. on p. 60).

[34] thyssenkrupp Materials Schweiz. "Metalle - die welt der werkstoffe." (), [Online]. Available: `https://www.thyssenkrupp-materials.ch/de/metalle` (visited on May 2023) (cit. on p. 64).

[35] Schaeffler Technologies AG & Co. KG. "Bearings for Screw Drives." (Mar. 2018), [Online]. Available: `https://medias-at.schaeffler.com/de/produkt/rotary/waelz--und-gleitlager/hochgenauigkeitslager/axial-hochgenauigkeitslager/axial-schraegkugellager-fuer-gewindegetriebe/zklfa0640-2rs/p/395569` (visited on Jul. 11, 2023) (cit. on p. 68).

[36] AB SKF. "W 606-2RS1 - Stainless steel deep groove ball bearing with integralsealing." (Jul. 11, 2023), [Online]. Available: `https://www.skf.com/group/products/rolling-bearings/ball-bearings/deep-groove-ball-bearings/productid-W%20606-2RS1` (visited on Jul. 11, 2023) (cit. on p. 68).

[37] igus® GmbH. "drylin® W profile guides - Assembled guide carriages, round." (), [Online]. Available: `https://www.igus.de/product/933?artNr=WW-16-60-10` (visited on Nov. 7, 2023) (cit. on p. 68).

[38] igus® GmbH. "drylin® W profile guides - Double rail, round, hard-anodised aluminium." (), [Online]. Available: `https://www.igus.de/product/732?artNr=WS-16-60` (visited on Jul. 11, 2023) (cit. on p. 68).

[39] "ECSS-E-HB-32-23A(16April2010) - Threaded fasteners handbook," European Cooperation for Space Standardization, Handbook, Apr. 16, 2010 (cit. on p. 69).

[40] "MIL-HDBK-60: Threaded Fasteners - Tightening to Proper Tension," United States of America - Separtment of Defence, Military Handbook, Mar. 12, 1990 (cit. on p. 69).

[41] Dr. Fritz Faulhaber GmbH & Co. KG. "Faulhaber Drive Calculator - Drive System: 3863X048CR + 42GPT 196:1." (Jun. 12, 2023), [Online]. Available: https://www.faulhaber.com/en/drive-calculator/fdc/showDetail/322339/30289-30479/ (visited on Jun. 12, 2023) (cit. on p. 72).

[42] Dr. Fritz Faulhaber GmbH & Co. KG. "Planetary Gearheads - High Torque: Series 42GPT." (May 24, 2023), [Online]. Available: https://www.faulhaber.com/en/products/series/42gpt/ (visited on Jun. 12, 2023) (cit. on p. 72).

[43] Dr. Fritz Faulhaber GmbH & Co. KG. "DC-Micromotors - Graphite Commutation: Series 3863 ... CR." (Feb. 11, 2021), [Online]. Available: https://www.faulhaber.com/en/products/series/3863cr/ (visited on Jun. 12, 2023) (cit. on p. 72).

[44] Ensign-Bickford Aerospace & Defence (EBAD). "TiNi™Pin Puller." (Mar. 18, 2022), [Online]. Available: https://www.ebad.com/tini-pin-puller/ (visited on Jul. 12, 2023) (cit. on p. 77).

[45] "ECSS-E-TM-10-25A(20October2010) - Engineering design model data exchange (CDF)," European Cooperation for Space Standardization, Technical Memoranda, Oct. 20, 2010 (cit. on pp. 80, 81).

Appendix

A

A.1 Calculation results

A.1.1 Additional data on the exemplary lander - 1-2-1 configuration

This section features additional information including the spreadsheets as well as MATLAB graphs for section 4.2 that were cut from the main body to make the structure clearer.

Lander Geometry, Mass, and Orientation			
Radius of lander [m]	2.500	Roll [°]	0.0
Height of lander [m]	6.000	Pitch [°]	15.0
Mass of lander [kg]	3100	apx. ground angle [°]	15.0
Number of landing legs	4		

General Coordinates of Leg Interfaces (for leg #1) and CoG:			
	x	y	z
IF1 - Primary Strut	2.169	0.000	0.534
IF2 - Secondary Strut (left)	2.115	-0.327	-0.100
IF3 - Secondary Strut (right)	2.115	0.327	-0.100
Center of Gravity	0.000	0.000	3.000

Calculation Parameters	
# of calculation steps	10
Ground clearance [m]	0.250

LEGEND
You **MUST** change cells shown in this color
You **CAN** change cells shown in this color
NEVER change cells in this color (unless you know what you're doing)
CAREFUL, value has been changed manually

Strut Lengths [m]						
	Leg #1	Leg #2	Leg #3	Leg #4	Leg #5	Leg #6
Primary Strut	1.925	1.925	1.925	1.925		
Secondary Strut (left)	1.440	1.440	1.440	1.440		
Secondary Strut (right)	1.440	1.440	1.440	1.440		
Primary Strut - upper Segment	1.875	1.875	1.875	1.875		
Primary Strut - lower Segment	0.050	0.050	0.050	0.050		

Mechanical Properties of Struts			
	Structure Struts	Primary Struts	Secondary Struts
E [N/mm²]	210,000	70,000	70,000
v	0.3	0.2	0.3
G [N/mm²]	80,769	29,167	80,769
R_{tube} [mm]	150	60	40
t_{tube} [mm]	50.0	5,0	2,5
A [mm²]	39,270	1,806	609
I_{11} [mm⁴]	638,136,008	5,983,752	914,928
I_{22} [mm⁴]	319,068,004	2,991,876	457,464
I_{33} [mm⁴]	319,068,004	2,991,876	457,464
k_{axis} [MN/m]	8.25	1.91	0.35

Fig. A.1.: MS Excel input for exemplary lander in 1-2-1 configuration

Date	Time
02.05.2023	16:42:00

Lander Geometry, Mass, and Orientation			
Radius of Lander [m]	2.250	Roll [°]	0.0
Height of Lander [m]	6.000	Pitch [°]	15.0
Mass of Lander [kg]	3100	ground angle [°]	15.0
Number of landing legs	4		

General Coordinates of Leg Interfaces (for leg #1) and CoG:			
	x	y	z
IF1 - Primary Strut	2.169	0.000	0.534
IF2 - Secondary Strut (left)	2.115	-0.327	-0.100
IF3 - Secondary Strut (right)	2.115	0.327	-0.100
Center of Gravity	0.000	0.000	3.000

Calculation Parameters	
# of calculation steps	10
Ground Clearance [m]	0.250

Mechanical Properties of Struts (for reference)			
	Structure	PS	SS
E [N/mm²]	210,000	70,000	70,000
v	0.3	0.2	0.2
G [N/mm²]	80,769	29,167	29,167
R_{tube} [mm]	150	60	40
t_{tube} [mm]	50.0	5.0	2.5
A [mm²]	39,270	1,806	609
I_{11} [mm⁴]	638,136,008	5,983,752	914,928
I_{22} [mm⁴]	319,068,004	2,991,876	457,464
I_{33} [mm⁴]	319,068,004	2,991,876	457,464
k_{axis} [MN/m]	8.25	1.91	0.35

Strut Lengths [m]						
	Leg #1	Leg #2	Leg #3	Leg #4	Leg #5	Leg #6
IF1 - Primary Strut	1.925	1.925	1.925	1.925		
IF2 - Secondary Strut (left)	1.440	1.440	1.440	1.440		
IF3 - Secondary Strut (right)	1.440	1.440	1.440	1.440		
Primary Strut - upper Segment	1.875	1.875	1.875	1.875		
Primary Strut - lower Segment	0.050	0.050	0.050	0.050		

Movement of IF1 [m]					
-0.142	0.131	0.917	0.131		

maximum absolute Forces on Footpads [N]						
Normal Force on Ground	2075	1316	1027	1316		
Downhill Force on Ground	1518	358	-282	357		
Absolute Friction on Ground	1518	1249	282	1249		

maximum absolute Forces on IF1 (in body coordinate-system) [N]						
x	-749	0	897	0		
y	0	-746	0	746		
z	1304	980	877	980		

Fig. A.2.: MS Excel output for exemplary lander in 1-2-1 configuration

A.1.2 Additional data on the exemplary lander - 2-2 configuration

This section features additional information including the spreadsheets as well as MATLAB graphs for section 4.3 that were cut from the main body to make the structure clearer.

Lander Geometry, Mass, and Orientation			
Radius of lander [m]	2.500	Roll [°]	10.7
Height of lander [m]	6.000	Pitch [°]	10.7
Mass of lander [kg]	3100	apx. ground angle [°]	15.0
Number of landing legs	4		

General Coordinates of Leg Interfaces (for leg #1) and CoG:			
	x	y	z
IF1 - Primary Strut	2.169	0.000	0.534
IF2 - Secondary Strut (left)	2.115	-0.327	-0.100
IF3 - Secondary Strut (right)	2.115	0.327	-0.100
Center of Gravity	0.000	0.000	3.000

Calculation Parameters	
# of calculation steps	10
Ground clearance [m]	0.250

LEGEND
You **MUST** change cells shown in this color
You **CAN** change cells shown in this color
NEVER change cells in this color (unless you know what you're doing)
CAREFUL, value has been changed manually

Strut Lengths [m]						
	Leg #1	Leg #2	Leg #3	Leg #4	Leg #5	Leg #6
Primary Strut	1.925	1.925	1.925	1.925		
Secondary Strut (left)	1.440	1.440	1.440	1.440		
Secondary Strut (right)	1.440	1.440	1.440	1.440		
Primary Strut - upper Segment	1.875	1.875	1.875	1.875		
Primary Strut - lower Segment	0.050	0.050	0.050	0.050		

Mechanical Properties of Struts			
	Structure Struts	Primary Struts	Secondary Struts
E [N/mm²]	210,000	70,000	70,000
v	0.3	0.2	0.3
G [N/mm²]	80,769	29,167	80,769
R_{tube} [mm]	150	60	40
t_{tube} [mm]	50.0	5,0	2,5
A [mm²]	39,270	1,806	609
I_{11} [mm⁴]	638,136,008	5,983,752	914,928
I_{22} [mm⁴]	319,068,004	2,991,876	457,464
I_{33} [mm⁴]	319,068,004	2,991,876	457,464
k_{axis} [MN/m]	8.25	1.91	0.35

Fig. A.3.: MS Excel input for exemplary lander in 2-2 configuration

Date	Time
02.05.2023	17:00:15

Lander Geometry, Mass, and Orientation			
Radius of Lander [m]	2.250	Roll [°]	10.7
Height of Lander [m]	6.000	Pitch [°]	10.7
Mass of Lander [kg]	3100	ground angle [°]	15.0
Number of landing legs	4		

General Coordinates of Leg Interfaces (for leg #1) and CoG:	x	y	z
IF1 - Primary Strut	2.169	0.000	0.534
IF2 - Secondary Strut (left)	2.115	-0.327	-0.100
IF3 - Secondary Strut (right)	2.115	0.327	-0.100
Center of Gravity	0.000	0.000	3.000

Calculation Parameters	
# of calculation steps	10
Ground Clearance [m]	0.250

Mechanical Properties of Struts (for reference)	Structure	PS	SS
E [N/mm²]	210,000	70,000	70,000
v	0.3	0.2	0.2
G [N/mm²]	80,769	29,167	29,167
R_{tube} [mm]	150	60	40
t_{tube} [mm]	50.0	5.0	2.5
A [mm²]	39,270	1,806	609
I_{11} [mm⁴]	638,136,008	5,983,752	914,928
I_{22} [mm⁴]	319,068,004	2,991,876	457,464
I_{33} [mm⁴]	319,068,004	2,991,876	457,464
k_{axis} [MN/m]	8.25	1.91	0.35

Strut Lengths [m]	Leg #1	Leg #2	Leg #3	Leg #4	Leg #5	Leg #6
IF1 - Primary Strut	1.925	1.925	1.925	1.925		
IF2 - Secondary Strut (left)	1.440	1.440	1.440	1.440		
IF3 - Secondary Strut (right)	1.440	1.440	1.440	1.440		
Primary Strut - upper Segment	1.875	1.875	1.875	1.875		
Primary Strut - lower Segment	0.050	0.050	0.050	0.050		

Movement of IF1 [m]						
	-0.095	0.624	0.624	-0.095		

maximum absolute Forces on Footpads [N]						
Normal Force on Ground	1822	1072	1072	1822		
Downhill Force on Ground	987	-337	-337	987		
Absolute Friction on Ground	1331	608	608	1331		

maximum absolute Forces on IF1 (in body coordinate-system) [N]						
x	-661	0	1024	0		
y	0	-1024	0	661		
z	1151	985	985	1151		

Fig. A.4.: MS Excel output for exemplary lander in 2-2 configuration

Declaration

I hereby declare that I am the sole author of this master thesis and that I have not used any sources other than those listed in the bibliography and identified as references. I certify that, to the best of my knowledge, this thesis does not infringe upon any proprietary rights. I further declare that I have not submitted this thesis, in whole or in part, at this or any other institution in order to obtain a degree.

Bremen, 23rd August 2023

Jan Alexander Bertram

Universität Bremen

Nachname **Bertram** Matrikelnr. **6091313**

Vorname/n **Jan Alexander**

Hinweise zu den offiziellen Erklärungen

1. Alle drei Erklärungen sind **unverändert im Wortlaut in jedes Exemplar** der BA-/MA-Arbeit **fest mit einzubinden** und jeweils **im Original zu unterschreiben**.

2. In der digitalen Fassung kann auf die Unterschrift verzichtet werden. Die Angaben und Entscheidungen müssen jedoch enthalten sein.

zu A

Bitte ergänzen Sie die notwendigen Angaben.

zu B

Die Einwilligung kann jederzeit durch Erklärung gegenüber der Universität Bremen mit Wirkung für die Zukunft widerrufen werden.

zu C

Das Einverständnis mit der Überprüfung durch die Plagiatsoftware *Plagscan* und der dauerhaften Speicherung des Textes ist freiwillig. Die Einwilligung kann jederzeit durch Erklärung gegenüber der Universität Bremen mit Wirkung für die Zukunft widerrufen werden.

Im Jahr 2019 wird die Software zunächst in einigen Fachbereichen eingesetzt.

Weitere Informationen zur Überprüfung von schriftlichen Arbeiten durch die Plagiatsoftware sind im Nutzungs- und Datenschutzkonzept enthalten. Diese finden Sie auf der Internetseite der Universität Bremen.

Universität Bremen

Nachname **Bertram** Matrikelnr. **6091313**

Vorname/n **Jan Alexander**

A) Eigenständigkeitserklärung

Ich versichere, dass ich die vorliegende Arbeit selbstständig verfasst und keine anderen als die angegebenen Quellen und Hilfsmittel verwendet habe.
Alle Teile meiner Arbeit, die wortwörtlich oder dem Sinn nach anderen Werken entnommen sind, wurden unter Angabe der Quelle kenntlich gemacht. Gleiches gilt auch für Zeichnungen, Skizzen, bildliche Darstellungen sowie für Quellen aus dem Internet.
Die Arbeit wurde in gleicher oder ähnlicher Form noch nicht als Prüfungsleistung eingereicht.
Die elektronische Fassung der Arbeit stimmt mit der gedruckten Version überein.
Mir ist bewusst, dass wahrheitswidrige Angaben als Täuschung behandelt werden.

B) Erklärung zur Veröffentlichung von Bachelor- oder Masterarbeiten

Die Abschlussarbeit wird zwei Jahre nach Studienabschluss dem Archiv der Universität Bremen zur dauerhaften Archivierung angeboten. Archiviert werden:

1) Masterarbeiten mit lokalem oder regionalem Bezug sowie pro Studienfach und Studienjahr 10 % aller Abschlussarbeiten
2) Bachelorarbeiten des jeweils ersten und letzten Bachelorabschlusses pro Studienfach u. Jahr.

☑ Ich bin damit einverstanden, dass meine Abschlussarbeit im Universitätsarchiv für wissenschaftliche Zwecke von Dritten eingesehen werden darf.

☐ Ich bin damit einverstanden, dass meine Abschlussarbeit nach 30 Jahren (gem. §7 Abs. 2 BremArchivG) im Universitätsarchiv für wissenschaftliche Zwecke von Dritten eingesehen werden darf.

☐ Ich bin nicht damit einverstanden, dass meine Abschlussarbeit im Universitätsarchiv für wissenschaftliche Zwecke von Dritten eingesehen werden darf.

C) Einverständniserklärung über die Bereitstellung und Nutzung der Bachelorarbeit / Masterarbeit / Hausarbeit in elektronischer Form zur Überprüfung durch Plagiatssoftware

Eingereichte Arbeiten können mit der Software *Plagscan* auf einen hauseigenen Server auf Übereinstimmung mit externen Quellen und der institutionseigenen Datenbank untersucht werden.
Zum Zweck des Abgleichs mit zukünftig zu überprüfenden Studien- und Prüfungsarbeiten kann die Arbeit dauerhaft in der institutionseigenen Datenbank der Universität Bremen gespeichert werden.

☑ Ich bin damit einverstanden, dass die von mir vorgelegte und verfasste Arbeit zum Zweck der Überprüfung auf Plagiate auf den *Plagscan*-Server der Universität Bremen hochgeladen wird.

☑ Ich bin ebenfalls damit einverstanden, dass die von mir vorgelegte und verfasste Arbeit zum o.g. Zweck auf dem *Plagscan*-Server der Universität Bremen hochgeladen u. dauerhaft auf dem *Plagscan*-Server gespeichert wird.

☐ Ich bin nicht damit einverstanden, dass die von mir vorgelegte u. verfasste Arbeit zum o.g. Zweck auf dem *Plagscan*-Server der Universität Bremen hochgeladen u. dauerhaft gespeichert wird.

Mit meiner Unterschrift versichere ich, dass ich die oben stehenden Erklärungen gelesen und verstanden habe.
Mit meiner Unterschrift bestätige ich die Richtigkeit der oben gemachten Angaben.

Datum Unterschrift